Genetically engineered defective interfering particles of influenza A virus for antiviral treatment and vaccination

Dissertation

zur Erlangung des akademischen Grades

doctor rerum naturalium

(Dr. rer. nat.)

von Tanya Dogra, M. Sc.

geboren am 11. August 1994 in India

genehmigt durch die Fakultät für Verfahrens- und Systemtechnik der Otto-von-Guericke-Universität Magdeburg

Promotionskommission:	Prof. Dr.-Ing. Udo Reichl (Gutachter)
	Prof. Florian Krammer (Gutachter)
	Prof. Judith Margarete Gottwein (Gutachter)

eingereicht am:	30.10.2024
Promotionskolloquium am:	26.03.2025

Abstract

The Influenza A virus (IAV) is a major human respiratory pathogen causing seasonal outbreaks and occasional pandemics. Owing to its continuous evolution, particularly of the surface proteins of IAV strains, annual updates to vaccine formulations are necessary. This process has several limitations including lengthy screening periods for identifying and generating strains for annual update of vaccines. Additionally, the emergence of antiviral-resistant IAV strains has challenged the efficacy of current treatments, necessitating the exploration of alternative therapeutic strategies. This dissertation investigates defective interfering particles (DIPs) of IAV as a promising antiviral approach. DIPs are naturally occurring viral mutants that produce particles typically with deletions in one of their eight viral RNA (vRNA) segments. Among these, DI244 is a well-characterized DIP with a deletion in segment 1 (seg 1), which encodes polymerase basic protein 2 (PB2). In addition, a new type of DIP “OP7” was identified by our research group that has been extensively studied. OP7 carries multiple point mutations in seg 7, which encodes matrix proteins. In a normal scenario, DIPs require co-infection with a standard virus (STV) for their replication, as the DIP is unable to generate a functional protein. However, during co-infection, DIPs can inhibit STV replication (both in vitro and in vivo), indicating their potential as natural antivirals. Additionally, the development of mutations that lead to resistance to DIPs is highly unlikely.

In previous collaborations, a modified IAV reverse genetics system was developed that utilizes PB2-expressing cells to generate clonal DI244-DIPs without STV contamination in the final virus harvest. This approach involved eight plasmids encoding seven full-length vRNA segments along with a seg 1 DI vRNA encoding plasmid. After transfection, PB2 protein expression from the host cell facilitated DIP propagation. Subsequently, genetically engineered suspension Madin-Darby canine kidney (MDCK) cells were used to optimize DIP production achieving high titer DIP preparations for antiviral applications. This innovative method formed the basis for this PhD project, which aimed to develop improved DIP constructs for use as antivirals or vaccines. Notably, the concept of using seg 1 DIPs as vaccine constructs has not been described previously.

In the first part of this thesis, evolutionary studies (performed by a colleague) are described in which novel deletion junctions with presumably better interference capabilities compared to the previously described prototypic and well-characterized DIP “DI244” were identified by next generation sequencing (NGS). Besides the emergence of diverse DIPs, differences in their propagation and accumulation were observed. It was hypothesized that DI vRNA displaying strong growth properties may also demonstrate high antiviral activity. In the context of this PhD thesis, for experimental validation, the aforementioned reverse genetics system was utilized to construct and reconstitute these newly identified seg 1 DIPs in a clonal population devoid of any infectious STV. Subsequent in vitro co-infection studies confirmed that rapidly propagating DIPs indeed exhibit higher antiviral activity compared to the slower growing DIPs, including DI244. Therefore, these newly identified seg 1 DIPs are promising candidates for antiviral therapy.

In the second part of this thesis, options for the generation of DIPs for use as live vaccines were explored. The primary objective was to harness the potential of DIPs to additionally induce adaptive immune responses against seasonal infections. Specifically, the surface glycoproteins of the DIPs should be replaced by those of seasonal vaccine strains. Such a live vaccine would be administered by a nasal spray via the mucous membranes. This strategy was designed to elicit mucosal immunity at the primary site of infection, thereby promoting a comprehensive immune response that includes cellular, humoral, and systemic adaptive immunity. Although these initial attempts were not successful, potential alternative experimental approaches to allow for the reconstitution of these constructs evolved and various promising strategies are currently under investigation.

OP7 has exhibited superior antiviral activity against STV replication compared to conventional DIPs like DI244 in various studies. In the last part of this thesis, the challenge of reconstituting OP7 DIPs free from infectious STV was addressed. Here, the reverse genetics approach for generating seg 1 DIPs was refined by introducing a ninth plasmid encoding seg 7-OP7. This change resulted in a population of DIPs that included OP7 chimera (with deleted seg 1 and mutated seg 7-OP7) alongside seg 1-DIP (with wild-type seg 7). Due to the deletions in seg 1, both DIPs were restricted to growth in PB2-expressing adherent MDCK cells and did not require any inactivation steps for further use. The seed virus obtained was

subsequently passaged in suspension MDCK cells in bioreactors and optimized (by our team) for high-yield production. In a next step, conducted by a collaborator (Dunja Bruder, Helmholtz Centre for Infection Research, Braunschweig, Germany), OP7 preparations were tested intranasally in mice. At high doses, they showed no toxicity and provided complete protection against a fatal STV challenge. This demonstrated the remarkable potential of OP7 chimera DIP preparations for use as an antiviral.

In the future, OP7 chimera DIPs will be used to establish GMP-compliant production processes advancing clinical development and enhancing pandemic preparedness with this new class of broad-spectrum antivirals.

Kurzfassung

Das Influenza-A-Virus (IAV) ist ein bedeutender menschlicher Atemwegserreger, der saisonale Ausbrüche und gelegentlich Pandemien verursacht. Aufgrund seiner kontinuierlichen Entwicklung, insbesondere der Oberflächenproteine von IAV-Stämmen, sind jährliche Aktualisierungen der Impfstoffformulierungen erforderlich. Dieser Prozess weist mehrere Einschränkungen auf, darunter lange Screening-Zeiträume zur Identifizierung und Generierung von Stämmen für die jährliche Aktualisierung der Impfstoffe. Darüber hinaus hat das Auftreten antiviral resistenter IAV-Stämme die Wirksamkeit aktueller Behandlungen in Frage gestellt, was die Erforschung alternativer Therapiestrategien erforderlich macht. Diese Dissertation untersucht defekte interferierende Partikel (DIPs) von IAV als vielversprechenden antiviralen Ansatz. DIPs sind natürlich vorkommende virale Mutanten, die Partikel produzieren, die typischerweise Deletionen in einem ihrer acht viralen RNA-Segmente (vRNA) aufweisen. Unter diesen ist DI244 ein gut charakterisiertes DIP mit einer Deletion in Segment 1 (Segment 1), das für das Polymerase-Basisprotein 2 (PB2) kodiert. Darüber hinaus wurde von unserer Forschungsgruppe ein neuer DIP-Typ „OP7“ identifiziert, der umfassend untersucht wurde. OP7 trägt mehrere Punktmutationen in Seg 7, das Matrixproteine kodiert. Normalerweise benötigen DIPs für ihre Replikation eine Koinfektion mit einem Standardvirus (STV), da das DIP kein funktionelles Protein erzeugen kann. Bei einer Koinfektion können DIPs jedoch die STV-Replikation hemmen (sowohl in vitro als auch in vivo), was auf ihr Potenzial als natürliche Virostatika hinweist. Darüber hinaus ist die Entwicklung von Mutationen, die zu einer Resistenz gegen DIPs führen, höchst unwahrscheinlich.

In früheren Kooperationen wurde ein modifiziertes IAV-Reverse-Genetiksystem entwickelt, das PB2-exprimierende Zellen nutzt, um klonale DI244-DIPs ohne STV-Kontamination in der endgültigen Virusernte zu erzeugen. Dieser Ansatz umfasste acht Plasmide, die sieben vRNA-Segmente in voller Länge kodieren, zusammen mit einem Seg 1 DI vRNA-kodierenden Plasmid. Nach der Transfektion erleichterte die PB2-Proteinexpression aus der Wirtszelle die DIP-Vermehrung. Anschließend wurden gentechnisch veränderte Madin-Darby-Hundenierenzellen (MDCK) in Suspension verwendet, um die DIP-Produktion zu optimieren und DIP-

Präparate mit hohem Titer für antivirale Anwendungen zu erhalten. Diese innovative Methode bildete die Grundlage für dieses Doktorandenprojekt, dessen Ziel die Entwicklung verbesserter DIP-Konstrukte zur Verwendung als antivirale Mittel oder Impfstoffe war. Insbesondere wurde das Konzept der Verwendung von Seg-1-DIPs als Impfstoffkonstrukte bisher nicht beschrieben.

Im ersten Teil dieser Arbeit werden evolutionäre Studien (durchgeführt von einem Kollegen) beschrieben, in denen mittels Next Generation Sequencing (NGS) neuartige Deletionsverbindungen mit vermutlich besseren Interferenzfähigkeiten im Vergleich zum zuvor beschriebenen prototypischen und gut charakterisierten DIP „DI244“ identifiziert wurden. Neben der Entstehung verschiedener DIPs wurden auch Unterschiede in ihrer Ausbreitung und Ansammlung beobachtet. Es wurde die Hypothese aufgestellt, dass DI-vRNA mit starken Wachstumseigenschaften auch eine hohe antivirale Aktivität aufweisen kann. Im Rahmen dieser Doktorarbeit wurde zur experimentellen Validierung das oben erwähnte Reverse-Genetik-System verwendet, um diese neu identifizierten Seg-1-DIPs in einer klonalen Population ohne infektiöse STV zu konstruieren und zu rekonstruieren. Nachfolgende In-vitro-Koinfektionsstudien bestätigten, dass sich schnell ausbreitende DIPs tatsächlich eine höhere antivirale Aktivität aufweisen als die langsamer wachsenden DIPs, einschließlich DI244. Daher sind diese neu identifizierten Seg-1-DIPs vielversprechende Kandidaten für eine antivirale Therapie. Im zweiten Teil dieser Arbeit wurden Möglichkeiten zur Erzeugung von DIPs als Lebendimpfstoffe untersucht. Das Hauptziel bestand darin, das Potenzial von DIPs zu nutzen, um zusätzlich adaptive Immunantworten gegen saisonale Infektionen zu induzieren. Konkret sollten die Oberflächenglykoproteine der DIPs durch die von saisonalen Impfstoffstämmen ersetzt werden. Ein solcher Lebendimpfstoff würde durch ein Nasenspray über die Schleimhäute verabreicht werden. Diese Strategie wurde entwickelt, um eine Schleimhautimmunität an der primären Infektionsstelle hervorzurufen und so eine umfassende Immunantwort zu fördern, die zelluläre, humorale und systemische adaptive Immunität umfasst. Obwohl diese ersten Versuche nicht erfolgreich waren, entwickelten sich potenzielle alternative experimentelle Ansätze zur Rekonstruktion dieser Konstrukte, und verschiedene vielversprechende Strategien werden derzeit untersucht.

OP7 hat in verschiedenen Studien eine überlegene antivirale Aktivität gegen die STV-Replikation im Vergleich zu herkömmlichen DIPs wie DI244 gezeigt. Im letzten Teil dieser Arbeit wurde die Herausforderung der Rekonstruktion von OP7-DIPs ohne infektiöses STV angegangen. Hier wurde der Reverse-Genetics-Ansatz zur Erzeugung von Seg-1-DIPs durch die Einführung eines neunten Plasmids verfeinert, das Seg 7-OP7 kodiert. Diese Änderung führte zu einer Population von DIPs, die OP7-Chimäre (mit gelöschtem Seg 1 und mutiertem Seg 7-OP7) neben Seg 1-DIP (mit Wildtyp-Seg 7) enthielt. Aufgrund der Deletionen in Seg 1 waren beide DIPs auf das Wachstum in PB2-exprimierenden anhaftenden MDCK-Zellen beschränkt und erforderten keine Inaktivierungsschritte für die weitere Verwendung. Das erhaltene Saatvirus wurde anschließend in Suspensions-MDCK-Zellen in Bioreaktoren passagiert und (von unserem Team) für eine ertragreiche Produktion optimiert. Im nächsten Schritt wurden OP7-Präparate von einer Mitarbeiterin (Dunja Bruder, Helmholtz-Zentrum für Infektionsforschung, Braunschweig, Deutschland) intranasal an Mäusen getestet. In hohen Dosen zeigten sie keine Toxizität und boten vollständigen Schutz vor einer tödlichen STV-Infektion. Dies zeigte das bemerkenswerte Potenzial von OP7-Chimären-DIP-Präparaten für den Einsatz als antivirales Mittel.

In Zukunft werden OP7-Chimären-DIPs verwendet, um GMP-konforme Produktionsprozesse zu etablieren, die die klinische Entwicklung vorantreiben und die Pandemievorsorge mit dieser neuen Klasse von Breitband-Antivirenmitteln verbessern.

Declaration

I hereby declare that the work presented in this thesis is my own original work, with certain sections taken from collaborators. The content, ideas, and conclusions expressed herein are entirely my own. AI tools, including Grammarly and ChatGPT, were utilized only to enhance the clarity and coherence of the language used in this document.

List of abbreviations

Adherent-HEK-293T-PA	Adherent HEK-293T cells stably expressing PA
Adherent-HEK-293T-PB1	Adherent HEK-293T cells stably expressing PB1
Adherent-HEK-293T-PB2	Adherent HEK-293T cells stably expressing PB2
Adherent-HEK-293T-PB2-PB1-PA	Adherent HEK-293T cells stably expressing IAV polymerases PB2, PB1 and PA
Adherent-MDCK-PA	Adherent MDCK cells stably expressing PA
Adherent-MDCK-PB1	Adherent MDCK cells stably expressing PB1
Adherent-MDCK-PB2	Adherent MDCK cells stably expressing PB2
Adherent-MDCK-PB2-PB1-PA	Adherent MDCK cells stably expressing IAV polymerases PB2, PB1 and PA
ATCC	American-Type Culture Collection
bp	Base pair
BSA	Bovine serum albumin
Cal H1N1	Pandemic influenza A/California/7/2009 of subtype H1N1
cDNA	Complementary DNA
CME	Complete medium exchange
CRM1	Chromosomal region maintenance 1
cRNA	Complementary RNA
cRNP	Complementary ribonucleoprotein
d.p.i.	Days post infection
d.p.t.	Days post transfection
DI vRNA	Defective interfering vRNA
DIP	Defective interfering particle

DMEM	Dulbecco's Modified Eagle's Medium
DPZ	German Primate Centre, Göttingen, Germany
ECACC	European Collection of Authenticated Cell Cultures
EDTA	Ethylenediaminetetraacetic acid
FBS	Fetal bovine serum
FDA	Food and Drug Administration
GFP	Green fluorescent proteins
GMEM	Glasgow Minimum Essential Medium
h.p.i.	Hour post infection
h.p.t.	Hour post transfection
HA	Hemagglutinin
HEK-293T	Human embryonic kidney cells, containing the SV40 large T antigen
HPAI	Highly pathogenic avian influenza
HZI	Helmholtz Centre for Infection Research, Braunschweig, Germany
IAV	Influenza A virus
IBV	Influenza B virus
IFITM	IFN-induced transmembrane
IFITMs	IFN-inducible transmembrane proteins
IFN	Interferon
IFNR	IFN receptor
IRF3/7	interferon regulatory factors 3 or 7
ISG	IFN-stimulated gene
JAK/STAT	Janus kinase/signal transducers and activators of transcription
LAIV	Live attenuated influenza vaccine
M1	Matrix protein 1 of IAV
M1	Matrix protein 1
M2	Matrix protein 2 of IAV
M2	Matrix protein 2
MD DSP	Medium dilution downstream production

MDCK	Madin-Darby canine kidney cells
MEM	Minimum Essential Medium
MODIP	Multiplicity of DIP
MOI	Multiplicity of infection
MPI	Max Planck Institute for Dynamics of Complex Technical Systems, Research group Bioprocess Engineering
mRNA	Messenger RNA
Mx	Myxovirus resistance
MyD88	Myeloid differentiation primary response protein 88
NA	Neuraminidase
NCR	Noncoding region
NEP	Nuclear export protein
NES	Nuclear export signal
NF-κB	Nuclear factor kappa-light-chain-enhancer of activated B cell
NGS	Next-generation sequencing
NIBSC	National Institute for Biological Standards and Control
NLS	Nuclear localisation signal
NP	Nucleoprotein of IAV
NS1	Non-structural protein 1 of IAV
NS2	Non-structural protein 2
ORF	Open reading frame
OvGU	Otto von Guericke University Magdeburg
PA	Polymerase acidic protein
PB1	Polymerase basic protein 1
PB2	Polymerase basic protein 2
PKR	protein kinase R
Poly(A)	Polyadenylated
PR8	Influenza virus strain A/PR/8/34 (H1N1)
PRR	Pattern recognition receptor
RdRp	RNA-dependent RNA polymerase
RIG-I	Retinoic acid-inducible gene-I
RSV	Respiratory syncytial virus

RT-qPCR	Reverse transcription-quantitative polymerase chain reaction
SARS-CoV-2	Severe acute respiratory syndrome coronavirus type 2
SD	Standard deviation
Seg	Segment
Seg 7-OP7	Seg 7 of OP7
SEM	Standard error of mean
SOE-PCR	Splice overlap exchange polymerase chain reaction
ssRNA	Single-stranded RNA
Suspension-MDCK	MDCK cells, derived from ECACC, and adapted to suspension growth in Xeno™
Suspension-MDCK-PB2	Suspension MDCK cells growing in Xeno™ stably expressing PB2
Suspension-MDCK-PB2-PB1-PA	Suspension MDCK cells growing in Xeno™ stably expressing IAV polymerases PB2, PB1 and PA
SXC	Steric exclusion chromatography
TLR	Toll-like receptor
UTR	Untranslated region
vRNA	Viral RNA
vRNP	Viral ribonucleoprotein
WHO	World Health Organization
WT	Wild-type

Table of contents

1. Introduction

According to the Global Burden of Diseases, Injuries, and Risk Factor study (GBD study) of 2019, chronic respiratory diseases rank as the third leading cause of death worldwide annually [12]. Data extrapolated from the WHO Global Health Estimate for 1999-2015 indicate that between 291,243 and 645,832 deaths each year are associated with influenza, making it a major respiratory disease [13]. Interestingly, individuals under the age of 65 account for 42% of these deaths, while immunocompromised or older people (>65 years) are more susceptible to infection, resulting in more fatal cases [13]. Influenza A viruses (IAVs) are contagious, airborne pathogens that typically cause symptoms of the common cold in the upper respiratory tract of those infected. In a small number of cases with moderate to severe infection, the infection can spread beyond the nose, throat, and bronchi into the lungs [9]. New variants of the virus, which can often be transmitted from animals to humans under conditions of reassortment and zoonosis, can cause severe lower respiratory tract infections that may be fatal. For instance, highly pathogenic avian influenza (HPAI) H5N1 was initially identified in 1997. Since 2022, human infections have occurred following unprotected contact with infected poultry. Although there is no evidence of human-to-human transmission, concerns persist about a potential pandemic if the strain adapts for human spread. Historically, pandemics such as the 1919 Spanish flu, originated after reassortment between H1N1 IAV strains of swine and avian origins [14]. Despite the availability of vaccines against seasonal strains and the immunity people develop over time from various infections, the emergence of new viral strains continues to pose a risk of new pandemics [15]. Seasonal vaccination, which requires intensive screening to identify the correct antigens, is necessary. However, mismatches between vaccine formulations and infecting strains in a particular region can greatly reduce vaccine effectiveness to only 28% as seen in Japan during the 2017-2018 season [16]. Yet vaccine formulation is a time-consuming process. Although antiviral medications that block influenza entry and replication are available for immediate relief, but the ongoing evolution of the virus and reassortment among IAV strains increase the risk of the development of resistance to these treatments [10]. Therefore, additional strategies are being

explored to complement current treatments for IAV infections during epidemics and to improve preparedness for future pandemics.

One such strategy involves the use of defective interfering particles (DIPs) of IAV [17-24]. These naturally occurring viral mutants are generated during virus replication and can inhibit the replication of the standard virus (STV) by out-competing it for resources and stimulating the innate immune system [25-27]. In preclinical studies utilizing murine and ferret models, intranasal administration of DIPs has demonstrated a potent antiviral effect. The application of DIPs as antiviral agents could provide immediate therapeutic benefits by activating the immune response and preventing subsequent infections, positioning them as potential prophylactic or adjunctive treatments in pandemic scenarios [28]. Furthermore, IAV DIPs exhibit broad-spectrum antiviral activity through non-specific activation of innate immunity, enabling the suppression of interferon-sensitive respiratory pathogens such as Influenza B Virus (IBV), Severe Acute Respiratory Syndrome Coronavirus 2 (SARS-CoV-2), and Respiratory Syncytial Virus (RSV). This broad antiviral potential highlights their promise as effective antiviral candidates [17, 28-31].

It is crucial to highlight that, historically, the primary method for producing large quantities of inactivated, live attenuated influenza vaccines (LAIV), or subunit vaccines involved cultivating the virus in embryonated chicken eggs [15]. This method had several drawbacks, including allergic reactions to egg components in some recipients and the challenge of scaling up the production of eggs during pandemics [32]. Despite these issues, egg-based IAV vaccine production remains predominant, even after the FDA approved cell culture-based methods in the 1990s. These included the use of MDCK or Vero cells and a high-yield H1N1/PR/8/34 (PR8) backbone for the production of IAV vaccines [15]. The transition towards cell-culture-based technology represents a significant advancement that may be exploited for the production of DIPs to use them as antivirals or vaccines against the influenza infection.

Previously, DIPs were produced using egg-based methods [2]. These particles, characterized by mutations like large internal deletions in their genome, cannot synthesize viral protein, necessitating co-infection with an STV in a host cell for

the missing viral protein production [33]. The first well-documented and reverse-genetically engineered IAV DIP is known as DI244 [2]. It features a deletion in segment 1 (seg 1), which prevents the generation of the full-length polymerase basic protein 2 (PB2) [2]. The reverse genetics for the generation of DI244 included side-by-side reconstitution of STV. Later, egg-based enrichment methods, followed by ultraviolet (UV) treatment were employed to deactivate any infectious STVs in the harvest. Despite UV treatment, DI244 exhibited antiviral properties against lethal STV challenges in ferrets and mice [17, 31, 34-36].

In recent studies, a more refined production system was developed for the clonal production of seg 1 DIPs, employing reverse genetics for IAV [6, 8]. In this system, supplementation of the missing PB2 protein in cell lines, eliminated the need for STV co-infection to propagate the DIP. The rescued DIPs were then produced in suspension cell cultures (expressing PB2 protein) and demonstrated protective activity against lethal STV infections in mice [37]. To enhance the use of DIPs as antivirals or vaccines, improving DIP constructs and their production methods seemed crucial.

In this thesis, the seg 1-based reverse genetics system was primarily utilized to create new DIP constructs. In the first chapter, new seg 1 DIPs were created, which were identified through next-generation sequencing (NGS) from a prolonged influenza A virus (IAV) infection in suspension cells [1]. In the second chapter, the DIP constructs were engineered to develop DIP-based live vaccines by incorporating seasonal strain-specific surface antigens. This modification was intended to further stimulate adaptive immunity against seasonal IAV infections. In the third chapter, the reconstitution of OP7 DIPs free of infectious viruses was aimed. OP7 DIP, a new type of DIP discovered by Kupke and colleagues in 2019 [5] is distinct from conventional DIPs due to the presence of multiple nucleotide substitutions within seg 7 vRNA, unlike the large internal deletions typically seen in conventional DIPs [5]. OP7 demonstrated enhanced antiviral effects compared to DI244, both in vitro and in vivo [5, 29, 38]. The objective was to generate a cell culture-based production system for OP7 without standard virus (STV) using reverse genetics.

2. Theoretical background

This section starts with a general overview to introduce IAVs, detailing their structure, morphology, and replication. Subsequent subsections will explore the origins of DIPs, their varieties, and how they interfere with STV replication. This is followed by an extensive overview of the methods used in IAV vaccine production, including the application of reverse genetics for creating IAV vaccines in cell cultures, and the role of DIPs as antiviral and/or use as vaccine.

2.1. Influenza A virus

2.1.1. Structure and morphology

Influenza viruses consist of types A, B, C, and D within the orthomyxoviridae family. Out of this, influenza A and B viruses (IAV, IBV) are the ones that lead to seasonal outbreaks, while IAV also leads to pandemics in humans [39]. IBV's host range is restricted to humans, whereas IAV can infect various species including birds, pigs, and horses, and can lead to severe illnesses [40]. IAV has a negative-sense, single-stranded (ss) RNA genome that is termed a vRNA. There are eight vRNA segments, and in total, they encode at least 17 proteins, depending on the strain [40]. In Figure 2.1.1, these segments are arranged in descending order of length, spanning from 2.3 to 0.9 kilobases (seg 1–8). Each segment is capable of encoding at least one protein. Additional proteins are generated through alternative splicing or ribosomal frameshifting mechanisms [41]. Regarding the latter, following the transcription of nascent mRNA from the genomic vRNA, the mature, spliced mRNA may encode multiple proteins due to the existence of several open reading frames (ORF). For instance, seg 7 can encode for up to four matrix proteins and seg 8 can encode for 2 NS proteins [42].

Regardless of the type of vRNA segment, all vRNA share a common structural organization that consists of an ORF positioned in the antisense direction (3’-5’) at its core [9]. The ORFs are flanked by untranslated regions (UTRs) at both the 3’ and 5’ ends. The coding and the UTR (also referred to as noncoding region, NCR) comprise packaging signals that are essential for the vRNA’s inclusion into progeny

virions. These traditional packaging signals are subdivided into incorporation signals, crucial for each vRNA segment's integration into the progeny, and are found within the 3’ and 5’ UTRs [43]. Bundling signals, necessary for the simultaneous and correct integration of all eight vRNAs in the progeny, are located at the ends of the coding region and are distinct for each vRNA segment [44]. The UTRs, range from 19 to 59 nucleotides in length, and are further divided into two motifs: one highly conserved across segments, located at the 3’ (12 nucleotides) and 5’ (13 nucleotides) ends [43]. These conserved regions are partially complementary and form the core promoter in vRNA segments [45]. The other motif encodes segment-specific noncoding regions and its length varies depending on the vRNA segment.

As shown in Figure 2.1.1, the vRNA segments are complexed with RNA-dependent RNA polymerases (RdRp) encoded by seg 1, 2, and 3, known as polymerase basic 2 and 1 (PB2, PB1) and polymerase acidic (PA), respectively. The single-stranded RNAs, being negatively charged, are inherently unstable. However, nucleoproteins (NP) encoded by seg 5, which carry a positive charge, stabilize the RNA by wrapping around it, making a twisted rod-like structure as depicted in Figure 2.1.1 [46]. This vRNP complex is crucial for the effective packaging and replication of the virus [47]. These eight vRNPs are organized in a configuration of 7+1 within the virion, with one central vRNP encircled by the other vRNPs [39, 47]. The eight vRNPs are enclosed within a lipid envelope derived from the host, lined with a matrix protein 1 (M1, encoded by seg 7) layer to preserve the virus's morphology [48]. Additionally, the surface of the virions is decorated with glycoproteins known as Hemagglutinin (HA) and Neuraminidase (NA), which are encoded by seg 4 and 6, respectively [9]. HA is instrumental in mediating the virus's entry into the host cell, as it binds to specific cell receptors, and facilitates the fusion of the virion (see section 2.1.2) with the cell membrane [49]. In contrast, NA plays a pivotal role in the virus's egress, enabling the cleavage of host cell receptors to facilitate the release of progeny virus [50]. The virion's surface also features M2 ion channels, which are expressed post RNA splicing from seg 7, and are embedded within the envelope. These ion channels are essential for virus entry, assembly, and budding processes [9]. Lastly, seg 8 is responsible for encoding non-structural proteins NS1 and NS2, which are majorly not incorporated into mature virions. NS1 plays a

critical role in circumventing the host's innate immune responses, thereby facilitating viral replication [51]. Nuclear export protein (NEP, also referred to as NS2), is essential in the export of vRNPs, along with M1, from the nucleus to the cytoplasm.

From clinical isolates, electron microscopy reveals that IAV may exhibit a filamentous morphology, which is believed to play a crucial role in virus replication and pathogenesis [52]. The exact mechanism behind this morphology's contribution to the virus's lifecycle, particularly its potential role in facilitating the transmission of viral progeny across cells within the respiratory mucosa, remains unclear. Furthermore, the most commonly utilized laboratory strains for studying influenza A virus H1N1 are PR8 and A/Wilson-Smith Neurotropic/33 (WSN), which typically display either mainly a spherical shape, as illustrated in Figure 2.1.1 [52]. The filamentous forms can stretch beyond 20 µm in length, whereas the spherical variants have diameters ranging from 80 to 120 nm [46, 48]. IAVs are categorized into various subtypes based on their 18 HA and 11 NA proteins. These viruses can undergo reassortment in animal hosts like pigs and poultry, which are susceptible to both human and avian IAVs and can result in the emergence of new variants. This process, known as antigenic shift, occurs when there is an exchange of antigenic proteins between different virus strains, leading to the creation of new virus subtypes. Additionally, the surface protein HA or NA, which is crucial for the virus's recognition by the immune system, can evolve rapidly within a particular strain by accumulating mutations in the genome. This evolution allows the virus to escape detection by the host's immune system, a phenomenon referred to as antigenic drift.

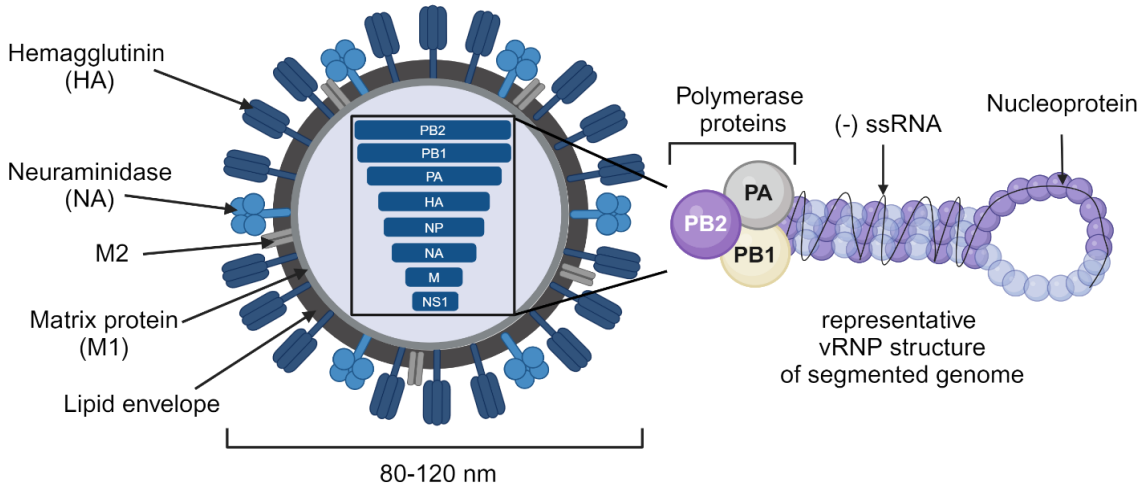

Figure 2.1.1. Structure of influenza A virus and its ribonucleoprotein. Influenza A virus (IAV) is a spherical, enveloped virion harbouring segmented, negative-sense, single-stranded RNA as its genome. The depicted RNA-dependent RNA polymerase complex consists of subunits from polymerase basic proteins 2 and 1, along with polymerase acidic (PA) protein, encoded by segments (seg) 1, 2, and 3, respectively. Nucleoproteins (NP), encoded by seg 5, encapsulate each viral RNA (vRNA) segment, and the vRNA ends associate with the polymerase complex to form the ribonucleoprotein (vRNP). The virion's surface features the glycoproteins hemagglutinin (HA) and neuraminidase (NA), encoded by seg 4 and 6. Matrix proteins M1 and M2, encoded by seg 7, with M2 forming an ion channel embedded within the envelope and M1 supporting the virion's structure. Proteins encoded by seg 8, non-structural protein 1 and 2 (NS1 and NS2), are not depicted. This figure is based on Krammer et al. [9] and modified using Biorender.com.

2.1.2. Virus replication

IAV is an infectious airborne pathogen that is transmitted through aerosols produced by sneezing or coughing, or via contact with contaminated surfaces. It infects new hosts when inhaled, initiating infection in the upper respiratory tract, including the nose, trachea, and sinuses. The viral surface proteins bind to sialic acid receptors expressed by epithelium cells. IAV strains that particularly infect humans mainly interact with α-2,6 sialic acid on epithelial cells. Whereas avian IAVs bind to α-2,3 sialic acid, commonly found in bird's gut, making it a primary infection site in birds [39]. In humans, α-2,3 sialic acid is less abundant and located mainly in the lower respiratory tract, explaining why some avian IAV (for instance HPAI) can cause deadly infections in humans by attacking the bronchioles and alveoli. This may lead to severe pneumonia with over 60% mortality [53]. Pigs express both sialic acid types in their trachea and thereby serve as a mixing vessel for generating reassortants from avian and human IAVs.

As depicted in Figure 2.1.2, the replication cycle of IAV is divided into six phases: attachment of the virus to the host cell, endocytosis of the virion, uncoating and membrane fusion, replication, transcription, and translation, and finally, the release of new virus particles [9].

The initial phase is facilitated by HA proteins, which enable the virus to bind to and fuse with the host cell membrane, allowing entry. HA proteins are trimeric, featuring a globular head and a stem [54]. Low pathogenicity H1 subtypes possess a monobasic cleavage site, leading to the cleavage of HA proteins into HA1, which includes sialic acid receptor binding sites, and HA2, which is responsible for the fusion of the viral envelope with host cell membranes [55]. This cleavage, essential for the virus infectivity in subsequent cycles, is performed by host trypsin-like proteases, predominantly found in the respiratory tract. Without cleavage, HA can attach to but not fuse with or enter the host cell [56]. Following entry, the virus undergoes endocytosis and is transported to an endosomal compartment. The acidic environment (around pH 5) in the endosome triggers conformational changes in HA proteins [57], exposing the fusion peptide and facilitating the fusion of viral and endosomal membranes [40]. This fusion creates a pore through which the viral genome, encapsulated as vRNPs, is released into the cytosol. Additionally in this step, the acidic conditions activate M2 ion channels, allowing H+ ions to enter the virus, leading to the dissociation of M1-RNP complexes and the release of vRNP into the cytoplasm [58].

Following uncoating and release into the cytoplasm, the vRNP complexes dissociates from the M1. This exposes the nuclear localization signals (NLS) on the RNPs, specifically on the polymerases and NP components [59]. The interaction between the NLS on the NP and polymerase proteins and the host cell's nuclear import factors, known as importins (such as α1, α5, β), facilitates the import of the vRNPs into the nucleus [60]. The nuclear pore complex (NPC) mediates the translocation of the importin-vRNP complex into the nucleus. Once inside the nucleus, the importins dissociate from the vRNPs, allowing the viral replication machinery to initiate replication. Initially, in the nucleus vRNA serves as a template for the RdRp complex, consisting of PB2, PB1, and PA, to produce two types of

positive-sense RNA species: mRNA (for transcription) and cRNA (for replication) [40, 61]. The immediate transcription of mRNA is crucial for the early synthesis of viral proteins necessary for replication, making this step more efficient than the replication of cRNA and vRNA. Whereas, the cRNA serves as a template for producing multiple vRNA copies [45].

cRNA replication occurs via a primer-independent mechanism (Newcomb et al., 2009). It starts with vRNA template introduction into the transcription initiation complex, where PB1 binds ATP and GTP ribonucleotide tri-phosphates (rNTPs), which is in alignment with U1 and C2 sequences at the vRNA 3' ends (Te Velthuis and Fodor, 2016). Complementary rNTP binding to the vRNA template forms the dinucleotide (pppApG) and locks the vRNA to PB1 within the RdRp complex (Deng et al., 2006). Transcript elongation generates cRNA, which detaches from RdRp as NP molecules attach. The polymerase complex binds to the cRNA-NP, forming the cRNP. This structure resembles vRNP, with 5' and 3' ends partially complementary in a loop facilitating RdRp association, while NP proteins coat the transcript (Zheng and Tao, 2013).

In the next phase of replication, vRNA is synthesized from the cRNP transcripts similarly to how cRNA is produced, leading to the creation of multiple vRNA copies. However, the initiation of this phase differs slightly, with two proposed mechanisms for the altered positioning of rNTPs, dinucleotide formation, and elongation [62]. The first mechanism suggests that rNTPs initially bind to the 4th and 5th positions at the 3' end of the cRNA, creating a dinucleotide that then detaches and rebinds to the 3' end of the cRNA transcript, initiating the transcription process that produces the vRNP transcript and leads to the assembly of the vRNP complex [62, 63]. The second mechanism proposes that the cRNA transcripts are positioned within the RdRp complex in a way that allows rNTPs to bind at the 3' end, form a dinucleotide, and continue with the elongation process to produce vRNA [62].

On the other hand, transcription to generate mRNA relies on a primer-dependent mechanism that incorporates a 5' cap structure and a 3' poly(A) tail [63]. IAV lacks the enzymes necessary for adding 5' caps to its mRNA transcripts. Therefore, it utilizes the host's nascent capped mRNA through a process known as "cap-

snatching.” In this process, the IAV PB2 protein (from the RdRp complex) binds to the 5’ cap of host mRNA using its cap-binding domain [39]. Following this, the PA subunit cleaves the capped RNA 10-13 nucleotides away from the 5’ cap, and the resulting RNA fragments, along with the cap, serve as primers for initiating transcription [11]. This cap structure is then positioned into the PB1 catalytic domain, where it anneals the cap to the vRNA (which serves as the template for mRNA synthesis) and promotes elongation [40]. At the 5’ ends of the vRNA, short poly(U) sequences are present that cause the RdRp to stutter, leading to the frequent detachment, repositioning, and reattachment of the mRNA to the vRNA at this site, as the poly(A) tail is synthesized [40].

Newly transcribed mRNA transcripts are transported from the nucleus to the cytosol for translation by cytoplasmic ribosomes. Here, nascent mRNA undergoes splicing into multiple protein-producing transcripts (e.g., seg 7 for M1 and M2 proteins, seg 8 for NS1 and NS2 proteins) via the host's cellular spliceosome machinery [48]. The resulting proteins, including polymerases, M1, NEP, and NP, play crucial roles in vRNA transcription and replication. Hence, they are subsequently imported back into the nucleus post-translation via nuclear localization signals [64].

During the final stages of virus assembly, proteins such as HA, NA, and M2, synthesized in the cytosol, are transported to the Golgi apparatus for post-translational modifications before being directed to the cell membrane [9]. Here, they integrate into the lipid membrane, facilitating packaging, budding, and the release of virions. Meanwhile, newly formed vRNPs must associate with NEP and M1 proteins to exit the nucleus [65]. This export, occurring in the infection's late stages, follows a sequential process where M1 binds to vRNPs and the cellular export protein, chromosomal maintenance 1 (CRM1), along with its co-factor RanGTP, enabling vRNP export via the CRM1-export pathway [65]. NEP plays a pivotal role in this process by enhancing the binding efficiency of M1 to vRNPs and facilitating M1's interaction with CRM1, as M1 alone cannot bind to CRM1. The assembly of this complex, crucial for the nuclear export of vRNPs, is driven by nuclear export signals (peptide sequence) in M1 and NEP proteins.

Budding is initiated by the accumulation of M1 protein near the membrane, attracting other viral components including the vRNPs to form a bud. To produce an infectious virion, the entire genome of the IAV, comprising all eight vRNA segments, must be incorporated into the progeny virions. Genome packaging occurs during the late stages of viral replication [66]. Early models of IAV packaging suggested a random process, where any number and combination of vRNA segments could be included in the progeny virions [66, 67]. This hypothesis was based on the presence of genome packaging signals in each vRNA segment, which were thought to be unable to distinguish between different vRNA segment types [67]. However, more recent models, supported by stronger evidence, propose a selective packaging mechanism [66, 68, 69]. According to this model, each vRNA segment is specifically packaged into the progeny virions through distinct packaging signals present on different vRNA segments, known as incorporation and bundling signals (see section 2.1.1 [44]). These packaging signals are believed to extend from the promoter regions to segment-specific non-coding regions (NCRs). Lastly, additional proteins like HA, NA, and M2 gather, with M2 initiating the detachment and scission of the virus bud from the membrane [39]. NA facilitates the release of mature virions by cleaving sialic acids from the cell surface. This action prevents HA from reattaching to the cell membrane, thereby ensuring the virions do not reattach to the cell surface [9].

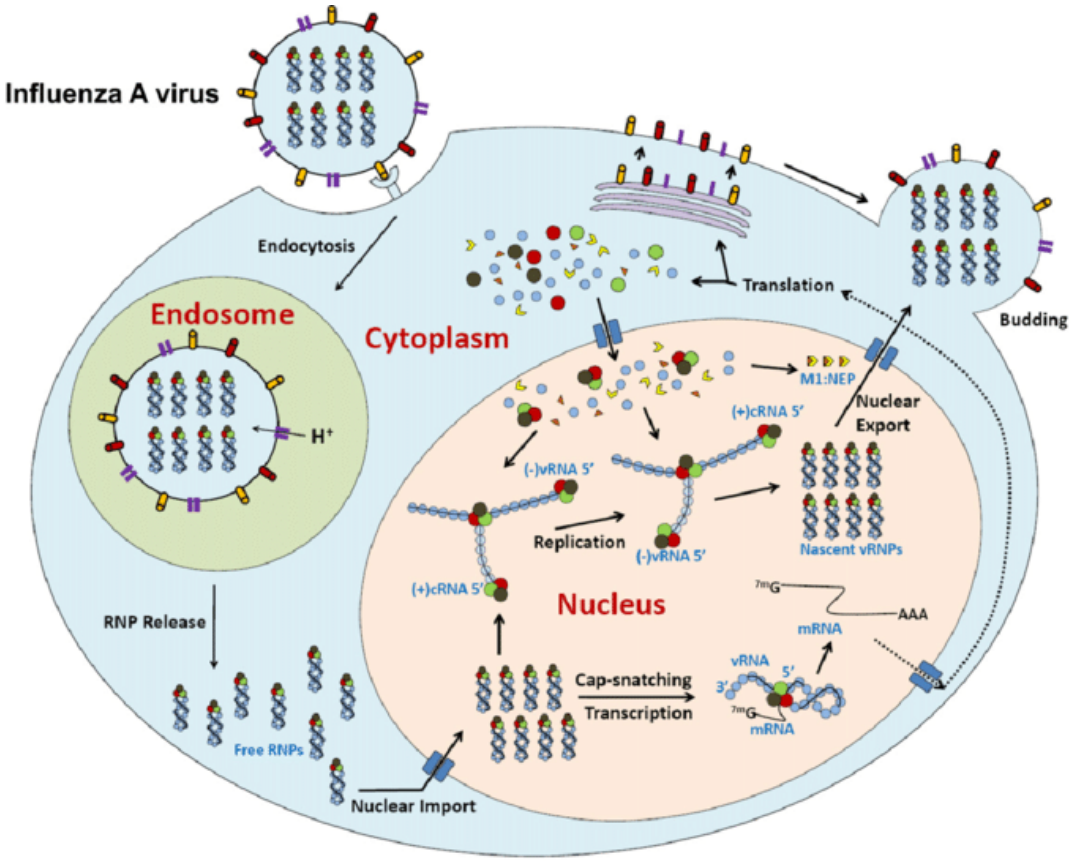

Figure 2.1.2. IAV replication process. Following the attachment of the virus to the cell via HA interaction with sialic acid receptors, the virus is internalized through endocytosis facilitated by receptor-mediated fusion. In the endosomes, a drop in pH triggers structural changes leading to the fusion of the viral membrane with endosomal membranes. Subsequently the uncoating of the virus and the release of vRNPs into the cell nucleus occurs. After nuclear import of the vRNPs, vRNA acts as a template for the production of complementary RNA (cRNA), and messenger RNA (mRNA) via replication and transcription processes. The mRNA is then transported to the cytoplasm where it directs the synthesis of viral proteins. The M1 and nuclear export protein (NEP) are transported into the nucleus to assist in exporting vRNPs to the cytoplasm. At the cell membrane, they are assembled into new virions that bud off from the cell. This figure is adapted from Zheng et al., [11].

2.2. Defective interfering particles

2.2.1. Origins and types of IAV DIPs

In the 1940s, von Magnus was the first to identify the presence of “incomplete virus particles” following serial passages of IAV in embryonated chicken eggs, and noted reduction in the ratio of infectious to total virus particles over time [70, 71]. This observation of non-infectious particles was not unique to IAV; similar phenomena

were noted for other viruses like the vesicular stomatitis virus and semliki forrest virus, suggesting a general pattern that is influenced by multiplicity of infection (MOI) [21, 25]. These non-infectious particles were dismissed as artifacts. In the 1970s “defective interfering particles”, term was coined by Huang and Baltimore; characterized by several key features: 1) they are morphologically similar to the STV, 2) miss a portion of the genome, 3) can replicate with the aid of a "helper virus," and 4) inhibit the production of this helper virus [72].

DIPs have been identified in both RNA and DNA viruses affecting a variety of plants and animals, as documented in literature [21, 26, 72, 73]. However, the emergence of DIPs is often attributed to the error-prone replication process of RdRp, which might explain why most research focuses on DIPs originating from RNA viruses [74]. Mutations that lead to the creation of DIPs can involve deletions or point mutations [74-76]. Analysis of DIPs derived from single-stranded RNA (ssRNA) has identified various categories [33]. The first category includes DIPs with a significant internal deletion within the ORF of the infectious genome, while still retaining the terminal ends. The second category consists of DIPs with large deletions that have been rearranged so that the terminal ends are in the reverse complement orientation, known as hairpin or copyback genomes. The third category involves the joining of non-adjacent sections of the genome, creating a mosaic [23-25, 75].

This thesis focuses on IAV DIPs, particularly those variants characterized by deletions that may occur in one or several segments of the IAV-segmented genome. Recent advancements in NGS technologies based on Illumina sequencing have facilitated the identification of deletion junctions across all eight vRNA segments, revealing that deletions span from the 5’ to the 3’ ends within the same segment [74, 77]. This suggests that such deletions likely result from the error-prone activity of the RdRp [78]. Additionally, mutations in the polymerase unit could influence the frequency of DIPs towards the end of an infection cycle [79]. Two models have been proposed to explain the generation of DIPs. The first, known as the "looping-out" model, posits that the RNA template's distal ends within the same segment are brought together, forming a loop recognized by the polymerase, which then replicates the RNA without detaching from the nascent

vRNA template [25]. The second and more recent model focuses on the polymerase's pausing activity on the nascent strand. Structural studies of RNA have shown that the polymerase complex features a closed tunnel-like structure through which the RNA template is threaded and replicated. This finding challenges the feasibility of the loop structure in replication as per the new insights into polymerase complex architecture. It is now theorized that deletion junctions are formed when the polymerase momentarily halts replication along the RNA template and then resumes synthesis further downstream [63, 80, 81].

2.2.1.1. DI244

DI244 was one of the earliest characterized IAV DI vRNA by Dimmock et al., featuring a specific deletion junction in seg 1, which encodes the PB2 polymerase. This DI vRNA retains 244 base pairs (bp) at the 3' end and 151 bp at the 5' end [2], as illustrated in Figure 2.2.1. The deletion largely removes the coding region, preserving only the terminal ends required for packaging into progeny virions. DI244 was initially identified in PR8 virus samples and subsequently reconstituted using reverse genetics with a helper virus, followed by propagation in embryonated chicken eggs. Although the DI vRNA can infect host cells, it must be co-infected with an STV for propagation, compensating for the absent gene proteins with those from the full-length virus [6, 82]. In vitro and animal studies, including those conducted in mice and ferrets, demonstrated the DIP's therapeutic potential, offering protection against an otherwise fatal STV infection challenges [17, 34, 36, 37, 83].

2.2.1.2. OP7

Traditionally, IAV DIPs are known for their large internal deletions. Previously, the BPE group unveiled a new IAV DIP genotype characterized by hypermutations in seg 7 of the virus, observed during high MOI experiments with the PR8 strain in MDCK cells in single-cell analysis experiments [5]. This hypermutated seg 7 exhibited mutations in critical areas, including the promoter, coding regions (M1 and M2), and the packaging region, totalling 37 distinct point mutations (as shown in Figure 2.2.1, right). This segment displayed characteristics similar to

conventional DIPs, such as being defective in virus replication and its ability to interfere with STV replication in a co-infection scenario. Similar to conventional DIPs, OP7 depends on co-infection with STV for propagation. Hence, from the initial production systems for OP7 DIPs contained STV in the final virus harvests [38]. Consequently, prior to testing the DIPs in animal models, the viral preparations had to be subjected to UV inactivation to eliminate any infectious STV [38]. Despite the final DIP harvest demonstrating robust antiviral activity in in vitro co-infections, the presence of STV during the production process raised regulatory and safety concerns regarding the use of these viral preparations as antiviral agents. Additionally, UV treatment led to a slight reduction in the antiviral efficacy of OP7 DIPs compared to non-UV-treated preparations when evaluated in vitro [38]. This suggests that future efforts should focus on producing clonal OP7 DIPs that are free from infectious STV in the final viral harvest.

Further studies noted that the interaction between OP7 and STV during co-infection leads to reduced infectious virus titers, surpassing the interference levels induced by DI244 [5, 29, 38, 83]. The OP7 co-treatment results in elevated levels of seg7-OP7 compared to seg 5 or 8, indicating a growth advantage and preferential amplification of this defective segment [5, 38]. Based on mathematical modelling observations, it is suggested that the "superpromoter" on seg 7-OP7 vRNA enhances its replication, leading to a depletion of viral proteins. This reduction in viral proteins subsequently diminishes STV genomic RNA replication, which appears to exert an antiviral effect [84].

Moreover, in the study by Ruediger et al., mathematical modelling was used to investigate various aspects of functional mutations [84], specifically superpromoter mutations and the role of the M1-OP7 protein in rendering OP7 a defective phenotype leading to the interference mechanism. Kupke et al., previously hypothesized that a supposed defective M1-OP7 protein could contribute to the defective replication of the OP7 DIPs [5]. As these mutated M1-OP7 binds to the vRNPs in the nucleus, leading to nuclear retention of vRNPs and thereby halting the replication [5]. Nevertheless, currently, it remains unclear whether M1-OP7 exhibits weak or no binding to vRNPs [84]. Further experimental work would be

necessary to confirm these findings and to determine which specific mutations are involved in the interference mechanism against STV propagation.

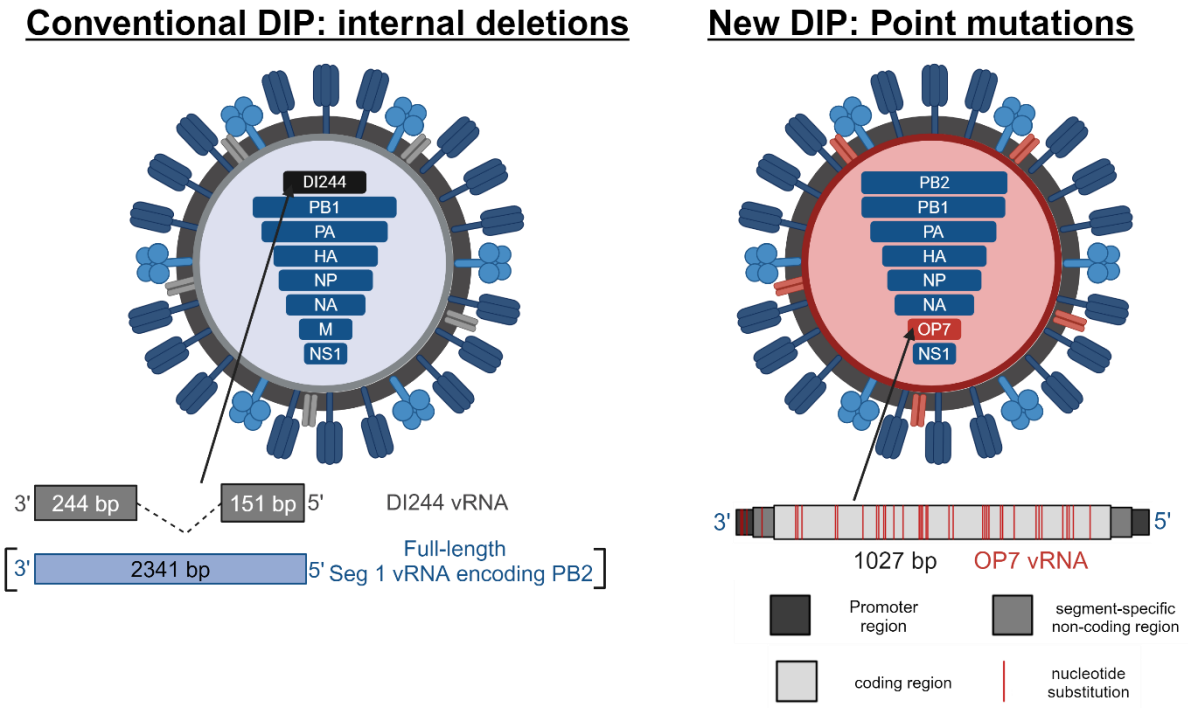

Figure 2.2.1. Types of IAV DIPs. Conventional DIPs contain at least one large deletion in one of the eight vRNA segments. For instance, DI244 is a conventional DIP that contains a large internal deletion in seg 1, which encodes the PB2 protein. The deleted DI vRNA includes a 3' end of 244 bp and a 5' end of 151 bp [2]. OP7 represents a new type of DIP, characterized by a hypermutated segment 7. In total, 37-point mutations are present, affecting functional regions such as the promoter, packaging, and protein-coding regions (M1 and M2). Figure adapted from Kupke et al., [5], and generated using Biorender.com

2.2.2. Interference by DIPs

DIPs of IAV, regardless of their genotype, whether internally deleted or possessing multiple nucleotide substitutions in the vRNA have been suggested to play a role in hindering the spread of STV. The initial hypothesis for this interference involved three main mechanisms such as 1) replication interference, 2) packaging disruption, and the 3) activation of innate immune responses [18, 28, 80, 85].

2.2.2.1. Replication interference

DIPs can compete for essential replication resources synthesized by the STV or host cells. Due to the shorter DI vRNA, it is hypothesized that DIPs replicate more

rapidly, thus outcompeting the full-length vRNA for essential replication resources [69]. In the case of conventional DIPs, it is assumed that the large internal deletion in the protein-coding regions renders the DIPs unable to generate a fully functional protein, thereby relying on the STV for replication resources [86].

Resources for viral replication include polymerase complexes, NP for encapsulating the DI genome, as well as structural proteins and glycoproteins necessary for the budding of virions containing DI vRNA. Due to the shorter DI vRNA potentially replicating preferentially by polymerases, they scavenge the resources from the full-length counterparts to replicate [28, 87].

The competitive advantage of DIPs is highlighted in studies involving the high-growth vaccine backbone strain PR8 at varying MOIs, which exhibit distinct infection dynamics. When MDCK cells are infected with the PR8 virus at a high MOI, both infectious and total virus titers are observed to be low [82, 88, 89]. This phenomenon is attributed to the presence of DIPs. After multiple replication rounds of the STV, DIPs arise and grow slowly over the cultivation period. These DIPs, based on the rapid replication of shorter DI vRNA segments compared to full-length vRNA segments, lead to competition for resources, thereby interfering with STV replication and significantly reducing their growth.

To achieve high infectious and total virus titers, vaccine viruses are cultivated at an optimal low MOI using a seed virus that is depleted of DIPs [90]. This approach minimizes the likelihood of co-infections with DIPs, thereby enhancing virus yield.

2.2.2.2. Interference in full-length vRNA packaging into progeny virions

One of the initial models for packaging mechanisms in IAV proposed a theory of random packaging. It was hypothesized that the increased production of non-infectious virus particles towards the end of infection suggested that vRNA segments were randomly packaged into progeny virions [91]. This assumption was based on the abundant presence of DI vRNA driving this phenomenon. According

to this theory, the interference by DI vRNA at the packaging stage, which resulted in reduced packaging of full-length vRNA, exerted antiviral activity [24, 68].

Subsequent investigations into the vRNA structure have elucidated that specific nucleotide sequences, comprising 26 nucleotides at the 3' end and 22 nucleotides at the 5' end of the vRNA, are crucial for the selective packaging of vRNA segments into progeny virions [69, 92]. This discovery suggests that the packaging process is more specific than random. In this refined model of selective packaging, it is postulated that vRNA segments are present in equimolar ratios [93]. Given that DI vRNA is highly replicated and thus more abundant than full-length counterparts within the cells, their incorporation into progeny virions is more probable. This model gained traction as it demonstrated that DI vRNA segments are more frequently incorporated into progeny virions than their full-length counterparts. The preferential incorporation of DI vRNA over full-length vRNA is attributed to their higher abundance [24, 68].

Recent advancements in Illumina-based sequencing analysis have challenged this preferential packaging model of DI vRNA. Although a significant intracellular presence of DI vRNA was confirmed, this was not reflected in the progeny virions released extracellularly [78]. Furthermore, Alnaji and colleagues observed that in co-infection experiments involving DIPs and STV, the presence of DIPs did not affect the packaging efficiency of WT vRNA in the extracellular virions [78]. However, additional evidence under varied experimental conditions is required to substantiate this theory. It is now posited that the type of deletion and its extent into the packaging signals could reduce packaging efficiency. RNA-RNA structure studies indicate that interactions between different vRNA species are necessary, and the absence of these critical signals may impair the packaging preference of DI vRNA during the packaging stage [94].

2.2.2.3. Stimulation of the innate immunity

The innate immune system is a primary barrier against viral infections, including IAV infections. The detection of most RNA viruses is initiated when its ssRNA, is recognized by pathogen recognition receptors (PRRs) such as retinoic acid-

inducible gene-I (RIG-I) in the host cell cytosol [95, 96]. This recognition triggers a signalling cascade, leading to the production of Type I interferons (IFNs) IFN-α/β, which play a crucial role in antiviral defense (Figure 2.2.2) [97]. The process begins with the identification of the virus by RIG-I receptors, which respond to the non-capped, 5’ phosphorylated vRNA in the cytoplasm. This interaction activates downstream signalling pathways involving interferon regulatory factors (IRF3 and IRF7) and nuclear factor-kB (NF-kB), culminating in the production of IFN-β by the host [7, 97]. The secreted IFN-β binds to IFNAR receptors (in autocrine or paracrine signalling), initiating the JAK/STAT pathway and subsequently inducing the expression of interferon-stimulated genes (ISGs). These ISGs encode antiviral proteins such as myxoma resistance proteins (MxA and MxB in human IAV), IFN-inducible transmembrane proteins (IFITMs), and protein kinase R (PKR) etc [51]. In mice, the production of Type I IFN leads to antiviral proteins like Mx1 (the equivalent of human MxA, found in the nucleus instead of cytosol) [98]. Additionally, other PRRs like TLR3 and TLR7 (Figure 2.2.2), located in endosomal compartments, are indicated to also recognize unidentified IAV RNA structures following the phagocytosis of IAV-infected cells [51, 99]. These receptors activate IFN signalling through adaptor proteins such as myeloid differentiation factor 88 (MyD88), activating IRF3/7 and NF-kB.

DIPs share structural similarities with STV and induce early and relatively strong IFN responses through similar PRR pathways [36]. It is largely accepted that RIG-I plays a crucial role in IFN-dependent antiviral activity, and IAV DIPs may preferentially bind to the PRR [23, 27, 96, 100-102]. However, it's crucial not to ignore other signalling pathways, such as the TLR 3/7 cascades, that also play a role in defense against IAV. These pathways might similarly activate in response to DIP infection, highlighting the need for additional research in this area. The rapid replication of DIPs, compared to full-length viral genomes, may enhance their efficacy in triggering a robust IFN response.

Furthermore, the induction of the innate immune responses by DIPs presents them as a natural adjuvant in vaccine preparations [99, 103, 104]. In this context, a specific involving DI244, a DIP, in conjunction with STV treatment in vivo, elicited an adaptive immune response against STV, in addition to the antiviral responses

[2]. This outcome was thought to result from the co-infection triggering the release of replication-deficient particles bearing STV surface proteins, subsequently recognized by the adaptive immune system. While, in a study conducted on ferrets, the use of an NA inhibitor compromised the antibody levels generated in response to STV, whereas DIP co-treatment did not diminish antibody responses to STV infection [36].

Recent progress in DIP research has enabled their clonal reconstitution and high-titer production in suspension cell cultures (see below and refer to section 2.5), allowing researchers to explore their potential as therapeutic or prophylactic agents against IAV infections. Notably, IAV DIP-induced Type I IFN expression offers broad antiviral protection, extending beyond IAV to viruses such as IBV, SARS-CoV-2, RSV, Zika, and Yellow Fever virus [17, 28-31]. While the immune responses elicited by DIPs are largely uncharacterized, ongoing studies suggest they may also modulate adaptive immune responses through Type I IFN-independent pathways [100]. For instance, in experiments with mice lacking both IFN Type I and III receptors to block IFN signalling after IAV or DIP co-infections, researchers observed reduced inflammation, enhanced multi-ciliated cell differentiation, and increased survival rates against lethal IAV infection. This indicates a role for replication interference and previously unidentified immune responses [105, 106].

Further research has elucidated that truncated proteins generated from IAV DIP polymerase segments exhibit inhibitory activity [107-109]. For example, a defective PB2 protein competes with the WT PB2 for binding with the PB1 protein in the polymerase complex, disrupting polymerase activity, as demonstrated in functional assays [110]. Additionally, a study identified a 10kDa peptide derived from a deleted PB2 segment that activates type-I IFN signalling in a RIG-I-dependent manner, further highlighting the immunostimulatory potential of DIP [107].

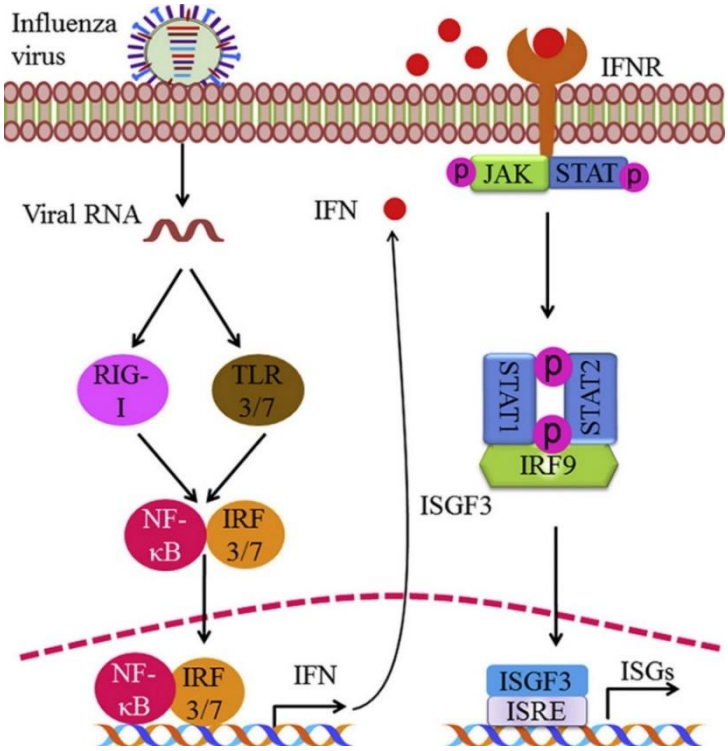

Figure 2.2.2. Innate immune response to IAV infection. Upon virus entry, vRNA is detected by intracellular pathogen recognition receptors (PRRs), like the retinoid acid-inducible gene-I (RIG-I) and toll-like receptors 3 and 7 (TLR3/7). This detection initiates a signalling cascade that culminates in the activation and expression of Type I interferon (Type I IFN). The infected cell then releases IFN, which can bind to their cognate receptors either on itself (autocrine) or on adjacent cells (paracrine signalling), thereby promoting the expression of interferon stimulated genes (ISGs) through the Janus kinase-signal transducer and activator of transcription (JAK-STAT) pathway. Figure is adapted from Goraya et al., [7].

2.3. Antivirals

To manage influenza infection like symptoms, healthcare providers may often prescribe antivirals that interfere with specific stages of the virus's life cycle, effectively stopping or slowing its proliferation in an infected host and facilitating recovery. Three primary categories of antiviral drugs have been identified for combating IAV infection: M2 inhibitors, polymerase inhibitors, and neuraminidase (NA) inhibitors, as illustrated in Figure 2.3.1 [10]. As detailed in section 2.1.2, upon infection, the virus enters the endosomal compartment of a cell. Here, the acidic environment triggers an influx of H+ ions through M2 protein ion channels, leading to the release of the viral genome. Drugs such as amantadine, the first antiviral against IAV approved by the FDA in 1966 [111, 112], and rimantadine, block these

ion channels, preventing the virus from replicating further [10, 113]. Compounds like baloxavir marboxil inhibit the virus's ability to hijack the host's mRNA for its protein synthesis, a process known as cap-snatching, by targeting the PA subunit of the viral polymerase complex [114]. This action significantly reduces the production of viral proteins and, consequently, the generation of new virus particles. Additionally, antivirals such as oseltamivir and zanamivir, both of which have received FDA approval, target the NA enzymes on the surface of the virus [112]. By blocking NA activity, these drugs prevent the newly formed virus particles from budding off the host cells, thereby halting the replication cycle.

Small molecule drugs have shown efficacy in treatment; however, their widespread use has led to the emergence of resistant strains [115-118]. Additionally, the therapeutic window for these drugs, given the presence of resistant strains, is limited to less than 24 h [119]. Furthermore, while these drugs remain in use, they are associated with adverse effects including diarrhoea, vomiting, nausea, and insomnia. Hence, there is a pressing need for alternative therapeutic approaches to augment the current standard of care for IAV treatment.

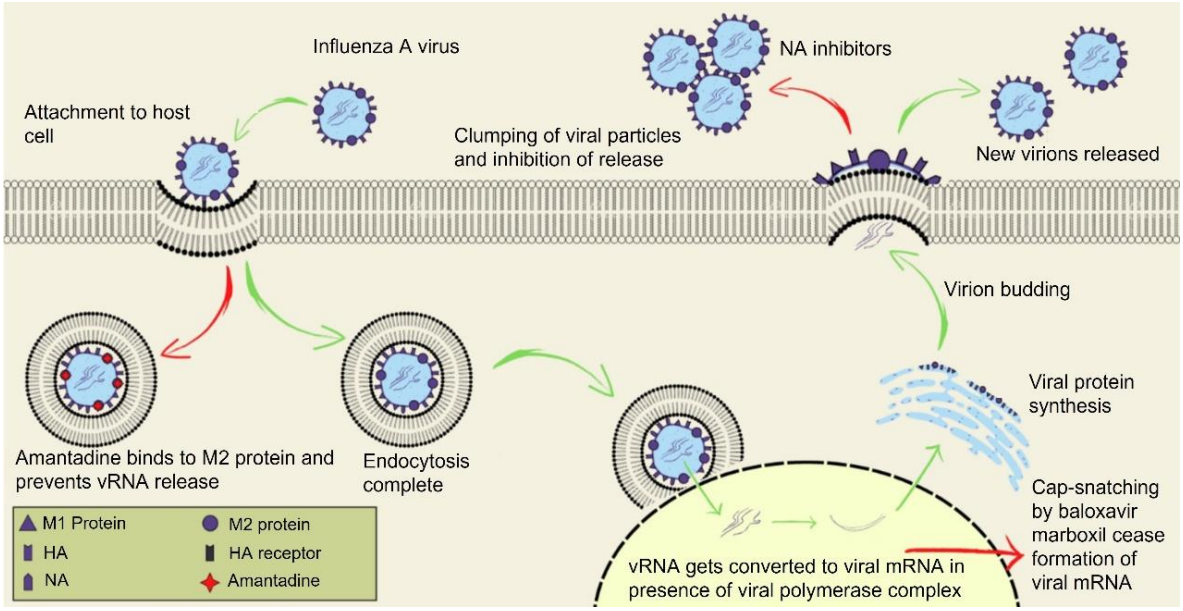

Figure 2.3.1. Antiviral targets in the IAV replication cycle. Antivirals can block IAV replication at three main stages: 1) Blocking of M2 ion channels to prevent uncoating and release of the virus genome, with drugs such as amantadine and rimantadine. 2) Inhibition of viral polymerase activity within the host cell nucleus, with drugs like baloxavir marboxil. 3) Prevention of progeny virion release by inhibiting NA receptor activity, with drugs including oseltamivir and zanamivir. The figure is adapted from Singh et al., [10].

2.4. Strategies for IAV vaccine production

2.4.1. Reassortment and egg-based vaccine production

Vaccination is the key strategy in preventing infections and establishing herd immunity. Since the first sanctioned production in the United States in 1945, embryonated chicken eggs have traditionally served as the medium for producing IAV vaccines [120]. These egg-based inactivated vaccines offered limited protection against the drifted IAV variants. The World Health Organization (WHO) later endorsed this method, which remains prevalent in nations worldwide. However, the six-month requirement to gather a significant quantity of embryonated eggs for a seasonal trivalent IAV vaccine production poses a challenge in responding swiftly to pandemics, thus constraining the ability to scale up vaccine availability [9]. Additionally, the risk of avian influenza jeopardizes the egg supply along with the presence of albumin, which can provoke allergic reactions in some individuals, diminishing vaccine effectiveness. In the 1960s, efforts to enhance vaccine strain production led to the adoption of the PR8 IAV strain, which, post-egg adaptation, proliferated more efficiently than other strains [121, 122]. This strain continues to serve as a master donor virus (MDV) for IAV vaccine production. The process for reassortment involves co-infecting an egg with the MDV PR8 and a seasonal virus, resulting in a vaccine virus strain with six internal genes from the MDV and the surface proteins (HA, NA) from the seasonal virus, forming a 6+2 genome constellation [9]. Next, a high-growth reassortant was selected using anti-PR8 serum to isolate virions expressing only seasonal antigens [123, 124]. Furthermore, RT-PCR analysis confirmed that the glycoproteins of these virions contained all the mutations responsible for antigenic drift [123]. Furthermore, egg-based technology facilitated the creation of live attenuated influenza vaccines (LAIVs). By attenuating the MDV through serial passages in eggs at lower temperatures, mutations are introduced that restrict the virus's growth at higher temperatures, confining replication in the nasal turbinate [125]. This method, which induces mucosal immunity, is administered intranasally via aerosol sprays. Russia in the 1980s and subsequently the United States, utilized different MDV strains (A/Leningrad/134/17/57 and A/Ann Arbor/6/60, respectively), and became pioneers in licensing LAIVs [125, 126]. This approach has since been

adopted in other European countries, where it has been a licensed product since 2013 and sold as a quadrivalent LAIV (Fluenz Tetra by AstraZeneca, containing H1N1, H3N2, and two strains of IBV) [127].

2.4.2. Reverse genetics and cell-culture-based vaccine production

The constraints of egg-based IAV vaccine production technologies led to progression into cell-culture-based systems for IAV. Since the 1990s, the FDA has approved the use of Vero and MDCK cell lines for the production of IAV vaccine viruses [128].

This advancement was complemented by the introduction of reverse genetics, a technique that enables the artificial construction of viruses by transfecting plasmids into host cells, facilitating the generation of viral progeny [8, 129]. This approach was initially applied to polioviruses to produce infectious particles, but for IAV, the encapsulation of vRNA with NP molecules was required [130]. Early work by Honda et al., demonstrated the separation of NP from the vRNA-polymerase complex, highlighting the essential role of NP in complete RNA transcript generation, as the polymerase complex alone could initiate but not elongate transcription without NP [131]. Further developments included a rather rudimentary reverse genetics system for reconstituting IAV with genetically modified genomes. Luytjes et al., introduced a novel approach by incorporating a plasmid with a reporter gene within the UTRs of seg 8, facilitating polymerase recognition of modified RNA [92]. These modified RNA transcripts were then incorporated into virus progenies using infections with helper viruses in eukaryotic cells (which were transfected with modified RNA transcripts). The field evolved further with Neumann et al., with the introduction of an RNA polymerase I (RNA pol I) promoter for vRNA transcription from cloned cDNA, alongside expression plasmids for polymerase subunits and NP proteins under an RNA polymerase II promoter, reducing the dependency on helper viruses by employing a total of 12 plasmids for transfection [132-134].

In the 2000s, Hoffmann et al., significantly advanced reverse genetics by creating the pHW2000 plasmid backbone, which generated both vRNA and mRNA from a

single cloned cDNA segment using RNA polymerase I and II promoters and terminators (Figure 2.4.1) [8]. This system utilized a human RNA polymerase I promoter and a mouse polymerase I terminator to produce vRNA in an antisense orientation, with protein production driven by cytomegalovirus (CMV) RNA polymerase II promoter and bovine growth hormone polyadenylation signals [8]. This innovation reduced the number of required plasmids for transfection and eliminated the need for helper viruses. Furthermore, Hoffmann et al., employed a co-culture of HEK-293T and MDCK cells, leveraging the high transfection efficiency of HEK cells to ensure reliable co-transfection, replication, and packaging of virions [8]. These virions could then infect and proliferate in MDCK cells to high titers. Therefore, establishing a plasmid-based transfection system that requires only eight plasmids, each containing a copy of viral cDNA, for generating IAV from cloned cDNA, marking a significant advancement in IAV vaccine production [8].

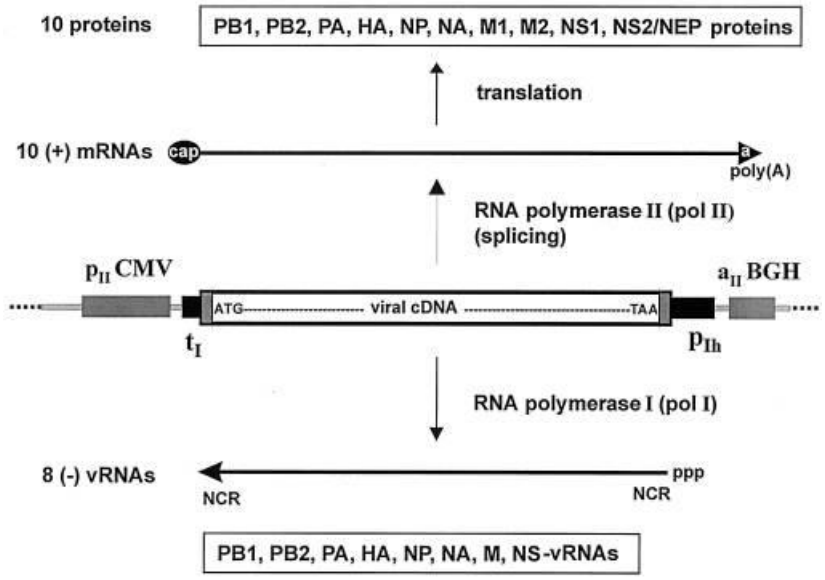

Figure 2.4.1. Scheme of vRNA and viral protein production from the pHW2000 plasmid based on the RNA pol I and II transcription systems. The viral cDNA for each segment is flanked by a human pol I promoter (pIh) and terminator (tI) to generate vRNA in the antisense orientation. The pol II system surrounds the pol I system and consists of a pol II promoter from human cytomegalovirus (pIICMV) and polyadenylation signals (bovine growth hormone, aIIBGH) for mRNA generation, thereby facilitating protein translation. Consequently, cellular transcription can yield two types of viral RNA species from a single cDNA cloned in such a system (plasmid backbone termed pHW2000). The figure is adapted from Hoffmann et al., [8].

2.5. Reverse genetics for DIP production

DIPs have been suggested as an alternative therapy to treat influenza infection [17-24, 34]. The potential for resistance development against DIPs is considered to be very low as it would require mutations in the viral polymerase gene that prevent it from recognising or replicating the DI genome [17, 135]. Additionally, it is possible that with advancements in cell culture technologies, employing DIPs as intranasal antivirals could be more cost-effective than treatments with small molecules like interferons [3, 6, 18, 38, 83].

DI244 is one of the initial examples of cloned DI vRNA that was generated through reverse genetics. This process involved the transfection of HEK cells with a total of 13 plasmids: eight for the viral genome, a ninth carrying the DI vRNA DI244 (under an RNA pol I promoter), and four expression plasmids for the polymerase subunits and NP (under an RNA polymerase II promoter) [2]. Following transfection at 24 h, MDCK cells were added to the culture, and the supernatant was collected on the seventh day. The harvested virus (enriched with the DI244 along with STV) was then amplified in embryonated chicken eggs to establish a seed virus bank, which underwent evaluation for antiviral efficacy and protective capability in both in vitro and animal models [17]. However, this method faced significant challenges, notably the presence of contaminating STV in the DIP preparations, necessitating UV treatment to inactivate infectious viruses [136]. Unfortunately, this UV treatment would also damage the DI vRNA, diminishing its antiviral properties [38]. Additionally, the reliance on eggs for virus propagation introduced further limitations associated with egg-based antiviral and vaccine production.

To address these issues, Bdeir et al., refined the plasmid-based system for influenza reconstitution, eliminating the need for eggs [6, 136]. They utilized a retroviral transduction technique with a self-inactivating vector to genetically modify HEK-WT and MDCK-WT cell lines for the constitutive expression of the PB2 protein, an essential component of the influenza virus polymerase complex (missing in seg 1 DIP, DI244, Figure 2.5.1). This method ensured that only cells that had successfully incorporated the antibiotic resistance marker and were expressing PB2 could survive and proliferate under antibiotic selection. Following validation of the cell line, the researchers initiated co-cultures of HEK-293T-PB2

and MDCK-PB2 cells and introduced eight plasmids encoding for the seg 1 DIP genome and the other seven complete viral RNA segments, using the pHW2000 plasmid system. This process led to the generation of clonally pure DI244 DIP particles [6]. Subsequent experiments showed that these DI244 particles could be cultivated in suspension cultures of MDCK-PB2 cells (that were similarly modified as adherent MDCK-PB2 cells), yielding high titers of DIPs that effectively inhibited the replication of STV in vitro and in vivo (Figure 2.5.1) [37, 83]. A similar approach to using PB2-expressing MDCK cell lines to propagate DI244 was also adopted by Yamagata and colleagues [137].

This PhD thesis is founded on the above-described plasmid-based reverse genetics system [6], which provides a robust platform for generating and evaluating new DIP-based antiviral and vaccine constructs. Utilizing this system, new antiviral constructs based on seg 1 DIPs identified through NGS were developed. The antiviral efficacy of these DIPs was validated by reconstituting them without infectious STV and conducting in vitro co-infection analyses.

Furthermore, the reverse genetics system was enhanced to reconstitute infectious STV-free OP7 chimera constructs based on new and potent seg 1 DIPs. Additionally, efforts were directed towards creating DIP-based vaccine constructs aimed at generating seg 1 DIPs capable of eliciting adaptive immune responses against seasonal IAV strains.

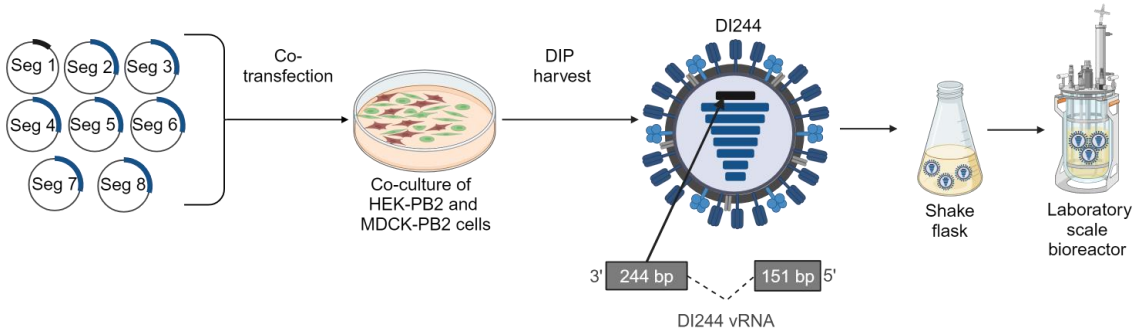

Figure 2.5.1. Overview of the production system for seg 1 DIPs. This diagram depicts the production process of a seg 1 DIP, DI244, utilizing a system devoid of infectious STV. It involves the co-transfection of eight plasmids from the pHW2000 series, including a plasmid encoding DI vRNA (with a deletion in PB2 encoding ORF), along with seven full-length vRNAs into a co-culture of mammalian cells that have been genetically engineered to express the PB2 protein. Specifically, HEK-293-T and MDCK cells are modified to stably produce PB2 proteins, labelled as HEK-PB2 (enhanced transfection efficiency) and MDCK-PB2 (increased virus yield), respectively. The process enables the harvest of clonal DIPs. The production can be scaled up through suspension cell cultivation in shake flasks. This production system is then transferred to a laboratory-scale bioreactor. The figure was created with Biorender.com.

3. Material and Methods

This section details the materials and methodologies employed in the research conducted for this doctoral thesis. The consumables, reagents, and equipment utilized are catalogued in sections 9–10. This chapter comprehensively outlines the cell lines utilized, their maintenance protocols, the methodologies for conducting infection experiments, the application of reverse genetics in developing antiviral and vaccine constructs, and finally, the techniques for virus quantification, including PCR assays. Please note parts of the Material and Methods have been taken from manuscripts [1, 3, 4]. Please note, that we refer to our standard operation procedures (SOPs) in this thesis whenever required. These SOPs can be requested from the Bioprocess Engineering group of the Max Planck Institute for Dynamics of Complex Technical Systems (Magdeburg, Germany), headed by Prof. Dr.-Ing. Udo Reichl.

3.1. Cells and viruses

MDCK cell culture

Adherent MDCK wild-type cells (MDCK-WT) from a European Collection of Authenticated Cell Cultures (ECACC, #84121903) were utilized for reverse genetics (sections 4.1.4–4.3.4), infection experiments (section 4.1.6), virus quantification (sections 4.1.4–4.3.7), and innocuity tests (sections 4.1.4, and 4.3.4–5). Cells were thawed according to SOP Z/02 and cultured following SOP Z/04 in Glasgow Minimum Essential Medium (GMEM, Thermo Fisher Scientific, #221000093) supplemented with 1% peptone (Thermo Fisher Scientific, #211709) and 10% fetal bovine serum (FBS, Merck, #F7524), referred to as “growth medium” (see SOP M/02 and M/03 for media preparation). The cells were maintained at 37°C in a 5% CO_2 atmosphere in 175 cm² tissue culture flasks (Greiner Bio-One). Working cell banks were prepared and cryopreserved in accordance to SOP Z/06. Weekly subculturing was performed as per SOP Z/04. In brief, cells were washed with PBS (prepared as per SOP M/01) and trypsinized with 6 mL of 1X trypsin (Gibco, 9002-0-7, prepared as per SOP M/07) at 37°C and 5% CO_2 for approximately 20 min. After incubation, 6 mL of growth medium was added to stop

the trypsinization process, and cells were detached by pipetting. Cell viability and count were assessed using a Vi-Cell™ XR cell counter (Beckman Coulter). Approximately 7.0 × 10^6 cells per flask were seeded into new flasks containing 50 mL of growth medium.

For rescue and propagation of seg 1 DIPs lacking the functional PB2 protein, MDCK-PB2 cells were used. These MDCK cells were retrovirally modified to express the IAV PB2 protein, as reported by Bdeir et al., [6], and were provided by collaborative partners from the German Primate Centre (DPZ), Göttingen. Weekly maintenance of this cell line was conducted similarly to MDCK-WT cells, using the same growth medium which was additionally supplemented with 1.5 µg/mL of puromycin (Thermo Fisher Scientific, #A1113803) as a selection marker for stable IAV PB2 protein expression. For seg 2 and 3 DIPs, which lack PB1 and PA proteins respectively, MDCK-PB1 and MDCK-PA cell lines were also provided by DPZ, Göttingen. These cell lines were cultured in growth medium supplemented with 5 µg/mL blasticidin (Sigma-Aldrich, 15205-25MG) and 500 µg/mL G418 (Roth, 0239.4), respectively. For cell lines expressing all three proteins (triple-positive MDCK-PB2-PB1-PA cells, also provided by DPZ, Göttingen [138]), the medium was supplemented with a combination of antibiotics: 1.5 µg/mL puromycin, 400 µg/mL hygromycin B (Thermo Fisher Scientific, #10687010), and 1 mg/mL G418.

HEK cell culture

Human embryonic kidney 293T cells (HEK-293T), referred to as HEK-WT in this thesis, were obtained from the American Type Culture Collection (ATCC, #CRL-3216) for reverse genetics experiments aimed at generating STV or OP7 clonal DIPs. Genetically modified HEK-293T cells (generated via retroviral modifications, akin to preparation of MDCK-complementing cells as described above) expressing individual IAV polymerase subunits PB2 [6], PB1, or PA [138], were designated as HEK-PB2, HEK-PB1, or HEK-PA, respectively. These modified cell lines were sourced from the DPZ, Göttingen [6, 138].

HEK-WT cells were cultured in Dulbecco's Modified Eagle Medium (DMEM, Gibco, #41966-052) supplemented with 10% fetal bovine serum (FBS), and 1%

penicillin/streptomycin (P/S, containing 10,000 units/mL penicillin and 10,000 µg/mL streptomycin, Thermo Fisher Scientific, #15140122), referred to as “DMEM growth medium”. The cells were incubated at 37°C in a 5% CO_2 atmosphere. SOPs Z/02, Z/06, and Z/04 were followed for thawing cell cultures, preparing working cell banks, cryopreserving, and subculturing, respectively, with minor deviations as described below.

Cells were passaged twice a week. The monolayer was rinsed with PBS, and cells were detached using 2 mL of 1x trypsin for 5 min at 37°C and 5% CO_2. Trypsinization was halted by adding 8 mL of DMEM growth medium. The cells were then resuspended to achieve a single-cell suspension. Cell viability and count were assessed using a Vi-Cell™ XR cell counter. Subsequently, 2×10^6 cells were seeded per T-75 flask in DMEM growth medium. For the genetically engineered HEK cells expressing single IAV polymerase proteins (HEK-PB2, HEK-PB1, or HEK-PA), the culture medium was supplemented with 1 µg/mL puromycin, 5 µg/mL blasticidin, or 1 µg/mL puromycin, respectively.

Calu-3 cell culture

Human alveolar epithelial cells, Calu-3, were obtained from Dunja Bruder’s lab (Helmholtz Centre for Infection Research, Braunschweig). The cells were cultured every week, with a total culture age not exceeding 20 passages. SOPs Z/02, Z/06, and Z/04 were followed for thawing cell cultures, preparing working cell banks, cryopreserving, and subculturing, respectively, with slight deviations.

Sub-culturing involved rinsing the cells with PBS, followed by trypsinization using 10 mL of 1x trypsin, and incubation at 37°C with 5% CO_2 for up to 20 min. The trypsinization process was stopped by adding 10 mL “Calu-3 growth medium”, which comprised Minimum Essential Medium (MEM, Thermo Fisher Scientific, #41090093) supplemented with 10% FBS, 1% P/S, and 1% sodium pyruvate (Thermo Fisher Scientific, #11360070). Cell viability and count were assessed using a Vi-Cell™ XR cell counter. For each T-175 flask, 5×10^6 cells were inoculated in the specified Calu-3 growth medium.

Please note, that all the cell lines used in this PhD thesis were sub-cultured up to a maximum of 20 passages.

Viruses

For infection experiments, STV based on influenza A/PR/8/34 (H1N1) seed virus, provided by the Robert Koch Institute (Berlin). This was amplified by previous group members and working seed virus was used at a titer of $1{,}10x10^9$ virions/mL. This strain is herein referred to as PR8. The DIP, DI244 (titer 2.5 Log_{10} (HAU/100 µL)) was produced by reverse genetics as outlined by Bdeir et al., [6] at DPZ, Göttingen, and its amplification in suspension cells [37]. This viral preparation served as the reference control in the interference assays.

3.2. Plasmids

For the reconstitution of the STV PR8 strain, eight plasmids based on the pHW2000 backbone, encoding the WT full-length segments (seg 1–8) as detailed by Hoffmann et al., [139] were provided by the DPZ, Göttingen, and designated as pHW191-198. To monitor transfection efficiency during the rescue experiments, a plasmid expressing GFP within the pMax backbone (gifted by DPZ, Göttingen) was used.

To generate OP7 chimera DIPs [3], a novel plasmid based on the pHW2000 backbone, containing the sequence for seg 7-OP7 (GenBank accession number: MH085234) was developed and referred to as phW-seg7-OP7. The sequence of seg 7-OP7 was first synthesized by GeneArt and delivered in the pMX vector backbone (construct ID 19ADX3QP). This vector was used as a template for further subcloning via Golden Gate cloning into the pHW2000GGAarI backbone (see details on Golden Gate cloning in section 3.3) by DPZ, Göttingen, and provided to us.

For the reconstruction of the A/California/04/2009 (Cal H1N1) strain, plasmids utilizing the pHW2000 backbone were obtained from the Institute of Bioorganic Chemistry, Polish Academy of Sciences, Poznan.

Please note, all the plasmids used in this PhD thesis were transformed into NEB10β competent *E. coli* cells (New England Biolabs, #C3019H) using the heat shock method followed by glycerol stock preparations as described in section 3.3

3.3. Cloning methods

To reconstruct newly identified DIPs based on seg 1, 2, and 3 of the IAV polymerase, it was necessary to engineer all the deletion junctions as illustrated in Figure 4.2A and detailed in Table 3.3-1 (refers to position and size of deletion). This was achieved through splice overlap extension polymerase chain reaction (SOE-PCR), a method that facilitated the creation of the required insert harbouring an internally deleted IAV gene segment (Figures 3.3.1A and 4.1.2A, B) [6]. Subsequently, this insert was incorporated into a pHW2000GGAarI vector backbone employing the Golden Gate cloning technique (Figures 3.3.1B and 4.1.2B), which enables simultaneous digestion and ligation processes [6]. An exemplification of this methodology to produce a plasmid harbouring a deleted seg 1 for seg 1 winner DIP reconstitution is provided in Figure 3.3.1 and for the procedure described below.

Table 3.3-1 Deletion junctions for new DIP candidates

DIP Candidate	Nucleotide number spanning deletion junction (5'-3')	FL size	DI vRNA size
Seg 1 Loser	129_2176	2341 bp	295 bp
Seg 1 Winner	217_2204	2341 bp	355 bp
Seg 1 De novo	269_2202	2341 bp	409 bp
Seg 2 Loser	137_2129	2341 bp	350 bp
Seg 2 Winner	139_2056	2341 bp	425 bp
Seg 2 De novo	218_2091	2341 bp	469 bp
Seg 3 Loser	361_1692	2233 bp	903 bp
Seg 3 Winner	137_1916	2233 bp	455 bp
Seg 3 De novo	124_1940	2233 bp	418 bp

Splice overlap extension PCR

The SOE-PCR process is divided into two stages. For seg 1 DIP construction to generate a pHW2000 plasmid harbouring seg 1 winner sequence, the pHW 191 plasmid served as the template. First step, specific primer sets (Thermo Fisher Scientific, see Table 3.3-2) were employed: "Seg 1 winner 5' forward (for)" primer

and “Seg 1 winner 5’ reverse (rev)” primers to amplify a 5’ fragment spanning nucleotides 1 to 217 (nucleotides spanning the deletion junction, Figure 3.3.1A and Tables 3.3-1, 3.3-2) by PCR. Simultaneously, “Seg 1 winner 3’ for” and “Seg 1 winner 3’ rev” primers to amplify a 3’ fragment covering nucleotides 2204 to 2341 (Figure 3.3.1A and Tables 3.3-1, 3.3-2) by PCR. The primer design incorporated AarI restriction sites (refer to Golden Gate cloning below for details) to streamline subsequent Golden Gate cloning steps and overlapping sequences to enable “stitching of the fragments” (Figure 3.3.1B, refer to primer design Table 3.3-2).

The PCR reaction mixture, with a total volume of 20 µL, comprised 8.8 µL of nuclease-free water, 4 µL of 5X High Fidelity buffer (Thermo Fisher Scientific, #F530L), 2 µL of magnesium chloride ($MgCl_2$, 10 mM, Thermo Fisher Scientific, #F530L), 1 µL of each primer set (10 µM, Table 3.3-2) and dNTPs (10 mM, Thermo Fisher Scientific, #R0182), 2 µL of plasmid template (10 ng), and 0.2 µL of Phusion high-fidelity polymerase (Thermo Fisher Scientific, #F530L). The PCR conditions are detailed in Table 3.3-3, with specific annealing temperatures for the splice PCR listed in Table 3.3-2. The PCR products underwent electrophoresis on a 2.5% agarose gel. As per the manufacturer's instruction, gel electrophoresed PCR products were subsequently purified via the Qiagen (QIAquick gel extraction kit, #28704) purification method (representative gel images depicted in Figure 4.1.2B).

In the second step, overlap PCR was performed from the newly generated spliced fragments Figure 3.3.1. This involved the same PCR reaction mixture components as described above, with both fragments added in a 1:1 ratio (based on length, using NEBioCalculator online tool) and subjected to cycling under conditions outlined in Table 3.3-3. Except, with a reduced cycle count of 15 for steps 2–4 and annealing temperatures as specified for overlap PCR in Table 3.3-2. In this step, denaturation of the dsDNA PCR products containing complementary base pairs occurs, followed by annealing of overlapping bases and subsequent extension. Therefore, primers were not added in this step. The resultant product, termed “SOE product” (Figure 3.3.1A), underwent an additional extension PCR. This step involved adding 1 µL of the primer sets “Seg 1 winner 5’ for” and “Seg 1 winner 3’ rev” (Table 3.3-2), and conducting PCR cycling under the conditions specified in Table 3.3-3, with an annealing temperature of 62°C applicable to all segments (1,

2, and 3). PCR products were subjected to a 2.5% agarose gel electrophoresis and purified using the QIAquick purification method.

Golden Gate cloning

The insertion of the SOE product into a vector was facilitated through Golden Gate cloning [140, 141], based on the complementary overhangs present in both the insert and vector following digestion with the Type IIs restriction enzyme, AarI. This enzyme is characterized by its unique property of recognizing a specific sequence while cleaving at distinct sites, thereby enabling a precise and orientation-specific ligation of the insert into the vector, as illustrated in Figure 3.3.1B. The cloning process was executed in a single reaction mixture, comprising a 10 µL volume that included 1 µL of 10x T4 DNA ligase buffer (New England Biolabs, #B0202S), Bovine Serum Albumin (BSA, Thermo Fisher Scientific, #B14) at a concentration of 1 mg/mL, 1 µL of the SOE PCR product, the vector pHW2000GGAarI at 10 ng (1 µL), 0.5 µL of T4 DNA ligase (New England Biolabs, #M0202S), 0.5 µL of AarI restriction enzyme (Thermo Fisher Scientific, #ER1581), and 0.2 µL of 50X oligonucleotides (0.025mM, Thermo Fisher Scientific, #ER1581). The conditions for the reaction cycles are detailed in Table 3.3-4. Subsequently, 5 µL of the reaction mixture was transformed into NEB10β competent *E. coli* cells using the heat shock method. The preparation of LB agar plates was performed as previously described by Seitz et al., [142]. Post-transformation, 10 µL of the bacterial culture was plated on LB agar plates containing ampicillin (Roth, #69-52-3) and incubated for 24 h at 37°C to select for ampicillin-resistant colonies. As the vector pHW2000GGAarI harbours an ampicillin resistance marker, only the bacterial cells that have been successfully transformed will grow on the LB agar plates supplemented with ampicillin.

Colony PCR was employed to verify the presence of DIP sequence-encoding plasmids within bacterial colonies. Bacterial colonies were selected from LB agar plates using toothpicks, which were also used for replica plating. Each colony was suspended in 20 µL of PBS and boiled at 95°C for 10 min to lyse the cells. PCR amplification was performed under conditions similar to those used for SOE PCR (using primer set Seg 1 winner 5’ for and Seg 1 winner 3’ rev), with specific cycling

parameters outlined in Table 3.3-3. Five colonies were analysed using this method, and the resultant PCR products were evaluated by 1% agarose gel electrophoresis, with representative gel images presented in Figure 4.1.2B.

Replica LB-agar plates supplemented with ampicillin were used to grow selected colonies. A toothpick touched to a specific colony (marked for colony PCR as above) was gently pressed against a marked spot on the agar plate, which was then incubated at 37°C for 16–24 h. Specific colonies identified by Colony PCR that contained the vector with the gene of interest were selected from the replica agar plate and grown in 5 mL LB broth medium containing ampicillin for 16 h at 37°C with shaking at 180 rpm. To generate glycerol stocks, 500 µL of the bacterial suspension was mixed with 500 µL of 50% autoclaved glycerol (Roth, #4043.3) and immediately stored at -80°C for future use in mini or midi preparations. Mini (QIAgen, #12125) and midi (QIAgen, #12143) preparations were performed according to the manufacturer's instructions.

Table 3.3-2 Primers for splice overlap extension PCR to generate seg 1, 2 and 3 DIPs

	Primer name	Sequence (5'-3")	Tm for splice PCR (°C)	Tm for overlapping PCR (°C)
1	Seg 1 Loser 5' for	CCCACCTGCCAGTGGGAGCGAAAGCAG	62	
2	Seg 1 Loser 5' rev	GCCTTCTCTCCTTTCGCGTACTTCTTGATTATGGCCA		67
3	Seg 1 Loser 3' for	TGGCCATAATCAAGAAGTACGCGAAAGGAGAGAAGGC	60	
4	Seg 1 Loser 3' rev	CCCACCTGCGCGCTATTAGTAGAAACAAGGTCGTTTTTAAACTA		
5	Seg 1 Winner 5' for	CGGTCACCTGCCAGTGGGAGCGAAAGCA	49	
6	Seg 1 Winner 5' rev	ACGTCTCCTTGCCCAATTATCCTCTTGTCTGCTGTA		66
7	Seg 1 Winner 3' for	TACAGCAGACAAGAGGATAATTGGGCAAGGAGACGT	60	
8	Seg 1 Winner 3' rev	CCCACCTGCGCGCTATTAGTAGAAACAAGGTCGTTTTTAAACTATT		
9	Seg 1 De novo 5' for	CAGTCACCTGCCGATGGGAGCGAAAGCAGGT	62	
10	Seg 1 De novo 5' rev	CCACGTCTCCTTGCCCAATTATTTTACTCCATAAAGTTTGTCCTTGC		66
11	Seg 1 De novo 3' for	GCAAGGACAAACTTTATGGAGTAAAATAATTGGGCAAGGAGACGTGG	64	
12	Seg 1 De novo 3' rev	CCCACCTGCTTTTTATTAGTAGAAACAAGGTCGTTTTTAAACTATTC		

13	Seg 2 Loser 5' for	CGTACACCTGCTTTTGGGAGCGAAAGCAGG	60	
14	Seg 2 Loser 5' rev	TGGTCTTCTGTATGAACTGCTATCCTGTTCCTGTCCCATG		67
15	Seg 2 Loser 3' for	CATGGGACAGGAACAGGATAGCAGTTCATACAGAAGACCA	58	
16	Seg 2 Loser 3' rev	CGCGCACCTGCCCGGTATTAGTAGAAACAAGGCATTTT		
17	Seg 2 Winner 5' for	GCACACCTGCTTTTGGGAGCGAAAGCAG	56	
18	Seg 2 Winner 5' rev	TCAAGTACTCCTCTTTGACTTGTATCCTGTTCCTGTCCCA		67
19	Seg 2 Winner 3' for	TGGGACAGGAACAGGATACAAGTCAAAGAGGAGTACTTGA	58	
20	Seg 2 Winner 3' rev	CCCACCTGCCCCCTATTAGTAGAAACAAGGCATTTTTTC		
21	Seg 2 De novo 5' for	CCGCACCTGCTTAAGGGAGCGAAAGCAG	56	
22	Seg 2 De novo 5' rev	AATTGCAGCACCTTTGGTGCGGTGCTCCAGTT		67
23	Seg 2 De novo 3' for	AACTGGAGCACCGCACCAAAGGTGCTGCAATT	58	
24	Seg 2 De novo 3' rev	GCGCCACCTGCCCCCTATTAGTAGAAACAAGGCATTTTTTC		
25	Seg 3 Loser 5' for	GCCACCTGCTATAGGGAGCGAAAGCAG	54	
26	Seg 3 Loser 5' rev	TGGGCCTTGAAACCTGTAATCATACAAATCTGGTA		63
27	Seg 3 Loser 3' for	TACCAGATTTGTATGATTACAGGTTTCAAGGCCCA	52	

28	Seg 3 Loser 3' rev	CCCACCTGCCCGGTATTAGTAGAAACAAGGTACTTTT		
29	Seg 3 Winner 5' for	CGCACCTGCTATTGGGAGCGAAAGCAGGT	56	
30	Seg 3 Winner 5' rev	AGACCTTCCCAATGGAACATTGCTGCAAATTTGTTTGTTTCG		63
31	Seg 3 Winner 3' for	CGAAACAAACAAATTTGCAGCAATGTTCCATTGGGAAGGTCT	53	
32	Seg 3 Winner 3' rev	CCCACCTGCCGCGTATTAGTAGAAACAAGGTACTTTTTTGG		
33	Seg 3 De novo 5' for	CGCACCTGCTCTCGGGAGCGAAAGCAG	51	
34	Seg 3 De novo 5' rev	ATACCGACTTTGCTAATAAAGTGTTTGTTTCGATTTTCAGGT		63
35	Seg 3 De novo 3' for	ACCTGAAAATCGAAACAAACACTTTATTAGCAAAGTCGGTAT	51	
36	Seg 3 De novo 3' rev	CGCACCTGCCCGGTATTAGTAGAAACAAGGTACTTTT		

* Please note, primers were designed to incorporate multiple specific features for seamless splicing overlap PCR followed by Golden Gate cloning.

1. **For 5’ forward and 3’ reverse primers:**
    - **Nucleotide clamp:** 2–4 nucleotides to enhance primer-template binding.
    - **AarI recognition sites:** For precise cloning.
    - **Segment-specific sequence:** Ensures binding to the target DNA.

- **Structure of the primer:** 5’- Nucleotide clamp: AarI recognition sites: segment-specific sequence -3’

In the table, these are depicted as: 5’ primer clamp AarI recognition site segment-specific sequence 3’ (highlighted by underlines and color).

2. **For 5’ reverse and 3’ forward primers (used for overlapping PCR):**

    - **Overhang sequences:** Facilitates joining of the DNA fragments.

    - **Segment-specific sequence:** Ensures binding to the target DNA.

Structure of the primer: 5’- Overhang sequence: segment-specific sequences -3’

In the table, these are depicted as: 5’ overhang segment-specific sequence 3’ (highlighted by underlines).

Table 3.3-3 Cycling conditions for splice overlap PCR

	Step	Temperature (°C)	Time	
1	Initial denaturation	98	3 min	
2	Denaturation	98	25 sec	25 cycles
3	Annealing	X (refer to table 3.3-2)	45 sec	
4	Extension	72	1 min	
5	Final extension	72	10 min	
6	Pause	4	∞	

Table 3.3-4 Cycling conditions for Golden Gate cloning

	Step	Temperature (°C)	Time (min)	
1	Digestion	37	5	50 cycles
2	Ligation	16	5	
3	Incubation	37	5	
4	Enzyme deactivation	80	5	

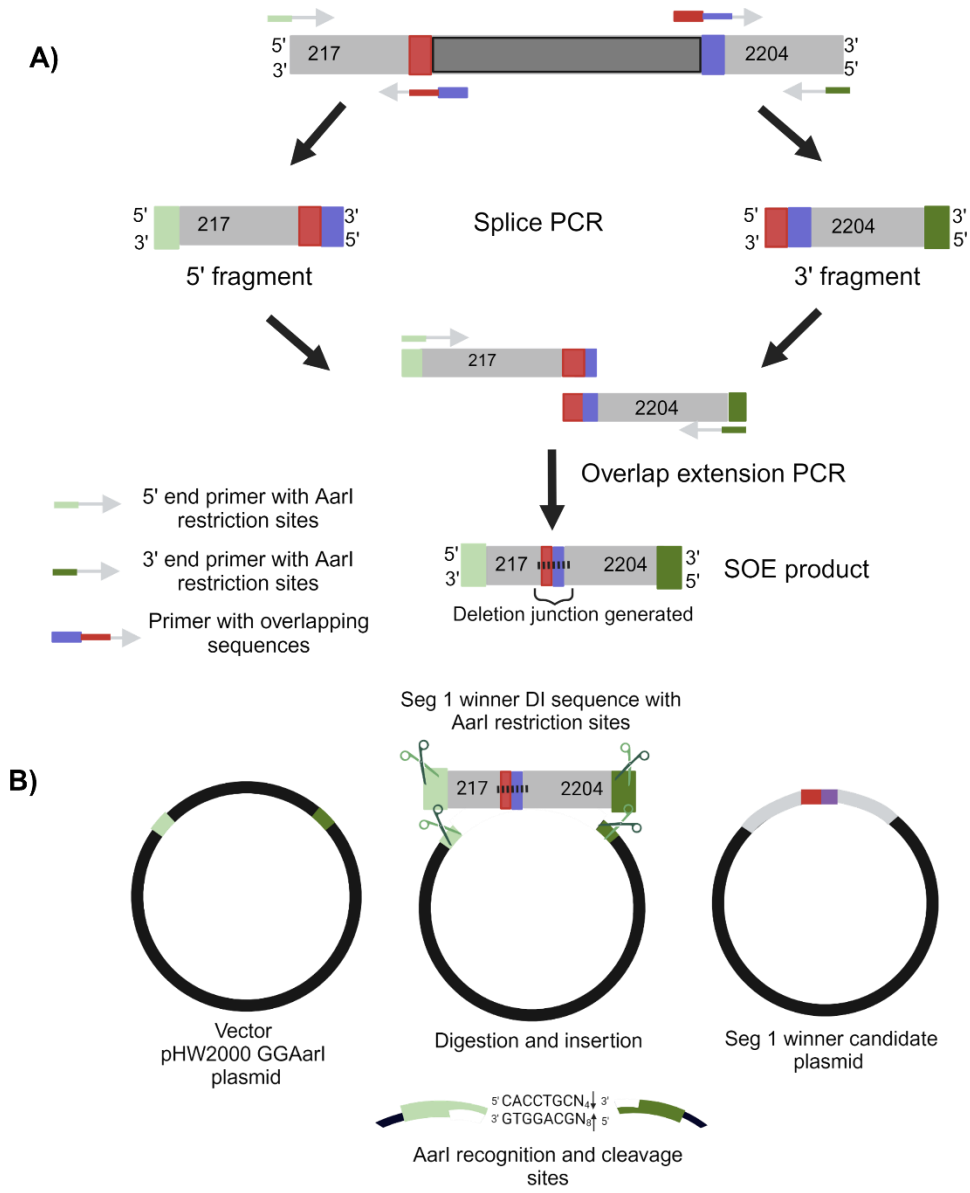

Figure 3.3.1. Overview on A) splice overlap PCR and B) Golden Gate cloning. The figure represents seg 1 winner DIP candidate cloning workflow. A) To create a deletion junction in seg 1, the pHW191 plasmid (encoding the full-length seg 1) was used as a template. Initially, a splicing polymerase chain reaction (splice PCR) with flanking end primers was conducted in two separate PCR reactions. This results in PCR products referred as 5' and 3' fragments. Subsequently, PCR products undergo overlap extension PCR with flanking primers incorporating AarI restriction enzyme sites at the ends. The vector (pHW2000GGAarI) and insert (SOE product) were digested and ligated using Golden Gate cloning with the AarI restriction enzyme. Image created using BioRender.

3.4. Reverse genetics

3.4.1. Reconstitution of seg 1, 2 and 3 DIPs

To generate clonal seg 1, 2, and 3 DIP candidates, a co-culture of HEK and MDCK cells expressing PB2, PB1 and PA proteins respectively, was utilized. Specifically, the PB2, PB1, and PA proteins were retrovirally transduced into adherent HEK-293T and MDCK cells (as previously described reference [6]), and provided by cooperation partners from DPZ, Göttingen. On the first day of transfection, 0.2×10^6 cells per well of HEK and 0.2×10^6 cells per well of MDCK cells expressing either PB2, PB1, or PA (for seg 1, 2, or 3 DIPs, respectively) were seeded in a 6-well plate with DMEM growth medium at 37°C in 5% CO_2. Cells were grown to a confluency of roughly 60–70% for 22–24 h. Eight pHW2000 plasmids (1 µg per plasmid) encoding seg 1–8 (pHW191–198) of IAV PR8 were co-transfected using the calcium chloride transfection method (refer to section 3.4.2 for details on the procedure) to generate a positive control PR8 virus (section 4.1.4). To assess transfection efficiency, 1 µg per well of GFP expressing plasmid (in the pMAX backbone) and 7 µg per well of empty pCAAGS were included. For DIP reconstitution, the plasmid amounts for seg 1 DI encoding plasmids and the remaining seven full-length WT segments are detailed in Figures 4.1.5 and 4.1.8 (sections 4.1.4–4.1.5). Positive control PR8 transfection was also performed for seg 2 and 3 DIPs (data not shown). For the DIP-based reconstitution (sections 4.1.4, 4.1.5, 4.2.1, 4.3.1, 4.3.2 and 4.3.4), a calcium phosphate method (section 3.4.2) was employed akin to PR8 reconstitution (with a slight modification mentioned in the section 3.4.2 and result sections 4.1.4, 4.1.5, 4.2.1, 4.3.1, 4.3.2 and 4.3.4), followed by blind amplifications (section 3.4.3) for improved virus titers and larger number of vials in the seed virus banks (sections 4.1.4, 4.1.5, 4.2.1, 4.3.2 and 4.3.4).

3.4.2. Calcium phosphate transfection method

A total of 8 µL of the eight plasmids (pHW2000 backbone) were mixed with 10 µL of 2.5 M calcium chloride (Carl Roth, #10035-04-8) and 82 µL of nuclease-free water, making the final volume 100 µL. Please note, in the case of 9 plasmid setups, 9 µL of plasmids were mixed with 10 µL of calcium chloride and 81 µL of nuclease-free water. Subsequently, 100 µL of cold (4 °C) HEPES-buffered saline (HBS, 2X, pH 7.2, see table 3.4-1 for preparation) was added, and the mixture was incubated for 5 min at

room temperature to allow for plasmid-calcium phosphate complex formation. A total of 200 µL of this mix was then transfected onto the medium, avoiding direct contact with cells. Plates were gently rocked to evenly spread the DNA-$CaPO_4$ complex, to allow for maximum contact with plated cells. 16 hour post-transfection (h.p.t.), the medium was refreshed with DMEM growth medium. At 24 h.p.t., transfection efficiency was evaluated using a fluorescent microscope to identify the GFP-transfected cells. Experiments were continued if visual transfection efficiency exceeded 70–80%. At 48 h.p.t., the cell culture medium was aspirated, and the cells were washed with PBS. Next, 3 mL of GMEM with 1% peptone, trypsin (5 U/mL, Sigma-Aldrich, T1426) (referred to as “GMEM infection medium”) and 0.2% BSA (AppliChem, #A1391) was added. Cells were incubated, and harvests were collected at 4, 6-, 8-, 10-, and 13 days post-transfection (d.p.t.). For harvesting, the supernatant was centrifuged at 3000×g for 10 min at 4°C and stored at -80°C until further analysis. Cells were each time refreshed with fresh GMEM infection medium with 0.2% BSA. A blind amplification in IAV-polymerase complementing cells was carried out (3.4.3).

Table 3.4-1 2X HBS buffer preparation

Chemicals	Quantity
Sodium chloride	16.4 g
Hepes	11.9 g
Disodium hydrogen phosphate	0.21 g
Water	1 L

*Dissolve the chemicals in water and measure pH

3.4.3. Blind amplification

Virus samples collected at various rescue time points were subjected to blind amplifications at an undefined MOI in MDCK-PB2 cells for seg 1 DIP candidates, or in triple MDCK-PB2-PB1-PA cells for seg 2 and 3 DIP candidates. Likewise, DIP candidates based on seg 1 DI vRNA, such as live-DIP vaccine (section 4.2.1) or OP7 chimera DIPs described in sections 4.3.2 and 4.3.4, blind amplification using MDCK-PB2 cells were performed. In general, for the amplification, 1×10^6 genetically engineered MDCK cells per well were seeded in a 6-well plate and cultured to form a monolayer over 24 h. The cells were then washed with PBS and infected with 300 µL of virus-containing supernatants for 1 h. Subsequently, 1.7 mL of GMEM infection

medium was added, and the cells were incubated until a visible cytopathic effect (CPE) exceeding 50% was observed, typically around 48 hour post-infection (h.p.i.). The supernatants were harvested, centrifuged at 3000×g for 10 min at 4°C, and stored at -80°C until further analysis in virus quantification assays or PCR analysis (sections 3.5 and 3.6).

3.4.4. DIP-based constructs for live vaccine

For the attempts to reconstitute a DIP-based vaccine (section 4.2.1), the reconstitution scheme and methods described above were employed. For the rescue of Cal H1N1, transfection plasmids based on the pHW2000 backbone, as detailed in section 3.2, were utilized. Please refer to the table in Figure 4.2.1 for plasmid concentration and genome constellations. Blind amplifications were performed in MDCK-PB2 cells as described in section 3.4.3.

3.4.5. Reconstitution of OP7 and OP7 chimera DIPs

The generation of OP7 chimera DIPs (sections 4.3.2 and 4.3.4) was based on a previously established plasmid-based reverse genetics system for the rescue of PR8-derived seg 1 DIPs. To complement the missing PB2 protein, a co-culture of HEK-PB2 cells and MDCK-PB2 cells was utilized for plasmid transfections. The OP7 chimera DIPs were generated on the seg 1 DIP backbone of DI244 or seg 1/winner (referred to as pHWS1b), seg1/loser, as illustrated in Figures 4.3.2 and 4.3.5 respectively. Essentially, in addition to the eight plasmids used for the generation of seg 1 DIPs, a ninth plasmid (pHW-seg7-OP7) was incorporated for the reconstitution of OP7 chimera DIPs using the above-described calcium phosphate transfection (section 3.4.2) method [3]. The quantities of plasmids are detailed in the tables of Figures 4.3.3 and 4.3.6 for the various OP7 chimera DIP constructs.

After reconstitution, the OP7 chimera DIPs were amplified three times in adherent MDCK-PB2 cells. For the production of OP7 chimera DIPs in MDCK-PB2 suspension cells using shake flasks [3] and bioreactors [4], we utilized an OP7 chimera DIP based on seg 1/winner backbone. This material underwent one round of blind passaging (sections 3.4.3 and 4.3.4), resulting in an infectious virus titer of 6.4×10^7 PFU/mL. This viral preparation was then propagated in MDCK-PB2 suspension cells to produce a seed virus with an infectious titer of 4.5×10^6 PFU/mL. This seed virus was

subsequently used for the cell culture-based production of OP7 chimera DIPs [3, 4] and for further animal trials [3].

The attempts to generate clonal OP7 DIPs and OP7-PR8 (see section 4.3.1) were performed similarly to the reconstitution of seg 1, 2, and 3 DIPs. However, in this case, HEK-WT and MDCK-WT co-cultures were employed. The amounts of plasmids and the various genome constellations (including the 8+1 scheme, which added an extra plasmid to the eight-plasmid scheme for DIP/STV rescue) tested in the reconstitution are described in the table of Figure 4.3.1.

3.5. Virus quantification

3.5.1. HA assay

The hemagglutination assay is a method used to quantify viruses, such as IAV, which express HA surface antigens. These antigens bind to sialic acid receptors on erythrocytes, preventing their sedimentation. At a specific concentration of viral particles, the binding is insufficient to form a lattice, causing erythrocytes to sediment at the bottom of a round well plate forming a dot. The HA assay [143] was employed to determine total virus titers, expressed as $\log_{10}$(HAU/100 µL). A detailed protocol is defined in the SOP (section 8), available upon request.

The concentration of DIPs (cDIP) was calculated from the HA titer using the equation

$$cDIP = 10^{Log_{10}\left(\frac{HAU}{100\ \mu L}\right)} \times cRBC$$

where cRBC represents the concentration of red blood cells, set at 2×10^7 cells/mL.

3.5.2. Plaque assay

To quantify infectious virus titers, a plaque assay was utilized. This method leverages the ability of IAV to cause cell lysis, leading to the spread of progeny viruses to neighbouring cells. The spread is confined, by employing a semi-solid medium based on agar, enabling easy visualization of the plaque. Refer to supplement section 8.1.1 for a detailed protocol.

In brief, adherent MDCK-WT cells were seeded in 6-well plates at a density of 0.75 × 10^6 cells per well and incubated at 37°C and 5% CO_2 for 48 h. Samples were prepared in serial ten-fold dilutions using GMEM infection medium. The cells were washed twice with PBS, and 250 µL of each dilution was added to the wells, followed by a 1 h incubation at 37°C with 5% CO_2. After supernatant was aspired from the wells; cells were overlaid with 2 mL of 1% agar in the infection medium. The plates were then incubated for 4 days at 37°C with 5% CO2. Subsequently, the agar was removed, and the cells were fixed with methanol and stained with a 0.2% crystal violet solution. Plaques were counted using light microscopy, and the virus titer was calculated as plaque-forming units per mL (PFU/mL). The formula for calculating the virus titer is as follows

Plaque titer (PFU/mL) = PFU×D×4

PFU = counted plaque-forming units

D= Dilution factor

Please note, for the quantification of seg 1 DIPs or DIP constructs based on seg 1 DI vRNA (including OP7 chimera constructs, live DIP vaccine), MDCK-PB2 cell lines were used in the plaque assay. For the seg 2 and 3 DIPs triple-positive MDCK-PB2-PB1-PA cell line was used.

3.6. PCR analysis

Segment-specific reverse transcription PCR (RT-PCR) was performed to detect the presence of DI or full-length vRNA (sections 4.1.4 and 4.3.5). Additionally, reverse transcription real-time PCR (RT-qPCR) was used to quantify vRNA of mutated seg 7-OP7, seg 1 DI vRNA, and seg 5, 7, and 8 (sections 4.1.4, 4.3.3, and 4.3.5). Cellular gene expression indicating innate immune responses following STV infections or STV and DIP co-infections was also assessed using RT-qPCR (section 3.6.1.3).

Extracellular viral RNA was purified using the NucleoSpin RNA Virus Kit (Macherey-Nagel, 740956) according to the manufacturer's protocol and stored at -80°C until further use. Intracellular RNA was extracted by lysing cells post-incubation with lysis buffer (Macherey-Nagel, #740961), and samples were stored at -80°C. RNA

purification from cellular lysates was performed according to the manufacturer's instructions.

3.6.1.1. Segment-specific RT-PCR to identify DIP contamination

To detect full-length and DI vRNA in DIP preparations, purified RNA was reverse transcribed to cDNA using the Uni12 primer (Table 3.6-1) and the RevertAid First Strand cDNA Synthesis Kit (Thermo Fisher Scientific, # K1631), following the protocol described by Frensing et al., [144]. During reverse transcription, the universal primer hybridizes to the conserved regions at the 3' end of the vRNAs across all eight segments of the influenza genome. Specifically, a 14.5 µL reaction mixture containing 10 µL of RNA, 1 µL each of dNTPs (10 mM) and Uni12 primer (10 µM, refer to Table 3.6-1 for primer sequence) was incubated at 65°C for 5 min and then cooled to 4°C. Subsequently, 4 µL of 5X reaction buffer, 0.5 µL of RevertAid H Minus Reverse Transcriptase (200 U/µL, Thermo Fisher Scientific, # EP0451), 0.5 µL of RiboLock RNase inhibitor (40 U/ µL, Thermo Fisher Scientific, #EO0384), and 0.5 µL of nuclease-free water are added to the reaction mixture. The final 20 µL reaction mixture is incubated at 42°C for 60 min, followed by 70°C for 10 min [144].

Next, each segment was amplified from the generated cDNA using segment-specific primers in a PCR reaction [144]. For the segment-specific PCR, the 20 µL reaction mixture, consisted of 8.8 µL of nuclease-free water, 4 µL of 5X High Fidelity buffer, 2 µL of MgCl2 (10 mM), 1 µL of each primer set (10 µM, Table 3.6-1), dNTPs (10 mM), 2 µL of cDNA, and 0.2 µL of Phusion High-Fidelity DNA Polymerase (2 U/µL). Refer to Table 3.6-2 for cycling conditions. The PCR-amplified products are then analysed on a 1% agarose gel using gel electrophoresis.

Table 3.6-1 Primers for segment-specific PCR

Reaction	Target	Primer name	Sequence (5´→3´)
RT	All segments	Uni 12	AGCAAAAGCAGG
PCR	Seg 1	Seg 1 Uni for	AGCGAAAGCAGGTCAATTAT
		Seg 1 Uni rev	AGTAGAAACAAGGTCGTTTTTAAAC
	Seg 2	Seg 2 Uni for	AGCGAAAGCAGGCAAACCAT
		Seg 2 Uni rev	AGTAGGAACAAGGCATTTTTTCATG
	Seg 3	Seg 3 Uni for	AGCGAAAGCAGGTACTGATCC
		Seg 3 Uni rev	AGTAGAAACAAGGTACTTTTTTGG
	Seg 4	Seg 4 Uni for	AGCAAAAGCAGGGGAA
		Seg 4 Uni rev	AGTAGAAACAAGGGTGTTTT
	Seg 5	Seg 5 Uni for	AGCAAAAGCAGGGTAGATAATC
		Seg 5 Uni rev	AGTAGAAACAAGGGTATTTTTC
	Seg 6	Seg 6 Uni for	AGCGAAAGCAGGGGTTTAAAATG

		Seg 6 Uni rev	AGTAGAAACAAGGAGTTTTTTGAAC
	Seg 7	Seg 7 Uni for	AGCGAAAGCAGGTAGATATTG
		Seg 7 Uni rev	AGTAGAAACAAGGTAGTTTTTTAC
	Seg 8	Seg 8 Uni for	AGAAAAAGCAGGGTGACAAA
		Seg 8 Uni rev	AGTAGAAACAAGGGTGTTTT

Table 3.6-2 PCR cycling conditions for segment-specific amplification

	Step	Temperature (°C)	Time	
1	Initial denaturation	98	3 min	
2	Denaturation	98	25 sec	25 cycles
3	Annealing	54	45 sec*	
4	Extension	72	1 min	
5	Final extension	72	10 min	
6	Pause	4	∞	

*** Please note, the annealing times were as follows: 2 min for seg 1–3, 1 min for seg 4–6, and 45 sec for seg 7–8.**

3.6.1.2. RT-qPCR for absolute vRNA quantification

RT-qPCR was used to quantify extracellular vRNA levels in DIP preparations like seg 1 candidates and the various OP7 chimera DIPs. For this, WT- full-length segments were quantified such as seg 5, 7 and 8 and DI vRNA based on seg 1 candidates (winner, loser or de novo) or seg 7-OP7.

Generation of RNA standards

To quantify seg 1 DI vRNA of the newly identified seg 1 DIP candidates, new synthetic RNA standards were generated to specifically detect the deletion junctions. In the first step, a PCR was employed to add the T7 polymerase promoter sequence to the 5' end of the template pHWS1a, pHWS1b and pHWS1c encoding DI seg 1 loser, winner and de novo sequences, respectively. The PCR mix contained 8.8 µL of nuclease-free water, 4 µL of 5X High Fidelity buffer, 2 µL of magnesium chloride (MgCl2, 10 mM), 1 µL of each primer set (10 µM), 1 µL of dNTPs (10 mM), 2 µL of plasmid template (10

ng), and 0.2 µL of Phusion high-fidelity polymerase. The primers used to add T7 polymerase promoter sequences are listed in Table 3.6-3 along with a forward primer called Uni1 for 5'-AGCGAAAGCAGGTCAATTAT-3'. The cycling conditions for PCR were the same as in Table 3.6-2, except 54°C annealing temperature and 35 cycles were used. The PCR products were analysed via agarose gel electrophoresis in 1% agarose gel to confirm their sizes, as shown for the different seg 1 DIP candidates in Figure 4.1.3B. The PCR products were then gel-extracted using the Qiagen purification method as per the manufacturer's instruction.

The purified PCR products were subjected to in vitro transcription using the TranscriptAid T7 High Yield Transcription Kit (Thermo Fisher Scientific, #K0441). A 20 µL reaction mix was prepared, containing 300 ng of PCR product, 4 µL of 5X TranscriptAid reaction buffer, 8 µL of rNTP mix, and 2 µL of TranscriptAid Enzyme mix. The reaction was incubated for 2 h at 37 °C, followed by purification with 10% DNase (30 min, 37 °C) and subsequently with 10% EDTA (15 min, 65 °C). All the contents mentioned were derived from the transcription kit. Further purifications were performed using the RNA isolation kit (Macherey-Nagel, 740955) according to the manufacturer's instructions. The generated RNA templates were subjected to electrophoresis on formaldehyde-agarose (FA) gels as previously described [144] to confirm the integrity and correct size of RNA templates generated. Figure 4.1.3C shows the RNA standards for the seg 1 DIP candidates.

Table 3.6-3 Primers for the addition of T7 polymerase promoter sequences

DIP candidate	T7 primer reverse primer (5'-3')
Seg 1 Loser	TAATACGACTCACTATAGGGAGTAGAAACAAGGTCGTTTTTAAAC
Seg 1 Winner	TAATACGACTCACTATAGGGAGTAGAAACAAGGTCGTTTTTAAAC
Seg 1 De novo	TAATACGACTCACTATAGGGAGTAGAAACAAGGTCG

RT followed by qPCR

Quantification of seg 7-OP7 vRNA was performed using primers and conditions as previously described [38]. For the quantification of the new seg 1 DI vRNA, a two-step hot RT-qPCR method was employed.

Initially, RT was conducted using tagged reverse primers, as detailed in Table 3.6-4. The segment-specific nucleotides are underlined in the primer sequences provided in the table. Newly generated RNA standards were subjected to RT in ten-fold serial dilutions ranging from 5 ng to 5×10^{-8} ng to create an internal calibration standard curve as described below for the purified RNA samples.

For the RT Maxima H minus first strand cDNA synthesis kit was used (Thermo Fisher Scientific, # K1652). Here, 1 µL of purified RNA samples was mixed with 1 µL of tagged reverse transcription primer (10 µM, Table 3.6-4), 1 µL of dNTPs (10 µM), and 11.5 µL of nuclease-free water. This mixture was incubated at 65°C for 5 min, followed by 55°C for 5 min. During the latter step, 4 µL of 5X RT buffer, 0.5 µL of nuclease-free water, 0.5 µL of Ribolock inhibitor (40 U/µL) and 0.5 µL of Maxima H minus reverse transcriptase (200 U/µL, ThermoFisher Scientific, # EP0751) were added to the reaction mix. The reaction was incubated at 60°C for 30 min and terminated at 85°C for 5 min.

The resultant cDNA (for RNA standards and samples) was diluted with 80 µL of nuclease-free water. The diluted cDNA was then quantified using qPCR with 2X QuantiNova SYBR Green qPCR Master Mix (QIAGEN, 208056), 0.5 µL of real-time forward primer tag (10 µM, Table 3.6-4), and 0.5 µL deletion junction sequence-specific reverse primers (10 µM, Table 3.6-4). The cycling conditions are specified in Table 3.6-5, and the quantification protocol follows the previously described methods by Frensing et al., [144].

To determine the absolute quantity of vRNA in a given sample, calibration curves were constructed by plotting the C_T (threshold cycle) values of the serially ten-fold diluted RNA reference standards (obtained from qPCR) against the $\log_{10}$ number of RNA molecules ($\mathrm{n_{molecules}}$), thereby generating linear regression-based calibration curves. The $\mathrm{n_{molecules}}$ were calculated based on the quantity of the standard ($\mathrm{m_{STD}}$, in ng), the fragment length ($\mathrm{N_{bases}}$, in bp), the average mass of 1 base (k = 340 Daltons/base pair), and the Avogadro constant ($\mathrm{N_A}$, per mole) [5, 144]. See equation below

$$\mathrm{n_{molecules}} = \frac{\mathrm{m_{STD}}}{\mathrm{N_{bases}} \times \mathrm{k} \times \mathrm{N_A^{-1}} \times 10^9}$$

The number of viral RNA molecules in a sample, denoted as ($\mathbf{Q_{sample}}$), was determined using its C_T value. The calculation included the slope (m) and y-intercept (b) of the calibration curve, the coefficient of dilution of RT reaction ($\mathbf{F_{RT}}$), and the total volume of the RNA sample ($\mathbf{V_{sample}}$) in microliters [5, 144]. See below for the equation

$$\mathbf{Q_{sample}} = \mathbf{10}^{\left(\frac{\mathbf{C_T - b}}{\mathbf{m}}\right)} \times \mathbf{F_{RT}} \times \mathbf{V_{sample}}$$

Table 3.6-4 Seg 1 DIP candidates RT and qPCR primers

DIP candidate	Tagged reverse transcription primer (5'-3')	Real time forward primer tag (5'-3')	Deletion junction specific reverse primer (5'-3')
Seg 1 Loser	ATTTAGGTGACACTATAGAAGCGAGCGAAAGCAGGT	ATTTAGGTGACACTATAGAAGCG	CTCTCCTTTCGCGTACTTCTTGATT
Seg 1 Winner	ATTTAGGTGACACTATAGAAGCGAGAACTACGAAATCTAA		CCTTGCCCAATTATCCTCTTG
Seg 1 De novo	ATTTAGGTGACACTATAGAAGCAGCGAAAGCAGGTCAA		TGCCCAATTATTTTACTCCAT

Table 3.6-5 Cycling conditions for q-PCR

Step	Temperature	Time	
Initial denaturation	95°C	5 min	
Denaturation	95°C	10 sec	40 cycles
Annealing	62°C		
Melting	65°C-90°C	5 min	

3.6.1.3. Measurement of innate immune responses

To measure innate immune responses induced in co-infections with STV and OP7-chimera (refer Figure 4.3.10), a RT-qPCR was employed as previously described [5]. Briefly, 500 ng of intracellular RNA was subjected to RT using the RevertAid First Strand cDNA Synthesis Kit. In the first step, a reaction mix included 1 µL each of dNTPs (10 µM) and oligo(dT) primers (10 µM, Thermo Fisher Scientific, #SO132) in a

total volume of 13.5 µL, incubated at 65°C for 5 min, followed by a 4°C pause. Concurrently, a second reaction mix was prepared containing 4 µL of 5X RT buffer (Thermo Fisher Scientific, #EP0752), 1 µL of RevertAid H minus reverse transcriptase (200 U/ µL), 0.5 µL of RiboLock RNase inhibitor (40 U/µL), and 1 µL of nuclease-free water, making a total volume of 6.5 µL. This second mix was added to the initial master mix, resulting in a final volume of 20 µL. First-strand synthesis was carried out by incubating the reaction mix at 50°C for 30 min, followed by enzyme inactivation at 85°C for 5 min. RT samples were diluted with 80 µL of nuclease-free water. The RT product was kept on ice before proceeding to qPCR.

Real-time PCR was performed using the cycling conditions defined in Table 3.6-5, with 5 µL of 2xSYBR green (Qiagen, #204074) and 0.5 µL of gene-specific primers (details in Table 3.6-6). Fold induction was quantified using the ΔΔCT method for IFN-β gene expression, with GAPDH serving as the reference housekeeping gene.

Table 3.6-6 Primers to measure innate immune responses

Target gene	Primer	Sequence (5'-3')
GAPDH	GAPDH for	CTGGCGTCTTCACCACCATGG
	GAPDH rev	CATCACGCCACAGTTTCCCGG
IFNβ1	IFNB1 for	CATTACCTGAAGGCCAAGGA
	IFNB1 rev	CAGCATCTGCTGGTTGAAGA

3.7. Infection experiments

3.7.1. MDCK cell-based interference assay

To evaluate the efficacy of seg 1 DIP candidates in inhibiting STV replication, an in vitro co-infection assay was conducted using MDCK-WT cells, following previously established protocols [5, 37, 38]. Briefly, MDCK-WT cells were cultured in 6-well plates for 24 h at 37°C with 5% CO_2. After this incubation period, the cells were washed twice with PBS. Three wells were then trypsinized using 0.5 mL of 1% trypsin-EDTA for 20 min. The trypsinization process was stopped by adding 0.5 mL of GMEM growth medium, and the average cell count from the three wells was used to determine the MOI. Subsequently, the cells were either infected only with STV at an MOI of 0.01 or co-infected with STV and 125 µL of the produced DIP material (normalised by dilution). The wells were then filled to a total volume of 250 µL with GMEM infection medium and incubated for 1 h at 37°C with 5% CO_2. Following this, the virus-containing

inoculum was removed, the cells were washed with PBS, and 2 mL of infection medium was added to each well. The cells were then incubated for 24 h at 37°C and 5% CO_2. After the incubation period, the supernatants were collected and centrifuged at 3000×g for 10 min at 4°C. The cell-free supernatants were stored at -80°C until further analysis.

3.7.2. Calu-3 cells

Growth kinetics of IAV in Calu-3 cells

To evaluate the growth of IAV in interferon-competent human alveolar cell lines, infections were conducted in duplicates. These experiments were performed by Ghada Hemissi [145].

Calu-3 cells were seeded at a density of $3x10^6$ cells per well in a 12-well plate and incubated for 24 h at 37°C and 5% CO_2 prior to infection. To determine the MOI, the average cell count from three wells was obtained by washing the cells once with 1X PBS, followed by trypsinization with 1 ml of 1X trypsin-EDTA. Trypsinization was stopped by adding 1 mL of Calu-3 growth medium. Cells from three wells were counted. For the infection process, cells were washed once with 1X PBS and infected with 250 µL of infection media at a MOI of 0.05. The cells were then incubated with the virus for 1 h, after which the Calu-3 growth medium was added up to a total volume of 2 mL. Virus-containing and cell-free supernatants were collected at 0, 6, 24, and 48 h.p.i. by centrifugation at 4°C, 3000 × g for 10 min. The harvested supernatants were stored at -80°C until further use in virus quantification assays (sections 3.5 and 3.6).

Interference assay based on Calu-3 cells

To determine the in vitro interfering efficacy of the produced OP7 chimera DIP material, an interference assay was used. Specifically, the inhibition of STV propagation after co-infection with OP7 chimera DIPs was evaluated. Calu-3 cells were seeded at a concentration of 3.0×10^6 cells per well in a 12-well plate and incubated for 24 h before infection. For infection, cells were washed with PBS and infected with STV PR8 at a MOI of 0.05 or co-infected with 125 µL of the produced OP7 chimera DIP material in a total volume of 250 µL in Calu-3 growth media. After

1 h, medium was added to a final volume of 2 mL. Supernatants were harvested at 6, 24, 48 h.p.i, centrifuged at 3000 × g for 10 min at 4°C and cell-free supernatants were stored at -80°C until virus quantification. To extract intracellular RNAs, 350 µL of RA1 buffer containing 1% β-mercaptoethanol was added to cells for lysis. RNA purification from these lysates was carried out according to the manufacturer's instructions (Macherey-Nagel, #740961) and samples were stored at -80°C until real-time RT-qPCR to measure IFN-β gene expression as described previously [5], see section 3.6.1.3 for details.

3.7.3. Innocuity assay

To evaluate the presence of infectious STV in the DIP preparations, two serial passages of the DIP harvests were conducted using MDCK-WT cells. MDCK-WT cells were seeded in T-75 tissue culture flasks at a density of 2.5×10^6 cells per flask and incubated for 24 h at 37°C with 5% CO_2 in growth media. After this incubation period, the cells were washed twice with PBS. Subsequently, the cells were incubated with 350 µL of the produced DIP material for 1 h, with gentle rocking every 15 min to prevent the cells from drying. Next, 13 mL of GMEM infection medium was added, and the flasks were incubated for 48 h at 37°C and 5% CO_2. Following this, the supernatants were collected and centrifuged at 3000×g for 10 min at 4°C. The resulting cell-free aliquots were stored at -80°C until further analysis in the HA assay. This process of infecting MDCK cells was repeated using the collected supernatants to perform the serial infections, and the samples were again subjected to the HA assay.

4. Results and Discussion

This section is structured into three distinct chapters, with each chapter addressing a separate aspect of the PhD work. The first chapter explores the discovery of novel DI vRNA based on seg 1, including their reconstitution and evaluation for antiviral properties, as documented in the publication by Pelz, Ruediger, and Dogra et al., [1]. The second chapter describes the development of a DIP-based live vaccine through the substitution of surface antigens using reverse genetics techniques. The final chapter employs modified reverse genetics for IAV to reconstitute OP7 chimera DIPs, ensuring that the resulting DIP material is free from any infectious STV. This work led to two separate publications by Dogra et al., [3] and Pelz et al., [4]. The content from these three publications, including text, figures, and tables, has been incorporated into the current thesis [1, 3, 4].

4.1. Identification and generation of new DIPs with superior antiviral activity than DI244

4.1.1. Long-term IAV infection in cell culture appears to accumulate highly competitive DIPs

Previous studies conducted by our group involved the establishment a continuous production process using a two-stage bioreactor system for the production of IAV-based vaccines [90, 136]. These studies highlighted periodic oscillations in both total and infectious virus titers, caused by DIP co-infections, thereby negatively affecting vaccine production titers. In a recent study, a similar cultivation system was adopted in a semi-continuous mode in shake flasks [1] (Figure 4.1.1A). Here, a DIP-depleted PR8 seed virus was used, to perform a long-term infection over 21 days in MDCK-WT suspension cells. The system comprised two shake flasks, one for cell growth and the other for virus infection. Both shake flasks were regularly fed with fresh medium (once in 12 h). Cells from the cell growth shake flask were continuously transferred to the virus infected shake flask. Every 12 h, virus-containing supernatants were harvested (Figure 4.1.1A). The results demonstrated the accumulation of deletions in all eight vRNA segments, as evidenced by RT-PCR results (data not shown). This finding potentially explained the observed fluctuations in total and infectious virus titers (Figure 4.1.1B) [136]. It is speculated that inhibition from DI vRNA on full-length

sequences arises due to the rapid replication of shorter sequences, leading to a high MOI of DIPs (MODIP) and thereby a reduction in STV replication (e.g., day 1-4) [89]. However, as STVs diminish, viral resources required for DI vRNA replication cease as well, resulting in the “washing out” of viruses and DIPs. Eventually, due to a low concentration of DIPs, an increase in STV replication and therefore the virus titers occurs again (e.g., day 4–5). The dynamics observed in virus composition (about STV and/or DIP accumulation), whether due to high MOI, low MODIP, or the reverse, were consistent with periodic oscillations in total virus titers and infectious virus titers. These oscillations in virus titers were reported using RT-qPCR (based on extracellular seg 5 vRNA) and $TCID_{50}$ measurements (Figure 4.1.1B). Additionally, the presence of DI vRNA was confirmed by segment-specific RT-PCR followed by agarose gel electrophoresis, where weak, blurred, or undefined DI bands emerged during the course of IAV replication in the long-term, semi-continuous cultivations (data not shown).

Overall, it was suspected that the exposure of DIPs to alternating selection pressures might have led to the accumulation of highly interfering and competitive DIPs towards the end of the cultivation. Hence, to precisely detect and quantify the various deletion junctions that were formed in the course of the semi-continuous process, next-generation sequencing (NGS) was employed (Figure 4.1.1C). A bioinformatics-based pipeline that included Illumina-based NGS sequencing, followed by a so-called “ViReMa” algorithm, was used to detect positions of individual deletion junctions (these studies were performed by Fadi Alnaji, cooperation partners at the University of Illinois [77]). The highest fractions of NGS reads and the greatest number of variations in deletion junctions were present on the polymerase-encoding segments, i.e., seg 1, 2, and 3 (encoding proteins PB2, PB1, and PA respectively). The remaining five IAV segments showed less than 2% of total NGS read fractions (data not shown). Upon close observation, deletion junctions in the polymerase segments showed differences in propagation, perhaps indicating at a competition in DI virus propagation and accumulation over the cultivation time. It was hypothesized that an individual DI vRNA could accumulate to high numbers toward the end of the cultivation owing to its high growth compared to other deletion junctions. Based on increases and decreases in their fractions, the deletion junctions were classified in various categories, such as top winners, losers, or de novo (Figure 4.1.1C). Deletion junctions were termed top

winners when these deletion junctions showed a high gain in their fraction from the seed virus to the end of the cultivation (21 d.p.i.). Top losers showed a loss in their fractions until the end of cultivation. Top de novo deletion junctions were spontaneously generated during the semi-continuous propagation and accumulated to a high fraction towards the end of the process.

In essence, a DI vRNA inhibits STV replication because the shorter DI vRNA replicates more rapidly, depleting cellular and viral resources needed for the replication of the full-length vRNA. Hence, it was hypothesized that DIPs capable of propagating to high fractions exhibit greater interference with STV replication compared to other DIPs that propagate slowly. To confirm this hypothesis, these deletion junctions were cloned and reconstituted to evaluate their interfering capacities in in vitro co-infection studies (Figures 4.1.2, 4.1.5, 4.1.6, 4.1.7, and 4.1.9).

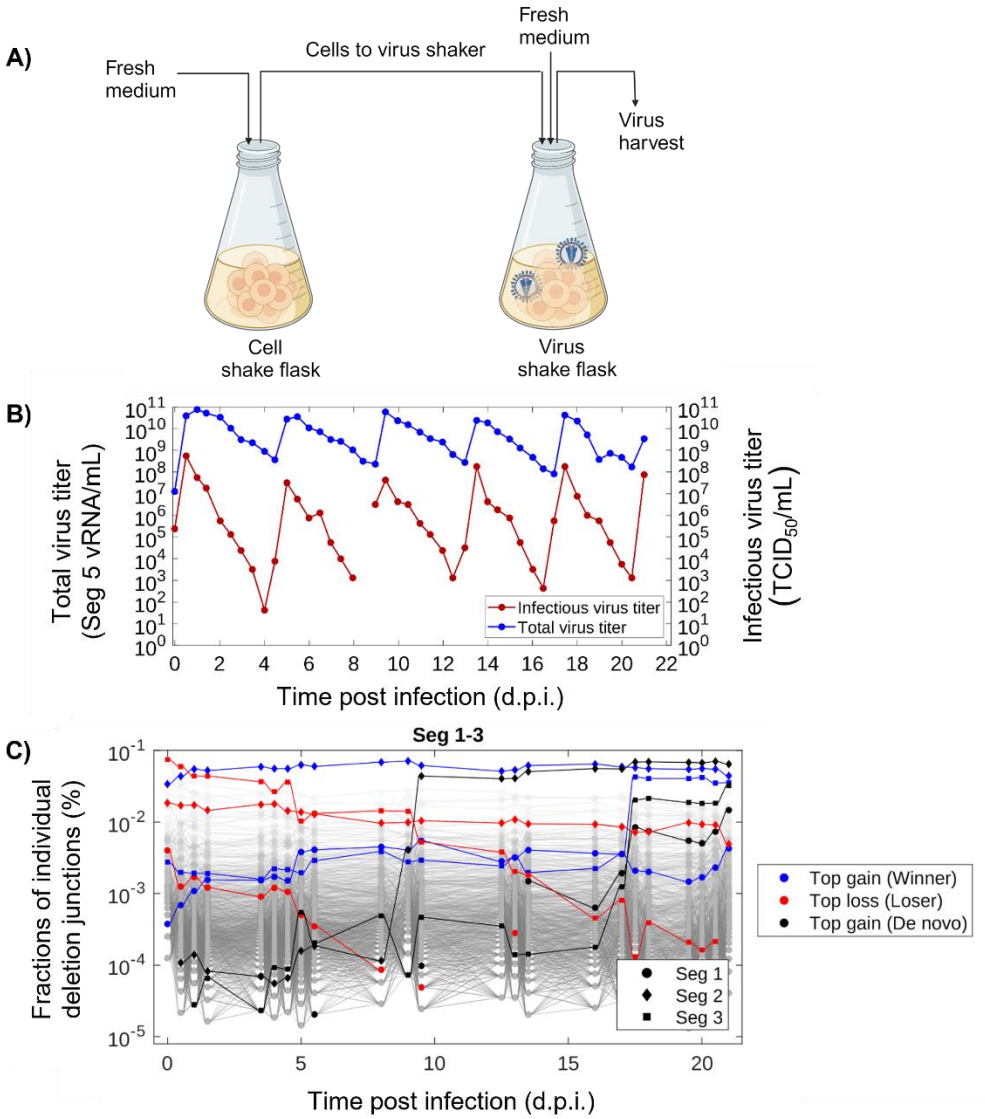

Figure 4.1.1. Long-term infection of IAV and its DIPs in semi-continuous mode, performed by Pelz et al., [1]**.** A) Experimental setup of two-stage cultivation consisting of shake flasks. MDCK-wild type (MDCK-WT) suspension cells were cultivated in cell and virus shake flasks. In the virus shake flask, MDCK-WT cells infected with standard virus (STV, H1N1 A/PR/8/34 (PR8)) seed virus at a multiplicity of infection (MOI) of 0.01 which was depleted in IAV DIPs. The semi-continuous mode was operated after 0.5 hour post-infection (h.p.i.), by transferring cells from the cell shake flask into the virus shake flask, while virus harvest obtained from the virus shake flask was subjected to analysis. B) Oscillations in infectious and total virus titers were observed over 21 days of infection, as indicated by the vRNA titers of seg 5 quantified by reverse transcription-real time PCR (RT-qPCR) and tissue culture infectious dose ($TCID_{50}$) assay respectively. C) Illumina-based next generation sequencing (NGS) for identification of different DI vRNA that propagated during semi-continuous propagation. ViRema algorithm analysis detected different deletion junctions on IAV polymerase seg 1, 2 and 3. Fractions for individual deletion junctions were calculated based on the ratio of the total number of NGS reads of the one individual deletion junction to the total number of NGS reads of all deletion junctions on all segments. The figure indicates the top three gains (winner and de novo) and loss (loser) DI vRNA on polymerase segments. Figures adapted from the publication by Pelz et al., 2021 and modified by Daniel Ruediger [1]. Panel A) generated using Biorender.com.

4.1.2. Generation of plasmids encoding for supposed highly interfering DI vRNAs

To reconstitute purely clonal DIPs without infectious STV, the newly identified deletion junctions had to be cloned in pHW2000 plasmids. Figure 4.1.2A shows the identified deletion junctions classified as top loser, winner, and de novo for each seg 1, 2, and 3. In the first step, to create large deletions, the splice overlap extension PCR (SOE PCR) was used. This method utilizes a carefully selected set of primers in two distinct PCR reactions (Figure 4.1.2B). The primers were designed to bind to the sequence regions flanking the desired deletion zone for splice PCRs (see Figure 3.3.1 in Material and Methods). Additionally, the sequences of primers contained overlapping sequences with each other. The resulting two PCR products (Figure 4.1.2B were then joined via complementary base pairing during a subsequent PCR step (overlap extension PCR, Figure 4.1.2B). Furthermore, during overlap extension PCR, the primer set introduced AarI restriction sites (a Type IIS restriction enzyme), enabling the use of the Golden Gate cloning technique. In the subsequent cloning step, the one-pot method allows to accurately orient and insert the fragments into the vector plasmid harboring an Aarl1 restriction site (pHW2000GGAarI). The plasmids were then transformed into *E. coli* NEB 10β competent cells, followed by colony PCR to identify positive clones that contained the plasmid with the DI vRNA sequence of interest (Figure 4.1.2B). Next, the resulting plasmids were purified and sequenced for the presence of correct deletion junctions (data not shown)

In sum, plasmids containing deletion junctions for seg 1, 2, and 3 of loser, winner, and de-novo deletion junctions were generated and then utilized in the reconstitution of clonal DIPs (Figures 4.1.5 and 4.1.8). Furthermore, these plasmids were used to create RNA standards (Figure 4.1.3) for seg 1 DI vRNA. This approach facilitated accurate and sensitive quantification of DI vRNA by reverse transcription real-time PCR (RT-qPCR) (Figures 4.1.4 and 4.1.7).

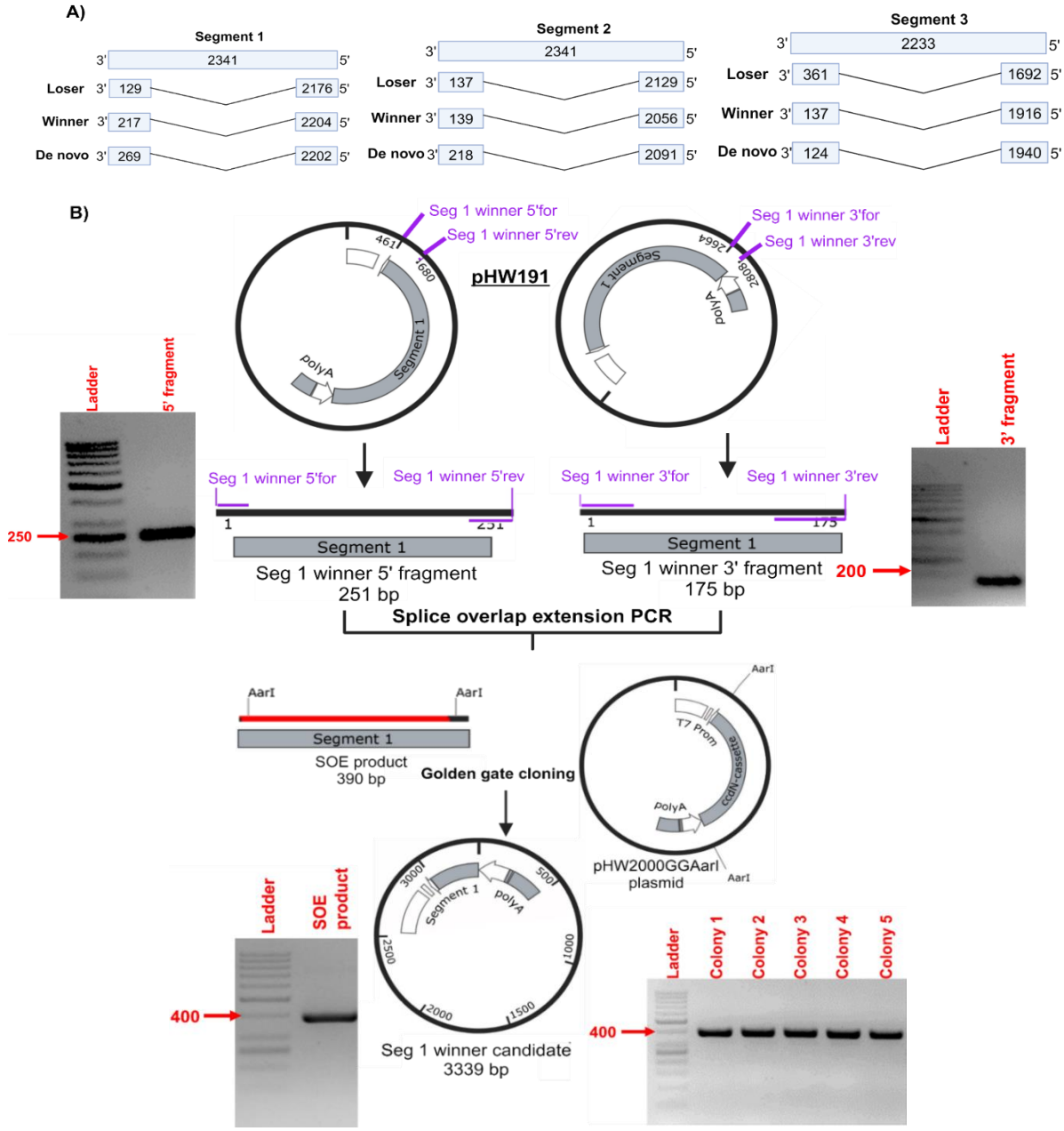

Figure 4.1.2. Construction of new deletion junctions entailed in pHW2000 plasmids for the reconstitution of the corresponding loser, winner, and de novo DIPs. A) The diagram illustrates the top three winner, de novo, and loser DI vRNAs on seg 1, 2, and 3. The panel highlights the deletion junctions at the 3' and 5' vRNA sequences. B) Cloning procedure. The figure presents the seg 1 winner as an example of the cloning technique applied for all the deletions. To create a deletion junction in seg 1, the pHW191 plasmid (encoding the full-length seg 1 in pHW2000 plasmid backbone) served as a template. First, a splicing polymerase chain reaction (PCR) with flanking end primers in two distinct PCR reactions was carried out. The PCR products (5' and 3' PCR fragments) were then analysed using agarose gel electrophoresis, with the relevant ladder band sizes (in bp) marked by arrows. Following this, the PCR products underwent splice overlap extension PCR (SOE PCR) with flanking primers incorporating AarI restriction enzyme sites at the ends. Please refer to the Materials and Methods section for a detailed description. Alongside, the agarose gel electrophoresis image shows the SOE PCR product. The vector (pHW2000GGAarI) and insert (SOE PCR product) were digested and ligated using Golden Gate cloning with the AarI restriction enzyme. To confirm the correct insert, colony PCR was performed on five randomly selected colonies. In total, nine plasmids for seg 1, 2, and 3 were created. The figure includes cropped gel images. The workflow image was sourced from SnapGene and assembled in BioRender.

4.1.3. Generation of new RNA standards for accurate quantification of deletion junctions

To employ a sensitive and precise method for the quantification of total DIP titers, specifically targeting the new deletion junctions (loser, winner, or de novo), an RT-qPCR methodology was established. For this, RNA standards of seg 1 candidates (i.e., loser, winner, and de novo) were generated. To produce the RNA standards, plasmids harbouring the newly identified seg 1 DI sequences (Figure 4.1.2B) served as templates. Initially, a primer pair targeting the terminal ends of the DI sequence was used to incorporate T7 polymerase promoter sequences through PCR (as depicted in Figures 4.1.3A and 4.1.3B). This PCR product was subjected to in vitro transcription using the T7 polymerase, a DNA-dependent RNA polymerase. Following transcription, the RNA standards were purified and their integrity was assessed via formaldehyde gel analysis (FA gel electrophoresis) as illustrated in Figures 4.1.3A and 4.1.3C. These RNA standards were then diluted to a concentration of 5 ng and used in ten-fold serial dilutions to establish calibration curves for absolute RNA quantification. This method with tagged primers was previously used for the detection of full-length segments (Figure 4.1.4A) [5, 87, 144, 146]. However, various DI RNA could be generated from the same full-length vRNA segment. For precise detection of individual seg 1 candidate deletion junctions in virus harvests, deletion junction-specific reverse primers were used for real-time PCR reactions (Figure 4.1.4A).

Figure 4.1.4B presents the calibration curves for seg 1 DIP candidates, derived from a ten-fold serial dilution of the synthetically produced RNA standards (Figure 4.1.3) to demonstrate the accuracy and reproducibility of the RT-qPCR workflow (n=3). To assess false amplification, controls without enzyme and template were used, to ensure the accuracy of results attributed to the reaction mix (data not shown). Additionally, to eliminate false positive detection of seg 1 FL, 5 ng of seg 1 FL RNA standards were introduced into the RT-qPCR workflow for quantification of various seg 1 DIP candidates, resulting in negligible detection (data not shown). Overall, this newly

established workflow allowed the precise and reproducible detection and quantification of the different seg1 DIP candidate RNA sequences.

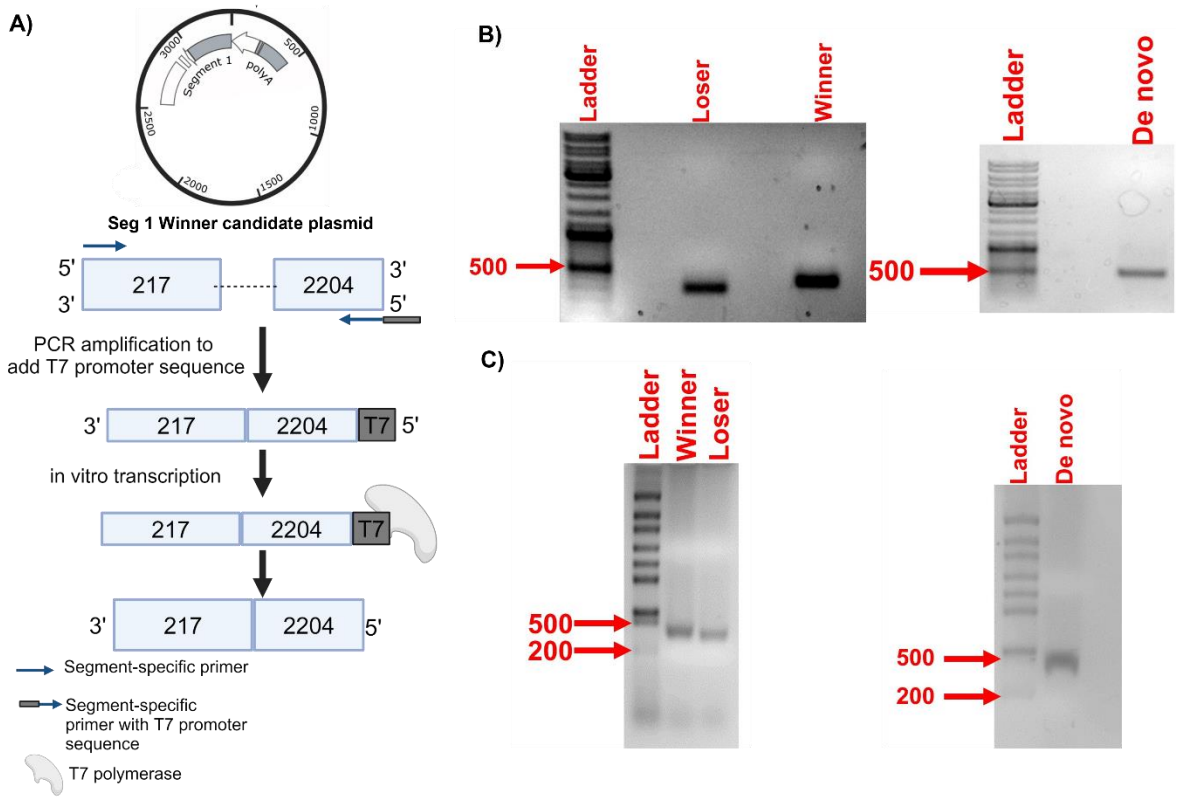

Figure 4.1.3. Production of seg 1 RNA reference standards for RT-qPCR quantification. A) The seg 1 DI sequence, harboured within the pHW2000 plasmid, serves as a template for RNA standard generation. The seg 1 winner is shown as an example. In an initial PCR, the product includes T7 promoter sequences through the use of segment-specific primers that encode T7 promoter sequences. This PCR product is then subjected to in vitro transcription using the T7 polymerase, resulting in RNA transcripts. B) Panel illustrates the PCR products of various seg 1 candidate, each incorporating T7 promoter sequences at their 5' termini, as visualized on agarose gels. The size of the corresponding ladder is denoted by an arrow. C) After in vitro transcription, DI-specific RNA standards for seg 1 candidates were analysed on formaldehyde gels, with ladder sizes indicated by arrows. Panel A image created with Biorender.com.

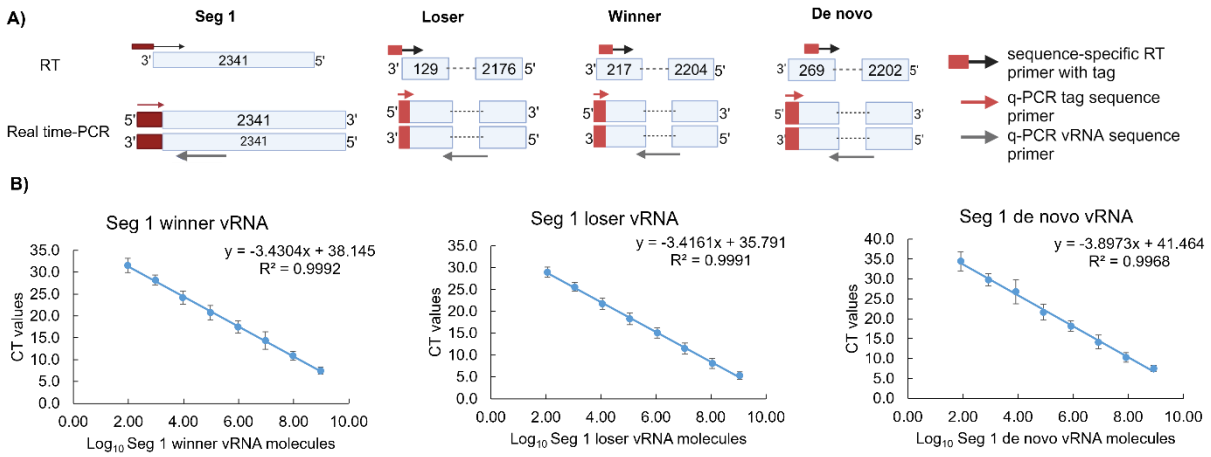

Figure 4.1.4. Strategy and calibration curves for RT-qPCR quantification of seg 1 DI vRNA candidates. A) The RT-qPCR analysis for DI vRNA quantification employs primers that encompass the deletion junctions, in contrast to those used for the full-length segment as shown on the left. B) Presented are the calibration curves for the different deletion junctions, constructed through linear regression based on serially diluted standards ranging from 5 ng to 5×10^{-8} ng (refer to Material and Methods for details). These plots summarize the average results from three independent experiments (n=3). Error bars indicate standard deviation (SD).

4.1.4. Seg 1 candidate DIP reconstitution

In the early 2000s, Hoffman et al., developed a new plasmid-based reverse genetics system for the reconstitution of IAV using cloned cDNA in a set of eight plasmids [8]. Each plasmid encoded for viral proteins as well as for vRNA, all required for virus replication in plasmid-transfected cells, thereby streamlining the recombinant IAV generation.

In the case of seg 1 DIPs, a deletion in seg 1 vRNA (encoding the PB2 protein) makes the DIP deficient in virus replication. DIPs therefore require co-infection with STV to compensate for the missing protein. Bdeir et al., modified the existing IAV reverse genetics system, such that the transfected cells (co-culture of HEK-293T and MDCK cells), expressed the missing PB2 protein [6]. Using a seg 1 DI sequence-encoding plasmid along with seven full-length IAV segment-encoding plasmids of strain PR8, a seg 1 DIP, “DI244” was reconstituted in their study [2, 6, 31, 36].

The newly identified seg 1 DIP candidates were reconstituted using the above-mentioned reverse genetics system (Figures 4.1.1 and 4.1.2A). Figure 4.1.5A illustrates that the seg 1 plasmid was designed to encode either the seg 1 loser, winner, or a de novo DI genome (refer Figure 4.1.2 for plasmid generation), whereas

the remaining seven plasmids encoded the full-length WT segments. Based on the backbone (pHW2000 plasmids), each plasmid was capable of encoding both the vRNA (due to RNA pol I promoter) and the corresponding protein(s) (due to RNA pol II promoter) for each segment. A co-transfection of these eight plasmids resulted in the generation of clonally pure seg 1 DIP candidates, which were subsequently amplified in MDCK-PB2 adherent cells.

It was suspected that self-interference in the DIP rescue may lead to extremely low or no virus titers post-rescue. Hence, to avoid such issues, two DI plasmid amounts (50 ng to 1 µg per well) were tested while the other seven full-length plasmids were kept at constant amounts of 1 µg per well (Figure 4.1.5B and C). Transfection efficiencies in each experiment were controlled using GFP transfected wells, evaluated under fluorescence microscope (data not shown). Positive controls, such as PR8 (STV) and DI244 were also included in the rescue attempts. Using 1 µg per well of DI plasmid and 1 µg per well of FL plasmids, it was possible to reconstitute the seg 1 winner construct, DI244 and PR8, as evidenced by positive infectious virus titers after transfection (at different harvest time points (Figure 4.1.5B)). In contrast, rescue attempts of seg 1 loser and de novo constructs did not yield virus titers. However, when the amount of the DI plasmid was reduced to 50 ng, both seg 1 winner and loser constructs were successfully reconstituted (Figure 4.1.5 B lower panel). Subsequent blind amplification (i.e., infection with an unspecified MOI of DIPs (MODIPs)) of the rescue material (50 ng DI plasmids with 1 µg of seven full-length plasmids, harvested at 13 d.p.t.) in MDCK-PB2 cells resulted in high infectious virus titers of about 1.0×10^{8} PFU/mL for both seg 1 winner and loser DIP candidates. Please note, that infectious virus titer quantifications post-DIP rescue was performed in MDCK-PB2 cells in the plaque assay.

Nonetheless, the seg 1 de novo construct failed to exhibit any infectious virus titer even after one round of virus amplification in adherent MDCK-PB2 cells. Segment-specific DIP PCR followed by agarose gel electrophoresis revealed a faint band for seg 1 de novo (Figure 4.1.6A), whereas distinct DI bands were observed for both winner and loser constructs. Yet, subsequent amplifications in suspension MDCK-PB2 cells yielded a high total virus titer for seg 1 de novo (Supplement figure 7.1). Virus harvests were subjected to agarose gel electrophoresis following a segment-specific PCR (Supplement figure 7.2). The results suggest that seg 1 de novo DIP could also

be rescued but required additional amplification rounds to achieve detectable infectious virus titers. Using suspension MDCK-PB2 cells, the further propagation of seg 1 DIP candidates at low MODIP notably contributed to the reduction of other contaminating DIPs. This was evidenced by agarose gel analysis following segment-specific PCR, as shown in Figure 4.1.6A, in comparison to Supplement figure 7.2.

After amplification, all constructs were sequenced to confirm the correct presence of deletion junctions (data not shown). Following this, the clonal DIP harvests were tested for contamination with infectious STV. Here, seed viruses underwent further amplification in MDCK-WT cells to check for any infectious viruses (Figure 4.1.6B). This process of multiple passaging (up to two rounds in this study) is known as innocuity assay. After each passage in MDCK-WT cells, the virus supernatant was analysed using HA assay to determine the presence of any detectable virus. The innocuity tests were negative for all three newly generated Seg 1 DIP candidates, suggesting that the new Seg 1 DIP candidate seed viruses were devoid of infectious STVs.

The newly established RT-qPCR analysis method (Figure 4.1.4) was employed to quantify the different deletion junctions of the seg 1 DIP candidates (amplified in adherent MDCK-PB2 cells, as illustrated in Figure 4.1.7). Seg 1 loser and winner, which exhibited high infectious virus titers (Figure 4.1.5C), also demonstrated significant total virus titers, as evidenced by seg 5 vRNA quantifications, and similarly high seg 1 DI vRNA titers. In line with previous results, the de novo and seg 5 vRNA quantifications again revealed lower total virus titers. In brief, the newly identified seg 1 DIP candidates were reconstituted using the modified reverse genetics system described by Bdeir et al., through a co-culture of mammalian cells expressing the missing PB2 proteins [6].

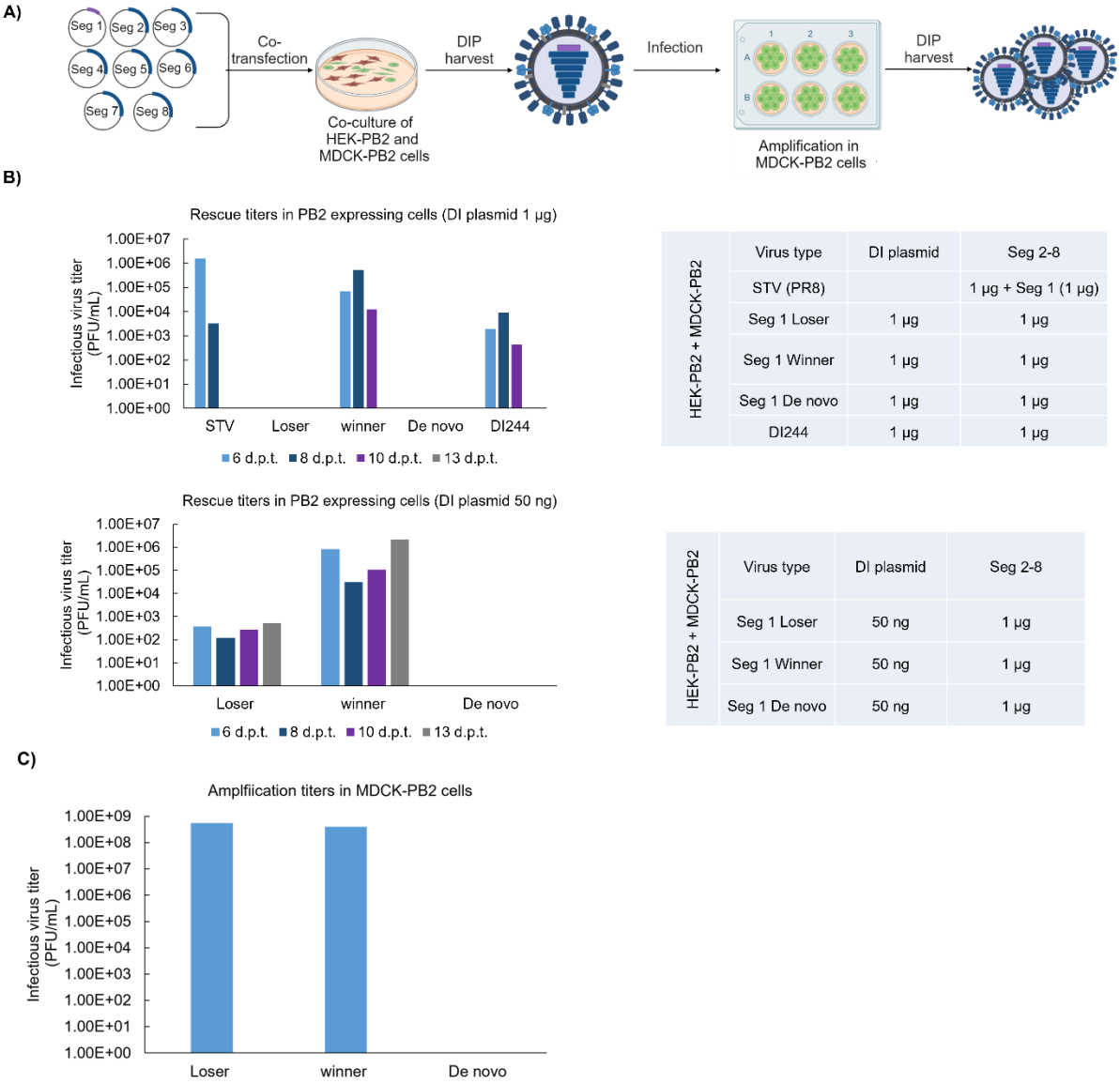

Figure 4.1.5. Seg 1 DIP candidate reconstitution and amplification. A) Illustration of the method used to create purely clonal DIPs. Eight plasmids are co-transfected, including a plasmid harbouring the seg 1 DI sequence (loser, winner, or de novo; plasmid generation as shown in Figure 4.1.2) and seven full-length-WT-encoding plasmids, into PB2-expressing mammalian adherent cells. For co-culture, genetically engineered HEK-293-T cells (HEK-PB2) for high transfection efficiency and MDCK-PB2 cells for high virus titers were utilized. This approach was adapted from Bdeir et al., 2019 [6]. The figure also depicts the subsequent amplification process in MDCK-PB2 adherent cells to improve virus titers and to establish a seed virus bank post-rescue. B and C) Panel displays the infectious virus yields post-rescue, quantified using the plaque assay, and expressed in plaque-forming unit (PFU) titers. The accompanying table details the different concentrations of DIP plasmids utilized. B) Post-rescue virus titers obtained with 1 µg per well of DIP encoding plasmid. C) Infectious titers achieved with 50 ng per well of DIP plasmids. D) Amplification of the rescue harvests from conditions where 50 ng per well of DIP plasmid was used (harvest at 13 d.p.t.) Plaque titers are indicated. After another round of amplification in suspension MDCK-PB2 cells, a virus titer for de novo Seg 1 DIPs could be detected (performed by Lars Pelz), as outlined in section 4.1.4 (please also refer to Supplement figures 7.1 and 7.2).

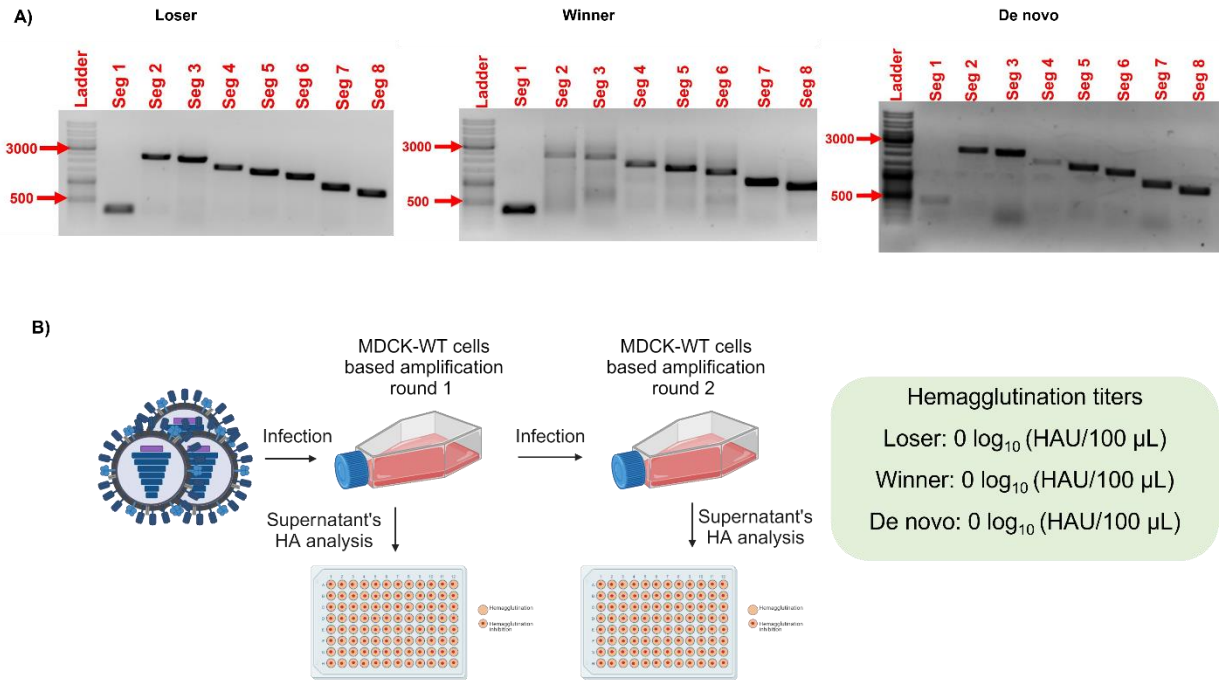

Figure 4.1.6. Purity of seg 1 candidate DIPs amplified in MDCK-PB2 cells. A) Seg 1 DIP candidates amplified in the PB2-expressing cells were subjected to segment-specific-reverse transcription (RT) PCR and agarose gel electrophoresis to assess contamination by other DIPs or infectious STV. Ladder: 3000 bp and 500 bp are marked by arrows. B) Innocuity assay. To test for the presence of infectious STV, the amplified DIPs were subjected to infections in MDCK-WT cells. Two consecutive passages were carried out, and each supernatant was analysed via HA assay. HA titers (all negative) are highlighted in the green box.

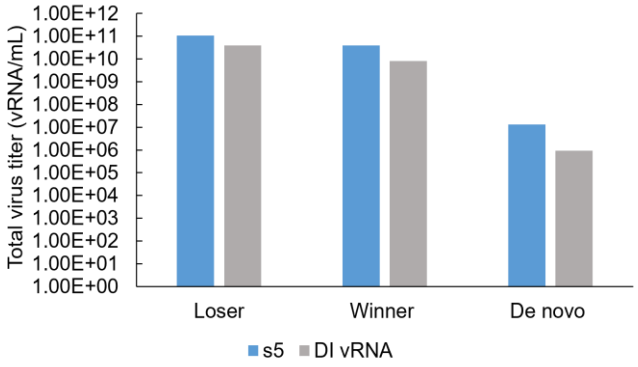

HEK-PB2 + MDCK-PB2

Virus type	DI plasmid	Seg 2-8
Seg 1 Loser	50 ng	1 µg
Seg 1 Winner	50 ng	1 µg
Seg 1 De novo	50 ng	1 µg

Figure 4.1.7. RT-qPCR quantification of amplified seg 1 DIP candidates. The table indicates virus types and plasmid concentrations for seven full-length or DI-encoding plasmids used for transfection. Samples were subjected to amplification in MDCK-PB2 and tested in RT-qPCR. The newly developed RNA standards and primer sets (Figures 4.1.3 and 4.1.4) were used to quantify the specific deletions for analysis. Additionally, quantifications of seg 5 vRNA were conducted to determine total virus titers. All vRNA measurements are reported in vRNA/mL.

4.1.5. Reconstitution of seg 2 and seg 3 DIPs

As outlined in section 4.1.1, the highest variations and fractions of deletion junctions identified through NGS analysis were found in segments encoding polymerases. Following the successful reconstitution of seg 1 DIP candidates, next steps aimed at reconstituting seg 2 and seg 3 DIP candidates (top winners, de novo, and losers). The process of generating pure seg 2 and seg 3 DIP candidates involved reverse genetics, mirroring the approach taken for seg 1 DIPs (including PR8 and gfp transfection controls). The seg 2 DIPs, which have deletions in their vRNA, render them unable to produce functional PB1 protein, necessitating the supplementation of PB1 protein. Therefore, a co-culture of HEK and MDCK cells expressing PB1 protein was used (cell lines generated by cooperation partners at DPZ, Göttingen). This co-culture of HEK-PB1 and MDCK-PB1 was co-transfected with eight plasmids, including seven full-length and the seg 2 DI-encoding plasmid, as illustrated schematically in Figure 4.1.8A. Similarly, for the generation of seg 3 DIP candidates, which are deficient in PA protein, co-cultures of HEK-PA and MDCK-PA (cell lines generated by cooperation partners at DPZ, Göttingen [138]) cells were co-transfected with seven full-length and seg 3 DI-encoding plasmid. To avoid the possibility of self-inhibition by the DI plasmid during the reconstitution of DIPs, two DI plasmid amounts (1 µg and 50 ng) were evaluated, while maintaining a constant amount of 1 µg per segment per well for WT seven full-length-encoding plasmids (refer to the tables in Figures 4.1.8A and 4.1.8B).

Plaque assays were conducted to assess the infectious DIP titers of seg 2 and seg 3 candidates from various rescue time points (4, 6, and 8 d.p.t. for seg 2 DIPs and 4 and 6 d.p.t. for seg 3 DIP candidates), using MDCK-PB1 or MDCK-PA adherent cells, respectively. Contrary to the results for seg 1 DIP candidates, no infectious virus titers could be detected for either seg 2 or seg 3 DIPs at any of the rescue time points. Next, more cycles of virus amplification were attempted to achieve detectable levels of infectious virus titers for various DIP candidates. As a result, blind amplifications were carried out in triple-positive MDCK-PB2-PB1-PA adherent cells (cell lines generated by Prerna Arora [138]). However, infectious virus titers were not detected post-amplification. The amplification was further explored in triple positive MDCK-PB2-PB1-PA positive suspension cells (performed by Lars Pelz). Yet, this approach also did not yield any detectable infectious virus titers.

In conclusion, the attempts to reconstitute seg 2 and seg 3 DIP candidates were unsuccessful. Despite multiple efforts to amplify virus titers using genetically engineered cell cultures to compensate for the missing DIP proteins, success was not achieved in either adherent or suspension formats.

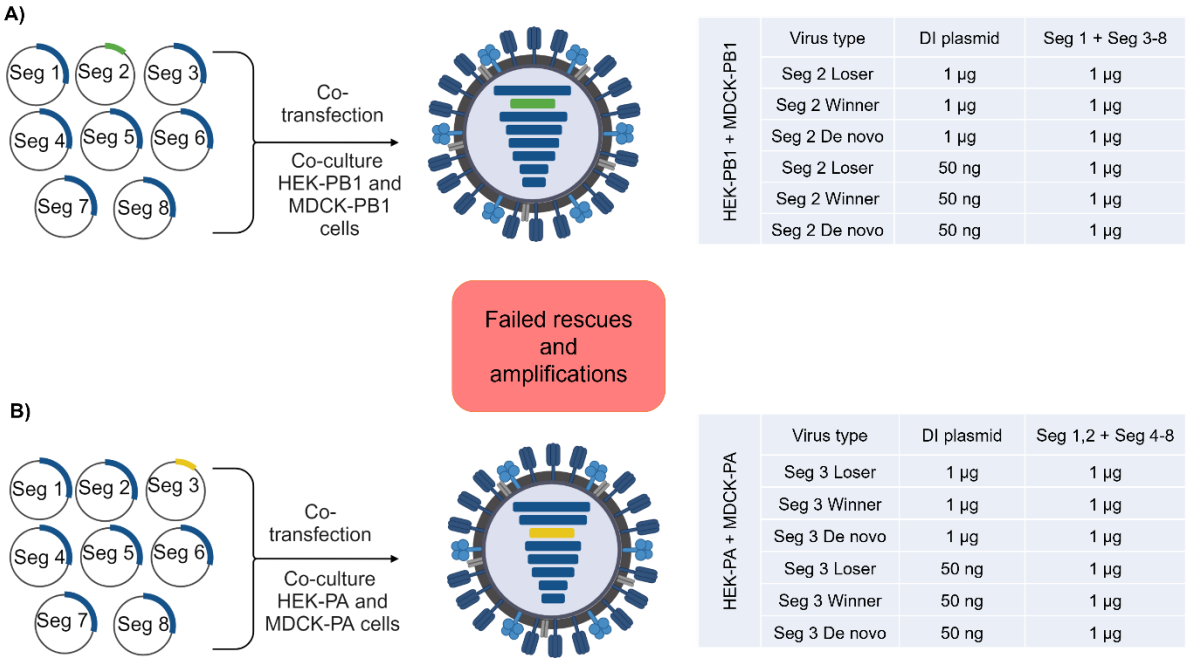

Figure 4.1.8. Reconstitution and amplification of seg 2 and 3 DIP candidates. A) A schematic condensed workflow for reconstituting seg 2 DIPs, involving the co-transfection of eight plasmids (including seg 2 DI encoding plasmid) in a mammalian co-culture expressing PB1 (missing protein in seg 2 DIPs). The table (right) displays the tested concentrations of the DI encoding plasmid and seven full-length encoding plasmids for the reconstitution. B) Illustrates a similar process for seg 3 DIPs, utilizing a PA expressing mammalian co-culture instead. The legend table details the concentrations of DI plasmid tested during the rescue. The resulting viruses from both seg 2 and seg 3 processes were further amplified in triple-positive MDCK-PB2-PB1-PA cells. The red box indicates the failure in rescuing or amplifying either seg 2- or seg 3-derived DIPs, indicating failure to detect any infectious or total virus titers.

4.1.6. Newly identified seg 1 DIP candidates demonstrate potent antiviral activity

To evaluate whether the new seg 1 DIP candidates that exhibited rapid propagation (Figure 4.1.1) would also display potent antiviral properties, an in vitro interference assay was conducted. The reconstituted DIPs (Figure 4.1.5) were amplified in suspension MDCK-PB2 cells (at an optimal MODIP of E-2, performed by Lars Pelz). This resulted in seed viruses with infectious virus titer of 8.0×10^7, 8.4×10^7, and 2.4×10^8

PFU/mL for the loser, winner, and de novo candidate, respectively. Additionally, the prototype seg 1 DIP, DI244, was included in the assay to compare its interfering efficacy. In the interference studies, MDCK-WT cells were infected with STV at an MOI of 0.01 for 24 h and co-infected with various DIPs to assess the inhibition of STV propagation by the DIPs. To facilitate direct comparison among different DIPs in the interference studies, the DIP input of the different seg 1 candidate DIPs and DI244 was normalised based on total virus titer (based on seg 1 winner titers, measured in $\log_{10}$ HAU/100µL).

STV replication reached 1.9×10^9 PFU/mL and was significantly reduced to a total infectious virus titer of 5.7×10^3 PFU/mL by co-infection with the de novo DIP (Figure 4.1.9A). This strong suppression of STV, exceeding five orders of magnitude, was significantly greater than that achieved by DI244 (resulting in infectious virus titers 2.1×10^5 PFU/mL). Similarly, strong suppression in STV titers was observed upon co-infection with the winner DIP, reducing the infectious virus titers to 2.4×10^4 PFU/mL. Conversely, the seg 1 loser DIP exhibited antiviral activity comparable to DI244, both reducing STV propagation by approximately four orders of magnitude. Similar trends of reduction in total virus titers could be observed in the HA assay (Figure 4.1.9B), although the effect is not very pronounced as reflected in the statistical analysis (no significance, using ANOVA analysis with Tukey's comparison test).

In summary, a semi-continuous process was utilized to cultivate STVs and DIPs over 21 days, and NGS was employed to identify new seg 1 DIPs. These DIPs were reconstituted using modified reverse genetics and tested for antiviral activity in vitro. Furthermore, the hypothesis derived from these evolutionary studies was confirmed: stronger antiviral activity is exhibited by fast-propagating DIPs compared to slow-propagating DIPs, leading to their accumulation in higher fractions. Consistent with this hypothesis, it was observed that the loser DIP (or the previously known and well-characterized DIP, DI244) exhibited weaker suppression of STV compared to either de novo or winner DIP in the interference assay.

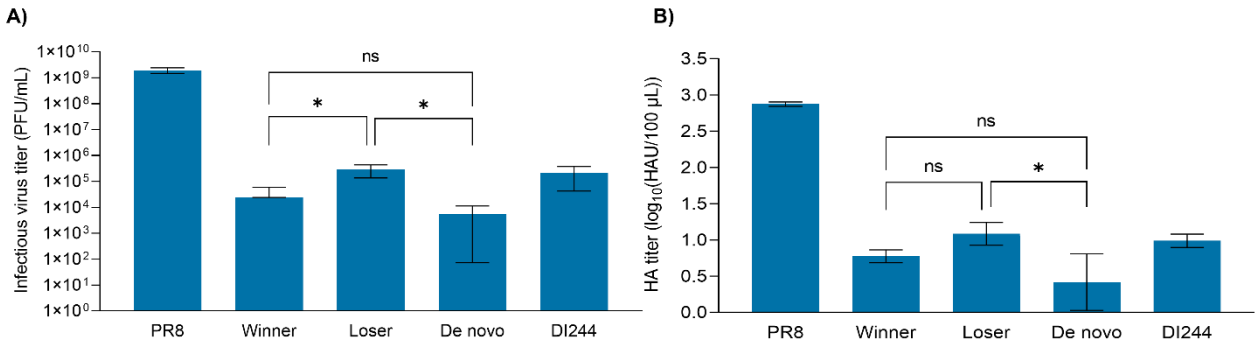

Figure 4.1.9. Evaluation of the interfering efficacy of novel seg 1 DIP candidates. The newly rescued seg 1 DIP candidates (Figure 4.1.5) were expanded in MDCK-PB2 suspension cells in shake flasks (conducted by Lars Pelz). Next, the seed virus material was tested in the interference assay. MDCK-WT cells were either infected with STV at a MOI of 0.01 for 24 h or co-infected with DIPs at a normalized quantity of 4.25×10^8 virions (virus particle count was calculated based on HA titers). DI244 served as a benchmark seg 1 DIP for comparison within the assay. A) Infectious virus titers, quantified by plaque assay. B) Total virus titers, expressed by HA titers. Three separate experiments were conducted (n=3). Statistical significance was assessed using ANOVA analysis with Tukey's comparison test, where $p<0.05$ indicates significance (*) and $p>0.05$ denotes non-significance (ns). Error bars indicate SD. Figure is adapted from Pelz, Ruediger, Dogra et al., [1].

4.1.7. Discussion I

Earlier studies on IAV DIPs to understand their mechanisms of action, such as the well-documented seg 1 DIP DI244 by Dimmock et al., were constrained because DIPs were propagated with STV in eggs [2, 17]. The resulting virus mixture needed to be enriched for the DIP and subsequently UV-inactivated (to eliminate the infectious STV) before testing for antiviral activity. This limited the elucidation of DIP replication mechanisms, their mode of actions and thereby their potential therapeutic uses [2, 36]. Bdeir et al., advanced DIP research by modifying the IAV reverse genetics system to generate DIPs using complementing cell lines. Specifically, their research focused on producing seg 1 DIP DI244, by using a co-culture of HEK and MDCK cells that express the PB2 protein [6]. While DI244 served as a model for proof-of-concept studies, its commercialization for antiviral or vaccine development that are based on DIP technology is hindered by existing patents.

To identify IAV DIPs with enhanced antiviral activity, the study was initiated by examining the natural occurrence and evolution of conventional DIPs in an in vitro system. A seed virus (PR8) depleted of DIPs was utilized and cultured in MDCK-WT cells within a shake flask-based semi-continuous system [1]. Periodic oscillations in

virus titers were observed in this setup (Figure 4.1.1). Different types of DIPs were generated from different IAV segments over a 21 day infection period. To analyse the diversity of DI vRNAs, an Illumina-based NGS approach combined with the ViReMa algorithm was employed [77], allowing for the identification of each specific deletion junction within the DIPs.

During semi-continuous infection, following an STV infection, oscillatory patterns emerge which are characterized by fluctuations in total and infectious virus particles. These oscillations in virus titers are influenced by the changes in DIP concentration over time. This is due to the interaction between STV and DIPs, marked by competition for resources (required for virus replication and growth), which results in a decrease in infectious virus titers as DIPs accumulate [90, 147]. Initially, at 0.5 d.p.i., a peak in infectious virus titers (high MOI) was observed, coinciding with the production of DIPs (Figure 4.1.1B). DIPs start to replicate faster than the STV and their accumulation (high MODIP) decreases replication of STV. Thereby, both the total virus and infectious titers decrease over time. As a consequence, due to the low STV concentration, DIP replication ceases as, and both the DIPs and STVs are out-diluted by the semi-continuous feeding [1]. This reduction in DIPs allowed the STV to resume its propagation, leading to high virus titers again. Subsequently, there is a gradual increase in the probability of co-infection with DIPs, which again leads to an accumulation of DIPs and perpetuates the cycle of oscillation.

NGS analysis of the viral harvest from different time points clearly suggested that the highest variation in deletion junctions was observed in the polymerase-encoding segments. This was consistent with other reports, where polymerase-based IAV DIPs are usually present in the in vitro cultivations [148, 149]. As the deletion junctions in non-polymerase-encoding segments were significantly less common, it was decided not to analyse them further [1].

It was hypothesized the length of these newly generated DI vRNA should play an important role in their propagation and accumulation. Since shorter DI vRNA can replicate faster [34, 150], it was assumed they would also have a stronger propagation profile over the infection period. Although a high abundance for shorter DI vRNAs was found, high fractions of DI vRNA were found around an optimum length with a mean ranging between 366 – 414 nucleotides for seg 1, 2 and 3, suggesting a balance

between length and replication efficiency. The position of deletion junctions has been indicated as significant, potentially influencing the packaging of DI vRNA [1, 25, 44]. In this study, it was found that the retention of nucleotides encoding for the incorporation signals (part of the packaging signals important for vRNA packaging into progeny virions) was necessary for the propagation of DIPs [151]. However, the complete bundling signal (which helps in the selective packaging of all eight different segments) was not necessary for the propagation of DIPs, particularly for seg 1 and 2 [1, 44]. This suggests that the replication and packaging of the DI vRNAs have specific requirements, which could impact our understanding of viral evolution, replication dynamics, and the development of antiviral strategies.

The study identified significant changes in deletion junction composition from 0 to 21 d.p.i.. Tracking these junctions revealed that the top winner and de novo DIPs accumulated notably more than other DI vRNAs (Figure 4.1.1C), while the top loser declined significantly. This indicated a competitive growth among DI vRNAs, resulting in a pronounced selection for certain DI vRNAs over others. This competition appears to be influenced by various factors, including length, position of the breaking points, and retention of essential packaging signals [1]. It was hypothesized that the fast-growing DIPs would exhibit stronger interfering activity due to their rapid replication compared to slow-growing DIPs. Consequently, these fast-propagating DIPs would sequester the cellular and viral resources necessary for STV replication more than slow-growing DIPs, thereby demonstrating higher antiviral activity.

To confirm this hypothesis, different DIP candidates had to be cloned and rescued before testing their antiviral activity. The initial step was to transfer the technology for clonal DIP reconstitution using reverse genetics from DPZ Göttingen to the MPI in Magdeburg, which constituted the foundation of this thesis. This involved establishing cloning methods, such as SOE, Golden Gate cloning, and reverse genetics systems, specifically developed for clonal DIP rescue. Moreover, the development of RT-qPCR techniques was necessary for the precise quantification of various deletion junctions in seg 1 DIP candidates.

Previously, it was suggested that self-interference might influence the DIP reconstitution process, leading to extended periods of reconstitution when compared to STV [6, 138]. In STV reconstitution experiments, a pronounced CPE was typically

observable by day 4 d.p.t., peaking at 6 d.p.t., when all cells in the transfected well had perished. Conversely, in the case of DIP rescues, the onset of CPE was not evident until 6 d.p.t., with the reconstitution process extending up to 13 d.p.t. Consequently, it was imperative to experiment with varying plasmid amounts encoding the DI vRNA (to rule out the effects of self-interference), which were typically tested at either 50 ng or 1 µg. For the seg 1 DIP winner, the successful rescue was achieved at both amounts, whereas for the seg 1 loser, only the 50 ng amount proved successful, as determined from various transfection harvest times (refer to Figure 4.1.5B). Despite no detectable virus titers for seg 1 de novo DIPs, a significant CPE was consistently observed (data not shown). To enhance the volume and titers of rescued seed virus banks, DIPs were propagated in adherent MDCK-PB2 cells. The literature indicates that any modified IAV requires propagation through numerous serial passages in either eggs or cells to facilitate growth and detection of the virus, a process also hoped to increase the titers of de novo DIP [152, 153]. Therefore, the seg 1 DIP candidates were amplified in MDCK-PB2 cells (Figure 4.1.5C) using reconstitution approaches with 50 ng of DI sequence-encoding plasmids (as shown in the lower part of Figure 4.1.5B). A decision to harvest was made when a CPE of over 50% was noted, marked by cell death and gaps in the cell layer. Supernatants were harvested at 48 h.p.i.. As depicted in Figure 4.1.5C, both seg 1 loser and winner candidates reached high titers, surpassing 1.0×10^8 PFU/mL. However, no titers were found for the de novo seg 1 DIP, despite the observation of a CPE in the plaque assay. Segment-specific PCR testing was used to ensure the integrity of the DIPs and to identify other contaminating DIPs. The PCR results for both the loser and winner seg 1 candidate showed a pronounced seg 1 DIP signal of expected sizes on agarose gels (Figure 4.1.6A), along with a weaker band for the de novo DIP (Figure 4.1.6A), suggesting that further amplification was necessary for the de novo DIP to reach detectable virus titers. To assess whether the de novo DIP could achieve detectable virus titers, Lars Pelz performed infections in MDCK-PB2 suspension cells. As shown in the Supplement figure 7.1, the seg 1 de novo DIP reached very high titers, approximately 2.8 $\log_{10}$(HAU/100 µL) at 24 h.p.i..

Segment-specific DIP PCR and agarose gel electrophoresis were repeated on samples amplified in suspension MDCK-PB2 cells to verify the absence of contaminating DIPs that were present in the initial amplifications in adherent MDCK-PB2 cells (Supplement figure 7.2 compared to Figure 4.1.6A). This procedure aimed

to determine if amplification under optimized, low MOI conditions, as opposed to blind amplifications, resulted in the dilution of contaminating DIPs in the final DIP harvest. This would produce samples more suitable for in vitro or in vivo antiviral activity testing, with the activity attributed to the specifically cloned DIP. To exclude contamination with infectious STV in the amplified samples, an innocuity assay was conducted (described in Section 4.1.4, Figure 4.1.6B), which confirmed the absence of infectious STV.

Subsequent interference studies in MDCK cells, as detailed in Figure 4.1.9, demonstrated that winner and "e novo, exhibited significantly stronger antiviral activity compared to the previously characterized DI244 and the loser DIP. This finding underscores the potential of experimental evolution approaches to identify superior DIPs that outperform other DIPs in terms of antiviral efficacy [73, 154, 155].

Unexpectedly, attempts to replicate these results with seg 2 and seg 3 candidate DIP were unsuccessful. Although a strong CPE was noted, infectious virus titers were absent. This was despite the presence of viral proteins in the complementing cell lines used for the DIP reconstitution, as confirmed by western blot analysis (see Supplement figure 7.3). Furthermore, attempts to amplify these DIPs using triple-positive suspension MDCK-PB2-PB1-PA cells (conducted by Lars Pelz), also failed to produce detectable virus titers. These results highlight the challenges faced in the amplification of both segments. Interestingly, the use of triple-positive cell lines for the rescue and amplification of a seg 1 and seg 3 double DIP resulted in a viable DIP with detectable virus titers [138]. This points to the potential use of chimeric viruses for the rescue of DIPs (WSN backbone with PR8 vRNA-based DI vRNA) [138]. The inherent challenges in generating DIPs with a PR8 backbone for seg 2 and 3, as opposed to the relatively easier rescue of WSN-based constructs, suggest that the choice of viral backbone plays a crucial role in the feasibility of DIP rescue and amplification. However, the use of WSN is further complicated by its neurotropism, which limits its practical applicability as an antiviral for human medical use [156, 157].

In conclusion, while the study faced challenges in rescuing and amplifying DIPs based on seg 2 and 3, the successful identification and characterization of potent antiviral DIPs from seg 1 provide a solid foundation for future investigations. The findings from this study highlight the importance of identifying DIPs that can be easily rescued and grown to high titers. For example, the seg 1 winner or de novo DIPs serve as promising

avenue for in vitro and in vivo antiviral activity studies but also hold potential for future applications in medical research, including the development of novel antivirals and vaccines (refer sections 4.2 and 4.3).

4.2. Improved DIP constructs for use as live vaccines

4.2.1. Reconstitution of seg 1-based DIPs for use as live vaccine

Following the successful generation of new seg 1 DIP backbones, which propagated to very high titers in suspension MDCK-PB2 cells and showed superior antiviral efficacy compared to DI244 [1], the next goal was to modify the DIP constructs further. These modifications would elicit adaptive immune responses against seasonal infections, facilitating the application of DIPs in vaccination strategies. For this, the focus was on developing a live seg 1 DIP-based vaccine. Figure 4.2.1A depicts the design of such a vaccine construct, in which the surface glycoproteins (HA and NA) of seg 1 DIP are replaced with those from the pandemic strain A/California/04/2009 (Cal H1N1) [123, 158] for the proof of concept. The WHO had recommended the Cal H1N1 strain for the 2009 pandemic vaccination campaigns and as a seasonal vaccine until 2016, using its surface antigens to direct immune responses. Evaluation of the vaccine seed viruses (previously generated using egg-based reassortment methods) revealed that in addition to HA and NA, the PB1 segment from the pandemic virus strain was frequently incorporated. This co-segregation of the segment provided a significant growth advantage over the PB1 gene segment derived from PR8 [76, 123, 159, 160]. Pursuing this approach, PB1 from Cal H1N1 was also included in the seg 1 DIP-vaccine construct (Figure 4.2.1A). As seg 1 winner DIP was easy to reconstitute over the range of different DI plasmid concentrations and was easily amplified to high titers in MDCK-PB2 suspension or adherent cells (Figures 4.1.5 B, C and 7.1). Therefore, seg 1 winner was used as the PR8 derived DIP backbone for live DIP-vaccine reconstitutions (Figure 4.2.1A and 4.1.5).

To verify the feasibility of reconstituting a pandemic strain within the PB2-expression system, reconstitution of Cal H1N1 (8 plasmid scheme, refer to condition 1 in Figure 4.2.1B and legend) was evaluated as a control. Based on literature, the pandemic virus exhibited slow growth and lower titers [123, 161]. The reconstruction of Cal H1N1

(condition 1) corroborated this observation, yielding a measurable infectious virus titer of 7.6×10^4 PFU/mL following a round of blind amplification of the rescue harvests in MDCK-PB2 adherent cells. A control vaccine strain virus rescue (condition 6, Figure 4.2.1B) was also conducted which comprised a 5+3 genome constellation with PB1, HA, and NA from Cal H1N1 with remaining segments derived from PR8. The reassortant strain achieved an infectious virus titer of 6.4×10^4 PFU/mL after blind amplification in MDCK-PB2 adherent cells.

The reconstitution of the DIP-vaccine construct was attempted following the successful creation of the vaccine strain virus construct. This was done by co-transfecting seg 2, 4, and 6 (which encode for PB1, HA, and NA) from the Cal H1N1 strain into the PR8 backbone including seg 1 winner DI-encoding plasmid and PB2 expressing cells (conditions 4 and 5, as shown in Figure 4.2.1B). However, this approach did not yield any viable virus after rescue and in the following blind amplification attempts in MDCK-PB2 cells. To investigate the possible mismatch in combining seg 1 DIP (due to a significant deletion in seg 1 vRNA, and based on PR8 strain origins) with a pandemic strain, seg 1 DI plasmid was introduced into the Cal H1N1 reconstitution setup (genome composition of 1+7, conditions 2 and 3, Figure 4.2.1B). However, this attempt also did not lead to the successful rescue or amplification of the virus.

Overall, the reconstitution of a Cal H1N1 virus-based CVV comprising a 5+3 genome constellation in the PR8 backbone was successfully achieved using the PB2-mammalian expression system. However, the efforts to reconstitute a seg 1-based DIP vaccine expressing Cal H1N1's HA and NA are still ongoing.

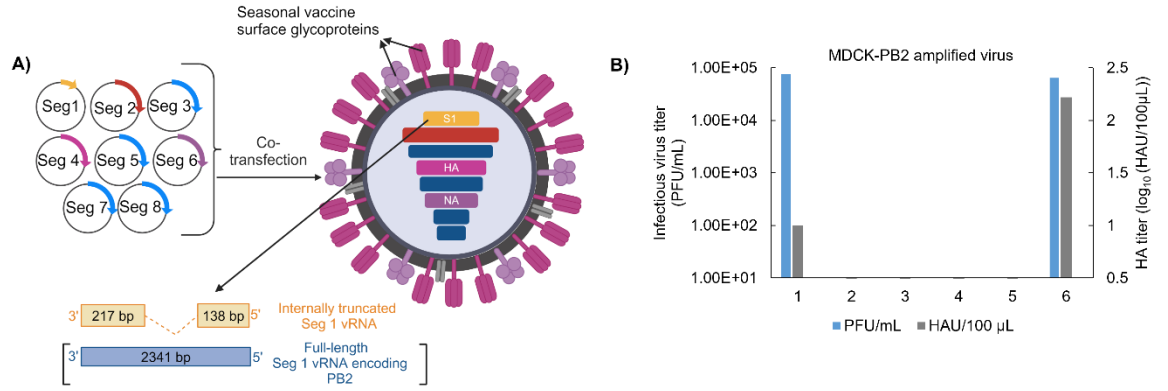

	Conditions labelled	Virus type (genome constellation)	DI plasmid	California-based plasmids (1 µg)	PR8-based plasmids (1 µg)	harvest time point
HEK-PB2 + MDCK-PB2	1	Cal H1N1 (8)	-	Seg 1-8	-	4 d.p.t.
	2	Seg 1 + Cal H1N1 (1+7)	1 µg	Seg 2-8	-	4 d.p.t.
	3	Seg 1 + Cal H1N1 (1+7)	50 ng	Seg 2-8	-	4 d.p.t.
	4	Seg 1 + Cal H1N1 (3+5)	1 µg	Seg 2,4,6	Seg 3,5,7,8	4 d.p.t.
	5	Seg 1 + Cal H1N1 (3+5)	50 ng	Seg 2,4,6	Seg 3,5,7,8	4 d.p.t.
	6	PR8 + Cal H1N1 (3+5)	-	Seg 2,4,6	Seg 1,3,5,7,8	4 d.p.t.

Figure 4.2.1. Reconstitution and amplification of live IAV DIP-vaccine construct. A) Visual representation for the reconstitution of seg 1 DIPs live vaccine constructs through the use of eight plasmids, including the seg 1 winner DI encoding plasmid alongside seven full-length encoding plasmids. The seg 2, 4, and 6 plasmids are derived from the A/California/04/2009 (Cal H1N1) strain, the remaining segments are derived from PR8. B) Conditions tested to generate controls or the DIP vaccine constructs. Experiments were conducted with 50 ng or 1 µg of the DI encoding plasmid, as detailed in the accompanying table. As controls in the experiments, condition 1 involved the rescue of the Cal H1N1 strain using all eight full-length encoding plasmids from the Cal H1N1 strain. Condition 6 represents seg 2, 4, and 6 of the Cal H1N1 strain and the remaining segments from PR8. For DIP vaccine constructs 5+3 and 1+7 genome constellations of PR8: Cal H1N1 were tested (conditions 2-5). Plasmid concentrations for segments (and their strain of origin) are mentioned in the table. Infectious virus titers were measured post-amplification using a plaque assay.

4.2.2. Discussion II

The segmented genome of IAV, plays a crucial role in the virus's ability to undergo reassortment. During reassortment, vRNA segments can be exchanged among different IAV strains when they co-infect a host cell. This exchange facilitates the creation of new virus variants, complicating the prediction of season's infection-causing strains [9]. Furthermore, the successful packaging of vRNA segments into new virions, essential for producing infectious offspring, depends on specific signals for proper assembly [44, 151]. This packaging process is closely linked to reassortment, highlighting the intricate mechanisms behind IAV's evolution and spread. Such complexity poses significant challenges to the development of vaccines.

Plasmid-based reverse genetics and cell culture technology significantly extended options to optimise vaccine candidate strains for immediate, direct, and vast-scale

production of the IAV vaccine [121, 129]. After the FDA approved these methods for generating IAV vaccine strains in 2012, widespread adoption was anticipated [158]. WHO recommended candidate vaccine viruses (CVVs) generated with reverse genetics are approved for use in many countries, including developed economies such as in USA and Europe. The process involves incorporating 6 internal genes from a high growth reassortant (e.g., PR8) along with 2 surface antigens derived from the donor vaccine virus (a seasonal strain). This allows to improve vaccine matching efficiency for eliciting an immune response to circulating strains. Subsequently, inactivated formulations of these viral constructs are used for vaccination purposes. But these inactivated vaccines compared to LAIVs have their drawbacks including weaker immune responses, administration routes etc.

Since the 1960s, LAIVs have been proposed as a substitute for conventional inactivated influenza vaccines. While inactivated vaccines are typically administered through intramuscular injections and are effective at inducing a strong systemic humoral immune response, primarily through IgG antibody production, which provides long-term protection [162]. In contrast, LAIVs are designed to stimulate local mucosal immunity. This includes T cell-mediated responses and the production of IgA antibodies [163]. These local immune responses offer enhanced protection against pathogens at the initial site of infection in respiratory diseases [164]. Despite these advantages, the development of LAIVs faces several challenges. These include the need to identify a safe viral backbone for the construction of vaccine, as there is a risk of reversion to the virulent parental strain in recipients. Additionally, LAIVs may have reduced efficacy in individuals with compromised immune systems [165]. To overcome these issues, seg 1 DIPs (potent antivirals as proven in different studies in vitro and in vivo so far), which cannot replicate in systems without PB2 expression [1, 4, 30, 37, 83] might be useful. By modifying these DIPs to express the surface antigens of seasonal IAVs (HA and NA), the aim is to stimulate adaptive immune responses against seasonal strains. This could offer several benefits such as mimicking natural infection that elicits broader immune responses (IgG and IgA responses with strong resident memory B and T cells). Besides, given the replication-deficient characteristic, the new DIP-based vaccine construct could demonstrate enhanced safety profile compared to conventional LAIVs.

The generation of seed virus using reassortment technique, either in eggs or cell cultures, involves an extensive screening process for the selection of a CVV with optimal growth and suitable seasonal surface antigens. This method was favoured and widely utilized over reverse genetics in recent years (between 2017-2023, seasonal CVVs for IAV as recommended by WHO [166]). This preference for reassortment, despite its complexity, may suggest challenges in the reconstitution using reverse genetics of new seasonal strains [166]. The genotypic analysis of the 2009 H1N1 pandemic vaccine virus strains suggested a high likelihood of co-segregation of specific vRNA segments apart from HA and NA. Notably, the PB1 vRNA segment from the seasonal vaccine strain was the most prevalent in the reassorted vaccine strain [123, 124]. This finding led to the exploration of the 5+3 genome configuration (condition 6, Figure 4.2.1B) along with the incorporation of the deleted seg 1 into this genomic constellation (conditions 4-5, Figure 4.2.1B). In this construct, emphasis was given to the critical role of the PB1 segment from the Cal H1N1 strain in the construct's reconstitution and growth [167]. However, all efforts to produce a seg 1 DIP expressing Cal H1N1 surface proteins were unsuccessful in this established “5+3” constellation.

Reassortment is a widely used method for reconstructing vaccine viruses, though its mechanism is not fully understood. Literature particularly regarding the 2009 H1N1 pandemic strains, emphasized on the role of PB1 segments derived from seasonal vaccines to generate a vaccine virus [123, 124]. Yet, research from various sources present conflicting perspectives on the significance of the PB1 segment from seasonal strains in vaccine strains.

Mostafa et al., found that the PB1 segment from the 2009 pandemic IAV isolate, A/Giessen/06/2009 H1N1, significantly enhanced the replication efficiency of PR8-derived recombinant vaccine viruses (5 (PR8) + 3 (PB1/HA/NA Giessen) constellation) [168]. Conversely, when reverse genetics were employed to create vaccine viruses for the H3N2, H5N1, H7N9, and H9N2 subtypes, using the PB1 segment from A/Giessen/06/2009 H1N1 along with strain-specific surface antigens in the PR8 backbone (5 (PR8) + 2 (HA/NA strain-specific) + 1 (PB1 Giessen) constellation), the resulting titers were comparable to those of viruses that contained the native PB1 segment from seasonal viruses in the PR8 backbone (5 (PR8) + 3 (PB1/HA/NA strain-specific) constellation) [168]. This indicates that the integration or co-segregation

phenomenon observed in certain pandemic vaccine viruses after reassortment is strain-dependent. Cobbin et al., similarly observed that selecting the PB1 segment from a seasonal strain (A/Udorn/307/72 H3N2) did not favour the emergence of a highly replicative virus [169]. This was shown by the reassorted vaccine strain exhibiting lower growth titers when compared to viruses that combined the PR8 PB1 with HA and NA from the seasonal strain within a PR8 virus backbone (5 (PR8) + 3 (PB1/HA/NA Udorn) constellation).

In our study, reconstitution of the Cal H1N1 virus (condition 1, Figure 4.2.1B), seg 1 winner DIP (Figure 4.1.5 B, C), and a CVV based on the co-segregation of seg 2, 4, and 6 of Cal H1N1 on a PR8 backbone under a 5+3 constellation (condition 6, Figure 4.2.1B) have been successfully reconstituted. However, the addition of a seg 1 DI vRNA from the PR8 strain introduced complexities in the CVV reconstitution process (conditions 4 and 5, Figure 4.2.1B). Potentially, the large internal deletion in seg 1 derived from the PR8 strain likely exacerbated these challenges, alongside the observed co-segregation phenomenon with seg 2, 4, and 6 from Cal H1N1. This concept is supported by previous research that demonstrated successful reconstitution of seg 1 DI vRNA from PR8 on a WSN backbone [138]. In contrast, our attempts to reconstitute the seg 1 DI vRNA of PR8 origin on the remaining 7 segments of Cal H1N1 were not successful (1+7 constellation; conditions 2 and 3, Figure 4.2.1B). This outcome suggests two critical factors for the development of a DIP-based live vaccine: backbone compatibility to propagate pandemic/seasonal IAV strains and the influence of UTRs and packaging signals on the co-segregation of vRNA from different strains.

To better understand these challenges, it is important to note that effective LAIVs require a backbone capable of propagating to high titers. Therefore, a mismatch in UTRs of the DI vRNA carrying segments (originating from the PR8 strain, a high-propagating IAV strain) and the UTRs of segments derived from seasonal strains may result in the failure to reconstitute CVVs or achieve low titers after multiple amplifications. Supporting this hypothesis, RNA structural studies have highlighted the importance of IAV strains involved in the reassortment process to generate a CVV [170]. These studies have been instrumental in elucidating how the structure of vRNA might influence reassortment due to mutations in the RNA structures within the UTRs (see below). This indicates that alterations at the RNA structural level may play

contribute to the adaptation of the RNA virus, providing insights into the emergence of new strains.

Dadonaite et al., showed that each IAV segment adopts unique RNA conformations within a virion, potentially influencing RNA interactions both within and between segments [171]. Therefore, any nucleotide changes could lead to alterations in RNA structure, affecting the interaction network among different segments. Thus, UTR compatibility is an important consideration. Furthermore, the significance and function of UTRs in RNA interactions have been thoroughly investigated, revealing that the assembly of virions is a highly specific process. Studies by Gao et al., and Zheng et al., have demonstrated that altering the UTR sequences between the HA segment and other segments significantly affects the reassembly and immunogenic properties of vaccine strain constructs [172, 173]. In their experiments, packaging signals from seg 4 and 6 were interchanged to create a chimeric virus. This involved flanking seg 4 of A/Hong Kong/4801/2014 (HK14) with the packaging signals of seg 6 from the PR8 strain and vice versa for seg 6 of HK14. The resulting chimeric segments were used to produce an HK14 swap virus, which elicited a stronger humoral antibody response to NA compared to the wild-type HK14. This enhanced response was attributed to increased NA expression on the virus surface, a consequence of swapping the UTRs of seg 4 and 6 from the PR8 strain. This swap likely facilitated better growth of the rescued virus in the PR8 backbone compared to using HK14 UTRs. Accordingly, this approach could serve as an alternative in our research. Substituting the UTRs of the HA and NA segments of the Cal H1N1 strain with those from PR8 should be considered and tested. This substitution could potentially facilitate the reconstitution of the conventional 6+2 genome constellation in vaccine strains, independent of the seasonal strain-derived PB1 gene segment, as illustrated in conditions 4 and 5 of Figure 4.2.1B.

Apart from the UTR compatibility between reassorting strains, packaging signals inside the coding regions could influence the RNA-RNA interactions, thereby influencing the generation of a CVV. For example, earlier it was assumed that only minimal terminal ends of the vRNA are necessary for proper incorporation of the DI vRNA in the virion [25, 34]. However, further research has highlighted the significance of internal packaging sequences that extend beyond UTRs into protein-coding regions [174-176]. Nevertheless, the existing body of research does not yet provide a thorough

understanding of the mechanisms behind the formation and selection of genome constellations after reassortment among various strains in the context of vaccine strain development. This would also mean that the size of the deletion junction, particularly sequences within the protein-coding region of seg 1 DI vRNA, might be crucial for establishing effective RNA interactions with the 2009 H1N1 strain. Such interactions could facilitate the reassembly of seg 1 DI vRNA with seg 2–8 of Cal H1N1 (refer to Figure 4.2.1B, conditions 2 and 3). A potential strategy for achieving this may involve substituting the seg 1 winner DI vRNA, which has a significant internal deletion, with another DI vRNA that has a smaller deletion junction. Hence, "increasing the packaging signal length" might increase the likelihood of successful rescue. If successful, this might allow for the creation vaccine strains with a deletion junction in seg 1, which are exclusively viable in PB2 expression systems.

However, this hypothesis is speculative at the moment, with the reduced number of constructs tested owing to the practical limitation of the number of varieties of constructs that could be tested in an experiment. To clarify whether the unsuccessful reconstitution is attributed to a discrepancy in UTRs between the vRNA segments of the Cal H1N1 strain and those of the PR8 strain or due to the significant deletion that excludes crucial packaging signals, it would be important to conduct a control experiment using a 1+7 constellation with seg 1 FL from PR8 and the remaining 7 segments from Cal H1N1 as controls to the 1+7 tested in the current experimental setup under conditions 2 and 3, Figure 4.2.1B.

Clearly, future studies are required to address the unanswered questions related to the integration, packaging, and modification in DI vRNA structures. These issues could significantly affect the manipulation of DIPs for use as a basis for developing new antiviral treatments or vaccine alternatives. Importantly, in the context of a pandemic, the priority is to adopt methods and processes that enable the rapid development of a vaccine strain that is simple to manipulate and can be propagated to high titers in cell cultures. Therefore, it's vital to persist in the exploration of DIPs, particularly those based on the PR8 backbone—a preferred choice for vaccine producers due to its high-growth capabilities—in terms of mutations and packaging. This will help identify the obstacles that hinder the generation of a versatile virus construct. The aim should be to introduce mutations that can adapt to seasonal strains and facilitate easy reconstitution and growth to high titers, or seek a new DIP backbone, similar to

ongoing efforts to enhance PR8-based LAIVs. Ultimately, the goal is to establish a DIP backbone platform that allows for easy manipulation and swift production of vaccine.

4.3. Generation of OP7 chimera DIPs without infectious standard virus

4.3.1. OP7 appears to be a defective particle

The point mutations harboured in seg 7-OP7 vRNA were not fully characterised yet. Previously, it was shown that OP7 shows interference with STV replication, similar to conventional DIPs [5, 38]. In addition, it was demonstrated that OP7 appears to be a defective viral particle, incapable of completing a virus replication cycle without co-infection with STV [38]. Yet, direct proof that OP7 virions are indeed defective in virus replication was missing.

To address this, a reverse genetics approach to reconstruct infectious PR8 was employed. As depicted in Figure 4.3.1, condition 1 involved co-culturing HEK-WT and MDCK-WT cells that are transfected with eight plasmids (each based on the pHW2000 backbone and encoding a full-length segment) at an amount of 1 µg per plasmid, to reconstitute clonal PR8 IAV as a control. At day 6 post-transfection, an infectious virus titer of 5.2×10^3 PFU/mL was observed, as determined by plaque assay (Figure 4.3.1). Transfection efficiency was also assessed using wells transfected with a GFP-encoding plasmid (data not shown). To explore the rescue of purely clonal OP7 DIPs containing seg 7-OP7 (but STV-free), a transfection was conducted using eight plasmids encoding full-length WT seg 1–6 and 8, with a plasmid for seg 7-OP7 at varying amounts (conditions 6–9, Figure 4.3.1). No infectious viruses were detected in any of the plaque assays following these rescues, regardless of the tested amount of the seg 7-OP7 plasmid. This absence of infectious virus titers thereby suggested the defective nature of seg 7-OP7 as OP7 may not be able to complete a replication cycle.

The next involved experimenting with an 8+1 plasmid constellation to co-rescue OP7 DIPs and STV. This involved the addition of a ninth plasmid encoding seg 7-OP7 to the eight plasmids used for PR8 rescue. Anticipating self-interference in the OP7 DIP rescue, varying amounts of the seg 7-OP7 encoding plasmid were tested (10 ng, 50 ng, 500 ng or 1 µg) as illustrated in conditions 2–5 of Figure 4.3.1. Notably, high infectious virus titers were detected for the PR8-OP7 rescue on the day 8 post-transfection, reaching 9.6×10^7 PFU/mL with 1 µg of the seg 7-OP7 plasmid.

Nevertheless, early infectious titers for the 8+1 construct were observed at lower amounts of the seg 7-OP7 plasmid (10 or 50 ng), with titers of 1.1×10^4 PFU/mL and 4.4×10^3 PFU/mL respectively by day 6 post-transfection, as shown in conditions 4 and 5 of Figure 4.3.1. Please note, that the 8+1 constellation presented here served as a prototype and was utilized as a control in this experiment. Future studies confirmed the presence of OP7 vRNA within the 8+1 constellation. This confirmation was achieved through RT-qPCR analysis, as detailed in sections 4.3.3 and 4.3.5 when OP7 vRNA is reconstituted with seg 1 DIPs. The RT-qPCR method precisely detected the presence of OP7 vRNA and monitored its propagation across successive passages. Additionally, this technique enabled the detection of seg 1 DI vRNA within the same sample sets rescued via the 8+1 reconstitution method (please refer to sections 4.3.2–4.3.5 for more details).

Previous efforts to recover OP7 DIPs by our collaborative partner at the DPZ, Göttingen, also failed to yield any infectious virus titers using an 8-genome constellation for OP7 rescue (see Supplement figure 7.4). The third attempt in our setup yielded similar outcomes (Figure 4.3.1, conditions 6-9). These repeated attempts have led to the conclusion that OP7 cannot be successfully recovered without addressing the underlying defect in seg 7-OP7. Until this defect is remedied, co-infection with STV, which compensates for the missing gene function of seg 7 WT, is necessary.

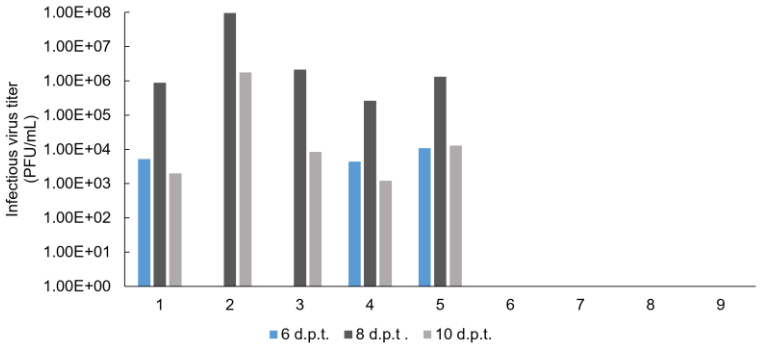

	Conditions labelled	Virus type (genome constellation)	PR8 plasmids (1 µg)	Seg 7-OP7 plasmid
HEK-WT + MDCK-WT	1	PR8 (8)	Seg 1-8	-
	2	PR8+OP7 (8+1)	Seg 1-8	1 µg
	3	PR8+OP7 (8+1)	Seg 1-8	500 ng
	4	PR8+OP7 (8+1)	Seg 1-8	50 ng
	5	PR8+OP7 (8+1)	Seg 1-8	10 ng
	6	OP7 (8)	Seg 1-6	1 µg
	7	OP7 (8)	Seg 1-6	500 ng
	8	OP7 (8)	Seg 1-6	50 ng
	9	OP7 (8)	Seg 1-6	10 ng

Figure 4.3.1. Attempt to reconstitute clonal OP7 DIPs using reverse genetics. IAV reverse genetics was employed to attempt the reconstitution of a clonal OP7 DIP. As a positive control, HEK-WT and MDCK-WT cells were co-transfected with eight plasmids, each encoding full-length WT segments, to create a PR8 virus (condition 1), detailed in the accompanying figure legend table. Infectious virus titers were measured using plaque assay following the rescues. As another control, to facilitate the rescue of OP7 DIP alongside STV, a ninth plasmid containing varying concentrations of the seg 7-OP7 sequence-encoding plasmid was introduced, depicted in conditions 2-5. To rescue a purely clonal OP7, a combination of eight plasmids was used, including one for seg 7- OP7 alongside plasmids for seg 1–6 and 8, all encoding full-length WT segments. This setup was further explored by testing different concentrations of the seg 7-OP7 plasmid (conditions 6–9 legend-table).

4.3.2. Reconstitution of OP7 DIP preparations free of infectious STV

So far, the research on OP7 has conclusively demonstrated its significant antiviral capabilities due to OP7 DI vRNA. Despite its strong antiviral activity, the identification of the mutations responsible for its defective phenotype is complicated due to the presence of the high number of mutations (37 point mutations) across different functional areas. This necessitates a comprehensive analysis before the development of an expression system aimed at rectifying this defect, akin to the system used for seg 1 DIPs that rely on PB2 expression.

Previous attempts to create an OP7 DIP virion-enriched virus material (Figure 4.3.1), showed that using a PR8-OP7 (8+1 genome constellation) rescue strategy led to the production of infectious virus titers potentially containing OP7 DIPs. Besides, the

earlier attempts to rescue only OP7 (8 genome constellation) failed to produce viable virus, likely due to OP7 being defective in virus replication. Inspired by the success of the 8+1 genome constellation method, the goal was to replicate this strategy, by employing the seg 1 DIP reconstitution framework to produce an OP7 DIP devoid of infectious STV.

The reconstitution process for seg 1 DIPs (Figure 4.3.2A–C) is based on an internally deleted seg 1, in which these newly generated DIPs can only grow in PB2-expressing cells. Figure 4.3.2A illustrates eight plasmids, with the first encoding the DI vRNA (in this case for the DI244 sequence), and the remaining plasmids encoding the seven full-length segments. These plasmids are co-transfected into PB2-expressing mammalian cells (Figure 4.3.2B), resulting in the production of a seg 1 DIP (Figure 4.3.2C).

The introduction and co-transfection of a ninth plasmid (Figure 4.3.2D) in the above system, led to the creation of a new DIP, termed “OP7 chimera” (Figure 4.3.2E). Through the co-transfection of nine plasmids, it is inferred that a population of DIPs is generated, including a conventional seg 1 DIP (containing DI244 vRNA, Figure 4.3.2C) and an OP7 chimera (containing DI244 and seg 7 OP7 vRNA, Figure 4.3.2E). The deletion in seg 1 limits the replication of these viruses to only PB2-expressing cells. Here, the presence of a fully functional WT seg 7 in the seg 1 DIP may act as a surrogate STV for the new OP7 chimera DIP during propagation in PB2-expressing cells. The mutations in seg 7-OP7 vRNA (that supposedly lead to the defect in virus replication of OP7) are compensated by the WT seg 7 of the seg 1 DIP.

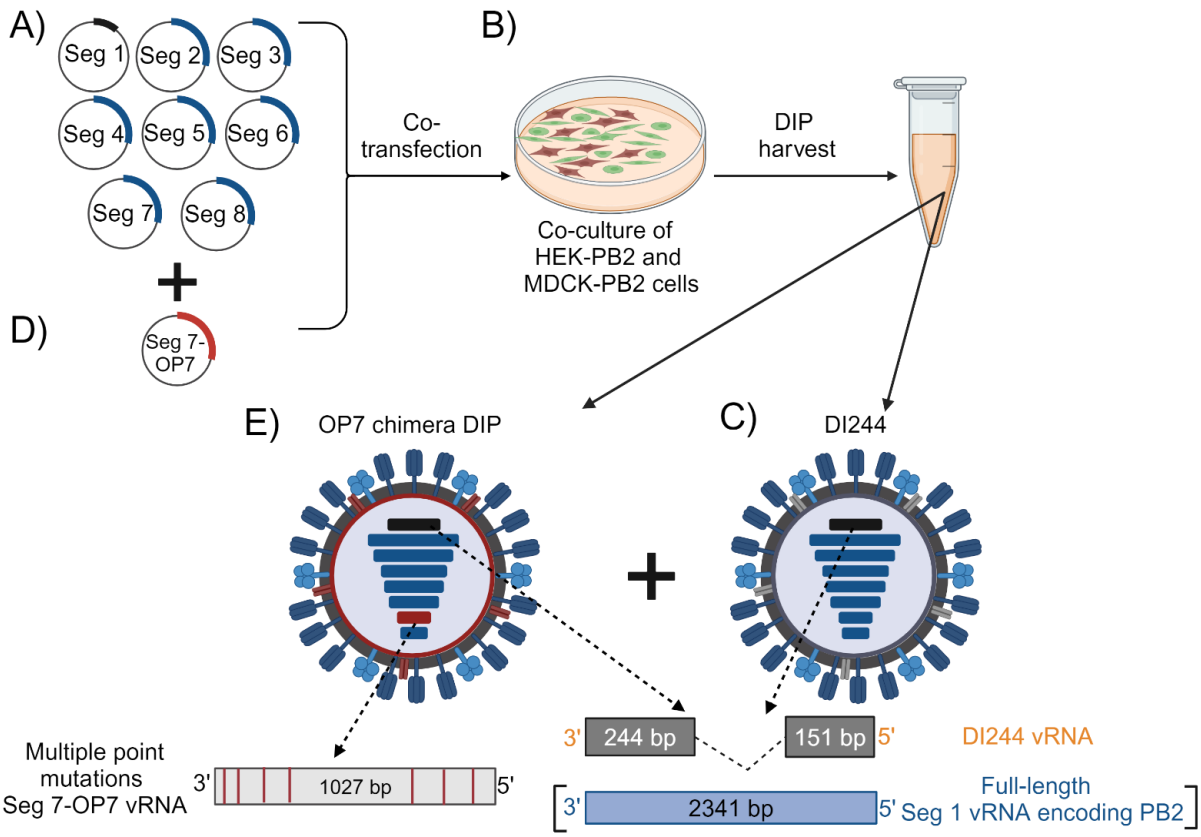

Figure 4.3.2. Reconstitution of OP7 chimera DIPs without infectious STV. A-C) Shows the reconstitution of seg 1 DIP, "DI244", using the modified reverse genetics scheme for seg 1 DIP rescue. Eight plasmids including a plasmid encoding for seg 1 DI244, along with seven full-length plasmids, are co-transfected into HEK-PB2 and MDCK-PB2 co-culture. The cells supply the PB2 protein, as DI244 in unable to encode complete and functional PB2 protein. D) The addition of a ninth plasmid encoding for seg 7-OP7 results in the reconstitute on of a population of DIPs, C) DI244, and E) OP7 chimera DIP, harbouring a deleted seg 1 (from DI244) and seg 7-OP7. Due to the deletion in seg 1, OP7 chimera exclusively propagate in PB2-expressing cells. The image was created with BioRender.com.

Based on learnings from the reconstitution of seg 1 DIP (section 4.1.4), a strong chance of self-interference during this rescue scheme was speculated. The introduction of an additional DI vRNA segment, particularly from OP7 (noted for its potent DI vRNA), was expected to complicate the rescue process further. Consequently, extensive screening was required to ensure successful reconstitution. Initially, as a baseline measure, the reconstitution of PR8-OP7 was reassessed using varying amounts of seg7-OP7 encoding plasmids. In these experiments, seg 7-OP7 plasmids were evaluated at amounts between 50 ng to 1 µg per well, while the amount of the remaining WT full-length encoding plasmids were maintained at 1 µg per plasmid per well (Figure 4.3.3A and table).

In contrast, as seen in Figure 4.3.3B, for the reconstitution attempts involving the OP7 chimera DIP with DI244 seg 1 vRNA, the seg 1 DI244 encoding plasmids were evaluated at amounts of 50 ng or 500 ng per well, with the amount of the OP7 encoding plasmid set at 50 ng per well. The reconstituted viruses were then propagated through blind amplification in MDCK-PB2 adherent cells, undergoing three serial passages of the virus supernatants for evaluation (Figures 4.3.3A, B and 4.3.4).

Additionally, Supplement figure 7.5 shows the results of further experiments using various amounts of plasmids encoding either the WT full-length segments, DI encoding seg 1, or seg 7. To mitigate the self-interference by the DIPs, plasmids encoding WT full-length segments were tested at a higher amount of 2 µg per plasmid per well. Using 50 ng of OP7 and 2 µg of DI244 encoding plasmid occasionally facilitated the reconstitution of the construct under specific conditions (1.2, 1.3, 2.2, 2.3, 3.3). Other tested variations with either lower amounts of plasmids encoding WT full-length segments (1 µg) or DI encoding segments (50 ng or 1 µg) were unsuccessful in supporting reconstitution. This underscores the importance of extensive screening for the successful reconstitution of complex DIP constructs and emphasizes the need to maintain the amount of seg 7-OP7 encoding plasmid at 50 ng per well in all reconstitution tests.

As an overall trend in the blind passaging of the PR8-OP7 construct, high levels of both total virus titers (measured in $\log_{10}$ HAU/100µL) and “infectious” virus titers (measured by plaque assays using MDCK-PB2 cells) were noted across various rescue conditions (as shown in Figure 4.3.3A), particularly during the first passage in MDCK-PB2 cells. Subsequent blind passages revealed a slight decrease in total virus titers, alongside a pronounced decline in infectious virus titers, suggesting potential interference by OP7. This observation implies that while virus particle production (as indicated by total virus titer) remains evident, the majority of these particles were non-infectious, possibly due to a higher prevalence of OP7-containing particles compared to infectious ones. Exceptionally, condition 6 is characterized by the absence of infectious virus titers in passage 2 and significantly reduced total virus titers, suggesting a substantial impact of MOI/MODIP on OP7 reconstitution. Specifically, during the second passage of the virus harvest, the infectious virus titers seemed to be markedly reduced due to OP7 interference, resulting in no detectable infectious progenies in the plaque assay. During the subsequent amplification (third passage of

the virus supernatant), the reduced MOI minimizes co-infections with the DIP, facilitating the growth of the infectious STV, which leads to a measurable plaque titer (conditions 6.2–6.3, Figure 4.3.3A).

On the other hand, Figure 4.3.3B, which illustrates titers of the DI244-OP7 chimera DIP after reconstitution across three consecutive passages, shows a more marked decrease in infectious virus titers through the passages. This suggests significant self-inhibition in the proliferation of infectious viruses, attributed to the inclusion of two DI vRNA types (DI244 and DI244-OP7chimera) in the progeny viruses.

In essence, serial passaging of constructs containing seg 7-OP7 resulted in a reduction in infectious titers, whereas the overall virus titers did not significantly decrease. This phenomenon may be explained by the inhibitory effect of seg 7-OP7 on the proliferation of STV.

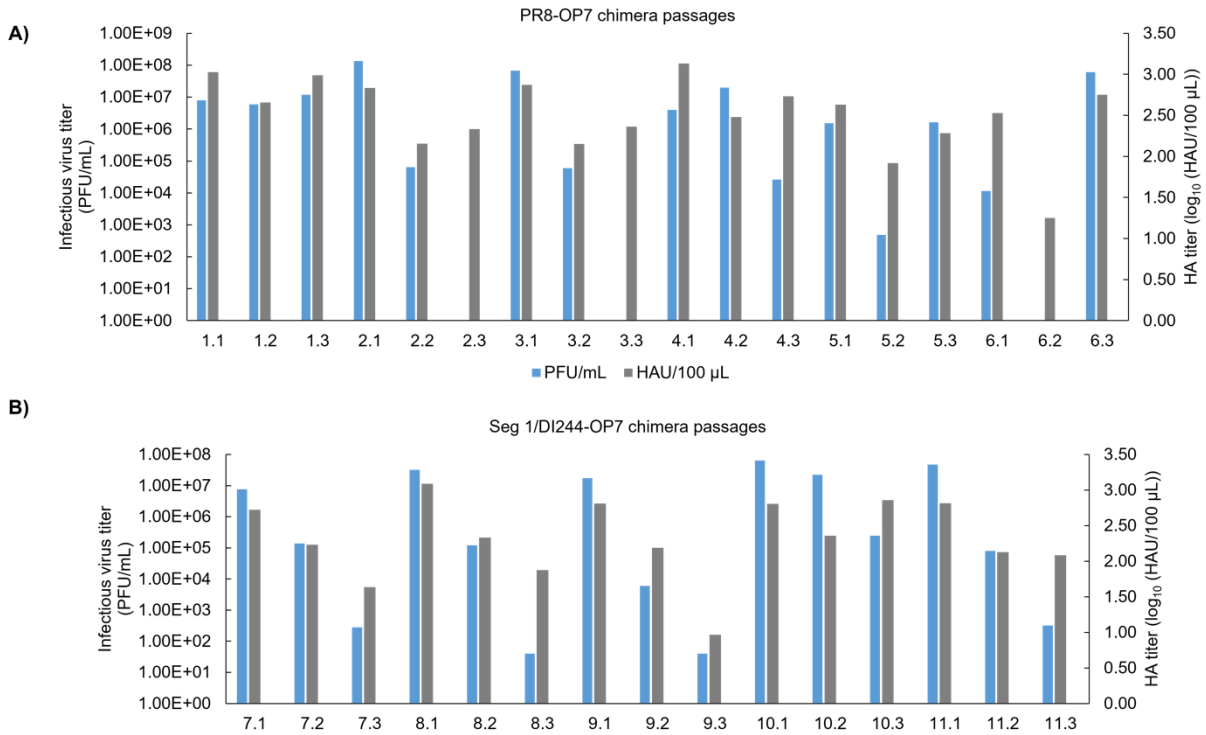

Figure 4.3.3. Sequential blind amplification of OP7 chimera DIPs after rescue. Virus samples collected from reconstitution experiments (as shown in Figure 4.3.2, conditions listed in the legend table, next page) at various time points post-transfection were subjected to three sequential blind amplifications in MDCK-PB2 cells. Virus titers were determined using the plaque and HA assay. A) As a positive control, for the generation of PR8-OP7 (8+1), various concentrations of seg 7-OP7-encoding plasmids were evaluated under conditions 1.1-6.3, as detailed in the associated figure legend table (next page). B) For generation of the seg 1/DI244-OP7 chimera DIP (Figure 4.3.2E), variations in the concentration of the DI244-encoding plasmid and seg 7-OP7-encoding plasmid (conditions 7.1-11.3) were used. For details on the conditions, see table on next page.

	Conditions labelled	Virus type (genome constellation)	PR8 plasmids (1 µg)	DI244 plasmid	Seg7-OP7 plasmid	harvest time point	Passage rounds
HEK-PB2 + MDCK-PB2	1.1	PR8+OP7 (8+1)	Seg 1-8	-	1 µg	4 d.p.t.	1
	1.2	PR8+OP7 (8+1)	Seg 1-8	-	1 µg	4 d.p.t.	2
	1.3	PR8+OP7 (8+1)	Seg 1-8	-	1 µg	4 d.p.t.	3
	2.1	PR8+OP7 (8+1)	Seg 1-8	-	1 µg	6 d.p.t.	1
	2.2	PR8+OP7 (8+1)	Seg 1-8	-	1 µg	6 d.p.t.	2
	2.3	PR8+OP7 (8+1)	Seg 1-8	-	1 µg	6 d.p.t.	3
	3.1	PR8+OP7(8+1)	Seg 1-8	-	1 µg	8 d.p.t.	1
	3.2	PR8+OP7(8+1)	Seg 1-8	-	1 µg	8 d.p.t.	2
	3.3	PR8+OP7(8+1)	Seg 1-8	-	1 µg	8 d.p.t.	3
	4.1	PR8+OP7 (8+1)	Seg 1-8	-	50 ng	4 d.p.t.	1
	4.2	PR8+OP7 (8+1)	Seg 1-8	-	50 ng	4 d.p.t.	2
	4.3	PR8+OP7 (8+1)	Seg 1-8	-	50 ng	4 d.p.t.	3
	5.1	PR8+OP7(8+1)	Seg 1-8	-	50 ng	6 d.p.t.	1
	5.2	PR8+OP7(8+1)	Seg 1-8	-	50 ng	6 d.p.t.	2
	5.3	PR8+OP7(8+1)	Seg 1-8	-	50 ng	6 d.p.t.	3
	6.1	PR8+OP7 (8+1)	Seg 1-8	-	50 ng	8 d.p.t.	1
	6.2	PR8+OP7 (8+1)	Seg 1-8	-	50 ng	8 d.p.t.	2
	6.3	PR8+OP7 (8+1)	Seg 1-8	-	50 ng	8 d.p.t.	3
	7.1	DI244+OP7 (8+1)	Seg 2-8	500 ng	50 ng	6 d.p.t.	1
	7.2	DI244+OP7 (8+1)	Seg 2-8	500 ng	50 ng	6 d.p.t.	2
	7.3	DI244+OP7 (8+1)	Seg 2-8	500 ng	50 ng	6 d.p.t.	3
	8.1	DI244+OP7 (8+1)	Seg 2-8	500 ng	50 ng	8 d.p.t.	1
	8.2	DI244+OP7 (8+1)	Seg 2-8	500 ng	50 ng	8 d.p.t.	2
	8.3	DI244+OP7 (8+1)	Seg 2-8	500 ng	50 ng	8 d.p.t.	3
	9.1	DI244+OP7 (8+1)	Seg 2-8	500 ng	50 ng	10 d.p.t.	1
	9.2	DI244+OP7 (8+1)	Seg 2-8	500 ng	50 ng	10 d.p.t.	2
	9.3	DI244+OP7 (8+1)	Seg 2-8	500 ng	50 ng	10 d.p.t.	3
	10.1	DI244+OP7 (8+1)	Seg 2-8	50 ng	50 ng	6 d.p.t.	1
	10.2	DI244+OP7 (8+1)	Seg 2-8	50 ng	50 ng	6 d.p.t.	2
	10.3	DI244+OP7 (8+1)	Seg 2-8	50 ng	50 ng	6 d.p.t.	3
	11.1	DI244+OP7 (8+1)	Seg 2-8	50 ng	50 ng	8 d.p.t.	1
	11.2	DI244+OP7 (8+1)	Seg 2-8	50 ng	50 ng	8 d.p.t.	2
	11.3	DI244+OP7 (8+1)	Seg 2-8	50 ng	50 ng	8 d.p.t.	3

4.3.3. vRNA content during serial passaging of OP7 chimera DIPs indicates seg 7-OP7 accumulation

Kupke et al., have elucidated that seg 7-OP7 vRNA can be consistently detected in co-infections with STV by observing a marked rise in OP7 vRNA levels across passages, in stark contrast to the reduction observed in other vRNA segments such as seg 5 and 8 [5]. The emergence of the OP7 phenotype is further evidenced by the progressive decline in infectious virus titers, as depicted in Figures 4.3.3A and B. The reconstitution of OP7 chimera DIPs (Figure 4.3.2E) also entails the simultaneous rescue of seg 1 DIP, identified here as DI244 (Figure 4.3.2C). It was suspected that OP7 also interferes with and may even outcompete the growth of DI244 DIP upon passaging in cells expressing PB2.

A RT-qPCR assay, specific to OP7 vRNA, was employed to accurately monitor the expansion of DIPs over passages. Figure 4.3.4 illustrates the levels of vRNA for seg 5, 8, DI244, and OP7, showcasing the presence of the "surrogate STV," DI244, and the "primary DIP," the OP7 chimera. Analysis of samples after three passages in PB2-expressing cells indicated a decrease in DI244, seg 5, and seg 8 titers, alongside an increase in OP7 vRNA (Figure 4.3.4). This pattern is consistent with the reduction in PFU titers for the same samples as shown in Figure 4.3.3 B. For instance, sample 1, after three passages in MDCK-PB2 cells as indicated in Figure 4.3.4 (labelled under conditions 1.1, 1.2 and 1.3 indicating passages), exhibited a reduction in DI244, seg 5, and seg 8 vRNA, aligning with the decrease in infectious virus titers observed in condition 7 of Figure 4.3.3 B. A similar trend is noted across the remaining samples when correlating the decline in infectious virus titers in Figure 4.3.3 B with the disproportionate rise in OP7 vRNA in the same sample set in Figure 4.3.4. Although, in each sample, initially, DI244 exhibits elevated levels of vRNA. Nevertheless, these levels are subsequently suppressed by the growth of OP7, as the OP7 DIP proliferates more robustly. Consequently, it appears that seg 7-OP7 vRNA outcompetes DI244 in terms of vRNA levels over time.

Additionally, the samples were tested in the innocuity assay (as outlined in the Materials and Methods, section 3.7.3), to verify the lack of any infectious STV following the propagation of the DI244-OP7 chimera constructs in MDCK-WT cells. The results from both passages showed no total virus titers (as indicated in the HA assay).

In summary, the findings presented in section 4.3.2 indicate a significant reduction in infectious titers across passages. This decline may be linked to elevated levels of vRNA OP7 observed over serial passages as indicated by RT-qPCR analysis. The rise in OP7 DIPs suggests an indirect suppression of surrogate STV "seg 1 DIPs" during co-infection, where OP7 acts as an inhibitor of the competing DIPs.

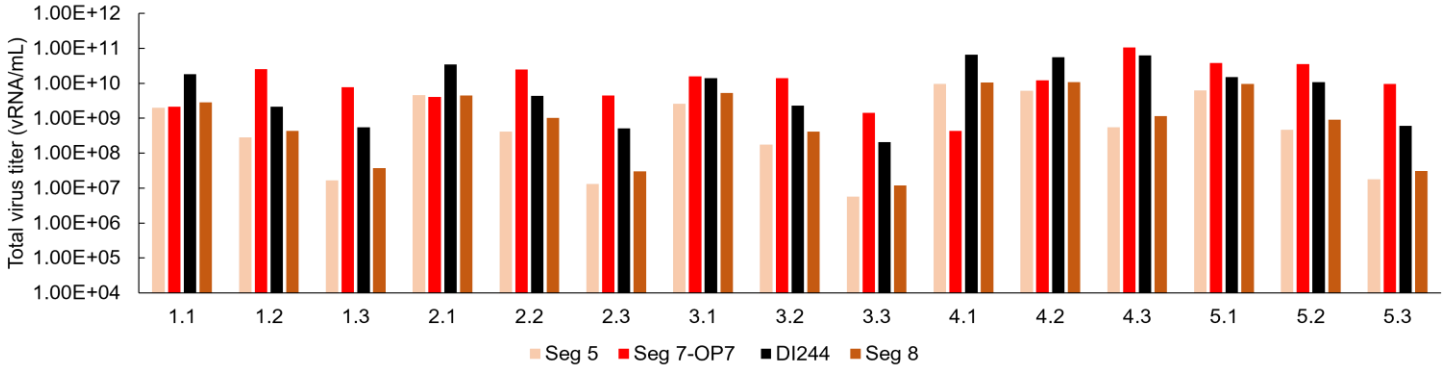

	Conditions labelled	Virus type (genome constellation)	PR8 plasmids (1 µg)	DI244 plasmid	Seg7-OP7 plasmid	harvest time point	Passage number
HEK-PB2 + MDCK-PB2	1.1	DI244+OP7 (8+1)	Seg 2-8	500 ng	50 ng	6 d.p.t.	1
	1.2	DI244+OP7 (8+1)	Seg 2-8	500 ng	50 ng	6 d.p.t.	2
	1.3	DI244+OP7 (8+1)	Seg 2-8	500 ng	50 ng	6 d.p.t.	3
	2.1	DI244+OP7 (8+1)	Seg 2-8	500 ng	50 ng	8 d.p.t.	1
	2.2	DI244+OP7 (8+1)	Seg 2-8	500 ng	50 ng	8 d.p.t.	2
	2.3	DI244+OP7 (8+1)	Seg 2-8	500 ng	50 ng	8 d.p.t.	3
	3.1	DI244+OP7 (8+1)	Seg 2-8	500 ng	50 ng	10 d.p.t.	1
	3.2	DI244+OP7 (8+1)	Seg 2-8	500 ng	50 ng	10 d.p.t.	2
	3.3	DI244+OP7 (8+1)	Seg 2-8	500 ng	50 ng	10 d.p.t.	3
	4.1	DI244+OP7 (8+1)	Seg 2-8	50 ng	50 ng	6 d.p.t.	1
	4.2	DI244+OP7 (8+1)	Seg 2-8	50 ng	50 ng	6 d.p.t.	2
	4.3	DI244+OP7 (8+1)	Seg 2-8	50 ng	50 ng	6 d.p.t.	3
	5.1	DI244+OP7 (8+1)	Seg 2-8	50 ng	50 ng	8 d.p.t.	1
	5.2	DI244+OP7 (8+1)	Seg 2-8	50 ng	50 ng	8 d.p.t.	2
	5.3	DI244+OP7 (8+1)	Seg 2-8	50 ng	50 ng	8 d.p.t.	3

Figure 4.3.4. RT-qPCR analysis after reconstitution and blind amplification passages of OP7 chimera DIPs. The analysis included measuring total virus titers (represented by vRNA levels of seg 5 and 8) and evaluating DI vRNA levels of DI244 and seg 7-OP7. The plasmids used in the rescue experiments, following a nine-plasmid scheme, are detailed in the accompanying table. This table also includes the specific rescue harvest time points evaluated during the serial passages of the selected five samples.

4.3.4. Generation of OP7 chimera DIPs based on the newly identified seg 1 DIPs

DI244, as previously mentioned, is currently under patent protection, complicating its commercialization as an antiviral agent. Kupke et al., holds a patent for OP7 DIP (EP18159908), which has demonstrated superior antiviral activity compared to DI244 in both in vitro and in vivo studies [5, 29, 37]. This makes OP7 DIP a more suitable candidate for licensing DIP technology-based antivirals or vaccines. The seg 1-OP7 chimera DIPs have been successfully generated (see Figures 4.3.2 and 4.3.3) using DI244 as a backbone, providing a proof of concept. These chimeras were reconstituted and cultured to high infectious titers in adherent MDCK-PB2 cells. The next objective is to use the newly identified, in-house seg 1 DIPs as a new backbone for OP7 chimera DIPs, as an alternative to DI244.

The recent identification of two types of DIPs on seg 1, known as winner and loser DIPs (Figure 4.1.1C and Figure 4.1.2A) was described in previous chapters. These DIPs were easily reconstituted and detectable in different viral identification assays. This was in contrast to the reconstitution and detection of seg 1 de novo DIP (Figure 4.1.2A and Figure 4.1.5 B, C), which required additional amplification rounds in suspension MDCK-PB2 cells. As a result, the winner or loser seg 1 DIPs were chosen as the backbone for creating OP7 chimera DIPs. Despite the fact that the loser DIP showed comparable interference to DI244 in the in vitro co-infection studies, its straightforward reconstitution and ability to grow to high virus titers made it the preferred choice for use in the OP7 chimera reconstitution scheme. Furthermore, it was assumed that the addition of seg 7-OP7 vRNA would allow the final DIP construct to demonstrate strong antiviral activity and allow to generate OP7 DIPs based on an easy-to-commercialise backbone and devoid of infectious STV in the final virus harvest. Regardless, following a similar approach as compared to the DI244-OP7 chimera reconstitution depicted in Figure 4.3.2, OP7 chimera DIPs utilizing either the seg 1 winner or loser were rescued. Figure 4.3.5 demonstrates the production of these OP7 chimera DIPs.

In the reconstitution experiments, either 50 ng or 500 ng of the seg 1 DI-encoding plasmid was utilized, in combination with 50 ng of the seg 7-OP7-encoding plasmid. The amount of the seven full-length-encoding plasmids was kept constant at 1 µg per

plasmid per well. Figure 4.3.6 and the associated table provide detailed information on the plasmid amounts used in various construct rescues. In line with observations from the DI244-OP7 chimera (Figures 4.3.3B, 7.5), both the seg 1/winner-OP7 and seg 1/loser-OP7 chimeras demonstrated a decline in infectious virus titers over successive passages after reconstitution in MDCK-PB2 cells.

It was hypothesized, based on the seg 1/DI244-OP7 chimera constructs, that combining a specific, low quantity of seg 7-OP7 (50 ng) with a seg 1 DIP (using either 50 or 500 ng of plasmid) facilitates the reconstitution of the chimera DIPs (see Figures 4.3.3B and 7.5). However, no clear relationship could be determined between the effectiveness of using 50 or 500 ng of the seg 1 DIP encoding plasmid with 50 ng of the seg 7-OP7 encoding plasmid. Hence, for the reconstitution of seg 1 loser-based OP7 chimera constructs, these conditions allowed the reconstitution of OP7 chimera DIPs that were detectable in the plaque assay, indicating that these conditions permit the rescue without hindrance (Figure 4.3.6 A). On the other hand, the process of DIP rescue is marked by significant complexity and stochasticity, necessitating extensive preliminary screening to determine the optimal plasmid quantities for reconstituting specific constructs. For example, using higher amounts of the seg 1 DIP plasmid to counteract OP7 DIP interference enabled the rescue of seg 1/winner-OP7 chimera DIPs. Conversely, employing a lower quantity of seg 1 DIP encoding plasmid (50 ng) for the winner backbone did not consistently result in infectious virus titers after multiple amplification rounds (samples 11-12, Figure 4.3.6B).

Overall, it was possible to successfully reconstitute OP7 chimera DIPs using the newly identified seg 1 DIPs. However, this success underscored the necessity for thorough screening of various plasmid amounts for different DI-encoding plasmids, which were then serially passaged over MDCK-PB2 cells to verify the rescue of infectious viruses in plaque assays.

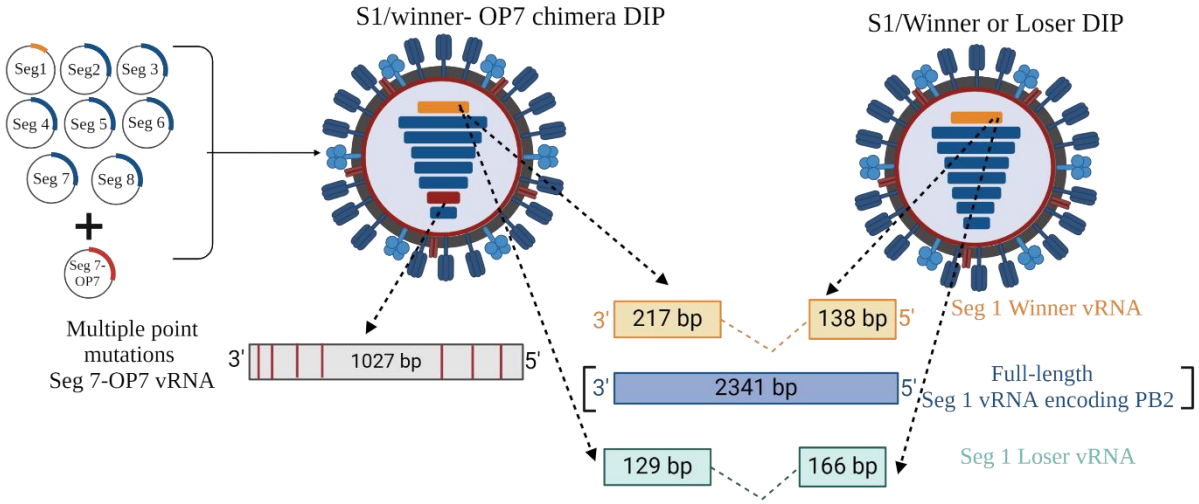

Figure 4.3.5. Generation of OP7 chimera DIPs based on the newly identified seg 1 DIPs. By co-transfecting nine plasmids, a population of DIPs was produced, including both, one seg 1 DIP (winner or loser) and their corresponding OP7 chimera DIP. Both type of DIPs are capable of replication in the absence of an infectious STV, by complementation of the missing PB2 protein expressing cells. Image generated with Biorender.com.

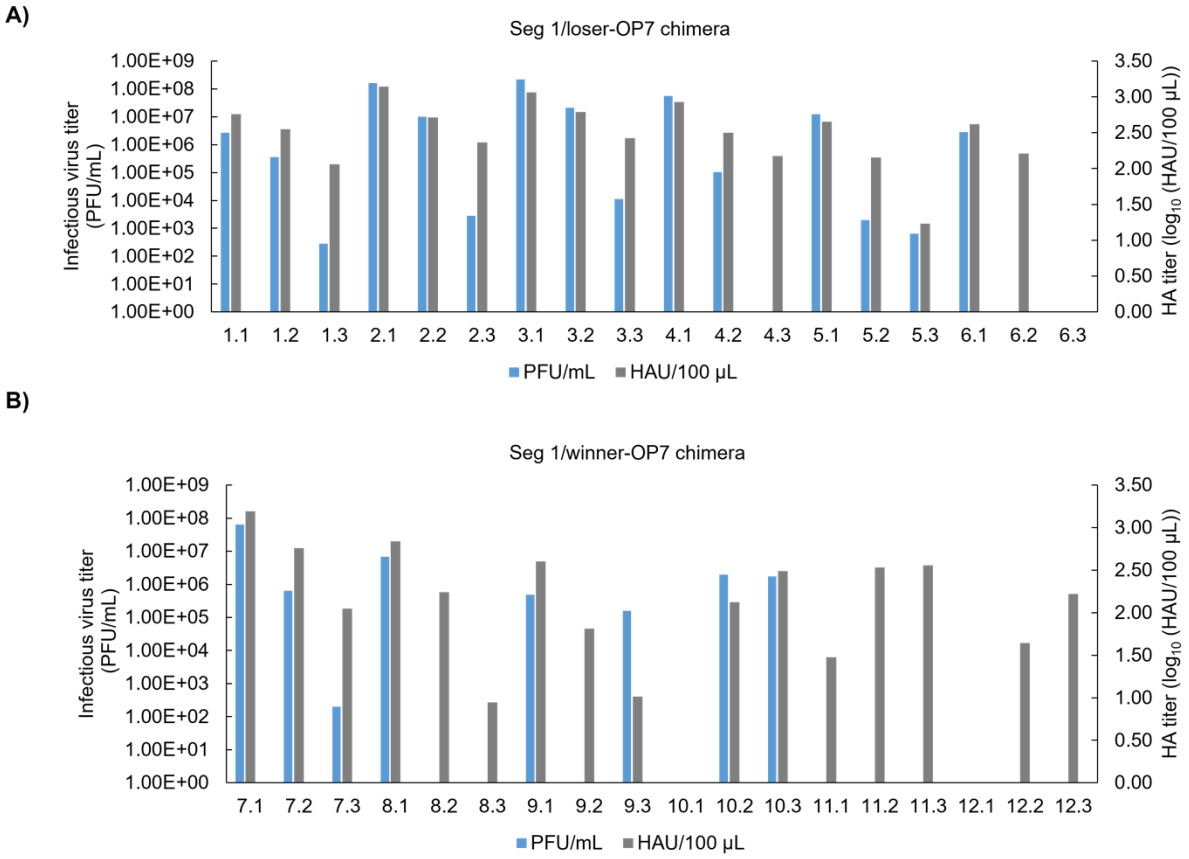

Figure 4.3.6. Sequential blind amplification of seg 1/loser-OP7 and seg 1/winner-OP7 chimera DIPs after rescue experiments (conditions listed in the legend table, next page). A) Virus titers during serial passaging of seg 1/loser-OP7 DIP. Generation of seg 1/loser-OP7 chimera: 50 ng of seg 7-OP7 encoding plasmid was combined with varying amounts of seg 1/loser plasmid (50 and 500 ng) under specific conditions (1.1-6.3) as outlined, see table on next page. B) Virus titers during serial passaging of seg 1/winner-OP7 DIP. Generation of seg 1/winner-OP7 chimera: 50 ng of seg 7-OP7 was combined with seg 1/winner plasmid in amounts ranging from 50-500 ng, following the conditions (7.1-12.3) detailed in the table (next page). For both chimera constructs, virus samples collected at different times post-transfection (6-10 days) underwent three consecutive blind amplification passages in MDCK-PB2 cells. These samples were then evaluated for infectious virus titers using the plaque assay, and for total virus titers using the HA assay.

	Conditions labelled	Virus type (genome constellation)	PR8 plasmids (1 µg)	DI plasmid	Seg7-OP7 plasmid	harvest time point	Passage rounds
HEK-PB2 + MDCK-PB2	1.1	Seg 1 Loser + OP7 (8+1)	Seg 2-8	Seg 1 Loser (500 ng)	50 ng	6 d.p.t.	1
	1.2	Seg 1 Loser + OP7 (8+1)	Seg 2-8	Seg 1 Loser (500 ng)	50 ng	6 d.p.t.	2
	1.3	Seg 1 Loser + OP7 (8+1)	Seg 2-8	Seg 1 Loser (500 ng)	50 ng	6 d.p.t.	3
	2.1	Seg 1 Loser + OP7 (8+1)	Seg 2-8	Seg 1 Loser (500 ng)	50 ng	8 d.p.t.	1
	2.2	Seg 1 Loser + OP7 (8+1)	Seg 2-8	Seg 1 Loser (500 ng)	50 ng	8 d.p.t.	2
	2.3	Seg 1 Loser + OP7 (8+1)	Seg 2-8	Seg 1 Loser (500 ng)	50 ng	8 d.p.t.	3
	3.1	Seg 1 Loser + OP7 (8+1)	Seg 2-8	Seg 1 Loser (500 ng)	50 ng	10 d.p.t.	1
	3.2	Seg 1 Loser + OP7 (8+1)	Seg 2-8	Seg 1 Loser (500 ng)	50 ng	10 d.p.t.	2
	3.3	Seg 1 Loser + OP7 (8+1)	Seg 2-8	Seg 1 Loser (500 ng)	50 ng	10 d.p.t.	3
	4.1	Seg 1 Loser + OP7 (8+1)	Seg 2-8	Seg 1 Loser (50 ng)	50 ng	6 d.p.t.	1
	4.2	Seg 1 Loser + OP7 (8+1)	Seg 2-8	Seg 1 Loser (50 ng)	50 ng	6 d.p.t.	2
	4.3	Seg 1 Loser + OP7 (8+1)	Seg 2-8	Seg 1 Loser (50 ng)	50 ng	6 d.p.t.	3
	5.1	Seg 1 Loser + OP7 (8+1)	Seg 2-8	Seg 1 Loser (50 ng)	50 ng	8 d.p.t.	1
	5.2	Seg 1 Loser + OP7 (8+1)	Seg 2-8	Seg 1 Loser (50 ng)	50 ng	8 d.p.t.	2
	5.3	Seg 1 Loser + OP7 (8+1)	Seg 2-8	Seg 1 Loser (50 ng)	50 ng	8 d.p.t.	3
	6.1	Seg 1 Loser + OP7 (8+1)	Seg 2-8	Seg 1 Loser (50 ng)	50 ng	10 d.p.t.	1
	6.2	Seg 1 Loser + OP7 (8+1)	Seg 2-8	Seg 1 Loser (50 ng)	50 ng	10 d.p.t.	2
	6.3	Seg 1 Loser + OP7 (8+1)	Seg 2-8	Seg 1 Loser (50 ng)	50 ng	10 d.p.t.	3
	7.1	Seg 1 Winner + OP7 (8+1)	Seg 2-8	Seg 1 Winner (500 ng)	50 ng	6 d.p.t.	1
	7.2	Seg 1 Winner + OP7 (8+1)	Seg 2-8	Seg 1 Winner (500 ng)	50 ng	6 d.p.t.	2
	7.3	Seg 1 Winner + OP7 (8+1)	Seg 2-8	Seg 1 Winner (500 ng)	50 ng	6 d.p.t.	3
	8.1	Seg 1 Winner + OP7 (8+1)	Seg 2-8	Seg 1 Winner (500 ng)	50 ng	8 d.p.t.	1
	8.2	Seg 1 Winner + OP7 (8+1)	Seg 2-8	Seg 1 Winner (500 ng)	50 ng	8 d.p.t.	2
	8.3	Seg 1 Winner + OP7 (8+1)	Seg 2-8	Seg 1 Winner (500 ng)	50 ng	8 d.p.t.	3
	9.1	Seg 1 Winner + OP7 (8+1)	Seg 2-8	Seg 1 Winner (500 ng)	50 ng	10 d.p.t.	1
	9.2	Seg 1 Winner + OP7 (8+1)	Seg 2-8	Seg 1 Winner (500 ng)	50 ng	10 d.p.t.	2
	9.3	Seg 1 Winner + OP7 (8+1)	Seg 2-8	Seg 1 Winner (500 ng)	50 ng	10 d.p.t.	3
	10.1	Seg 1 Winner + OP7 (8+1)	Seg 2-8	Seg 1 Winner (50 ng)	50 ng	6 d.p.t.	1
	10.2	Seg 1 Winner + OP7 (8+1)	Seg 2-8	Seg 1 Winner (50 ng)	50 ng	6 d.p.t.	2
	10.3	Seg 1 Winner + OP7 (8+1)	Seg 2-8	Seg 1 Winner (50 ng)	50 ng	6 d.p.t.	3
	11.1	Seg 1 Winner + OP7 (8+1)	Seg 2-8	Seg 1 Winner (50 ng)	50 ng	8 d.p.t.	1
	11.2	Seg 1 Winner + OP7 (8+1)	Seg 2-8	Seg 1 Winner (50 ng)	50 ng	8 d.p.t.	2
	11.3	Seg 1 Winner + OP7 (8+1)	Seg 2-8	Seg 1 Winner (50 ng)	50 ng	8 d.p.t.	3
	12.1	Seg 1 Winner + OP7 (8+1)	Seg 2-8	Seg 1 Winner (50 ng)	50 ng	10 d.p.t.	1
	12.2	Seg 1 Winner + OP7 (8+1)	Seg 2-8	Seg 1 Winner (50 ng)	50 ng	10 d.p.t.	2
	12.3	Seg 1 Winner + OP7 (8+1)	Seg 2-8	Seg 1 Winner (50 ng)	50 ng	10 d.p.t.	3

4.3.5. Confirmation of the OP7 phenotype

To verify the presence of OP7 vRNA in various OP7 chimera constructs, RT-qPCR was employed. Figure 4.3.7 illustrates the OP7 phenotype, demonstrating an increase in OP7 vRNA with each serial passage, in contrast to other full-length segments such as seg 5 and 8 for both the seg 1/winner or loser-OP7 chimera constructs. While seg 1/ winner or loser mostly showed over proportional levels in the first passages, later passages displayed a decrease in the seg 1 DI vRNA, while seg 7-OP7 levels increased.

For the development of antiviral agents based on OP7 DIPs, the constructs were produced in suspension MDCK-PB2 cell cultures, it was therefore essential to thoroughly characterize the constructs for integrity. Figure 4.3.8 presents the results of the segment-specific PCR conducted on seed viruses of a sample from condition 4.1 (Figure 4.3.6A for infectious and total virus titers) to identify the seg 1/loser-OP7 chimera DIP (Figure 4.3.8A). In Figure 4.3.8B, for the seg 1/winner-OP7 chimera DIP, seed virus samples tested were from 7.1 (Figure 4.3.6B, representing infectious and total virus titers).

The results indicate that no significant accumulation of other DI vRNAs or seg 1 full-length were observed (Figure 4.3.8). Testing in the innocuity assay confirmed the absence of any infectious STV upon propagation in MDCK-WT cells (data not shown).

Please refer to the data in the supplements for MOI-dependent growth of OP7 chimera DIPs in suspension MDCK-PB2 cells showing strong antiviral activity (sections 7.1.4 – 7.1.6). MODIP screenings were conducted by Lars Pelz using the seg 1/winner-OP7 chimera construct (Supplement figure 7.6). Here, low MODIP conditions gave rise to high total virus titers (Supplement figure 7.6) and infectious virus titers (data not shown). MODIP screening revealed an optimum MODIP of 1E-3 and 1E-4, that showed high virus titers with strongest interfering capacities (Supplement figure 7.8). Additionally, no significant accumulation of DIPs on seg 2–8 was observed following segment-specific PCR and agarose gel electrophoresis (Supplement figure 7.7).

Furthermore, Sanger sequencing was performed on the suspension-amplified seg 1/winner-OP7 chimera constructs to confirm the deletion junction in seg 1 DI vRNA.

While OP7 vRNA was confirmed with RT-qPCR analysis along with mass spectrometry analysis to specifically detect for mutated OP7 protein (data not shown, refer to [3])

In sum, all the OP7 chimera constructs were rescued and the absence of any infectious STV and presence of a specific DI vRNA deletion in the seg 1 were confirmed. OP7 vRNA presence and levels were also confirmed via RT-qPCR. The seed viruses prepared could be directly used for large scale production in MDCK-PB2 suspension cells.

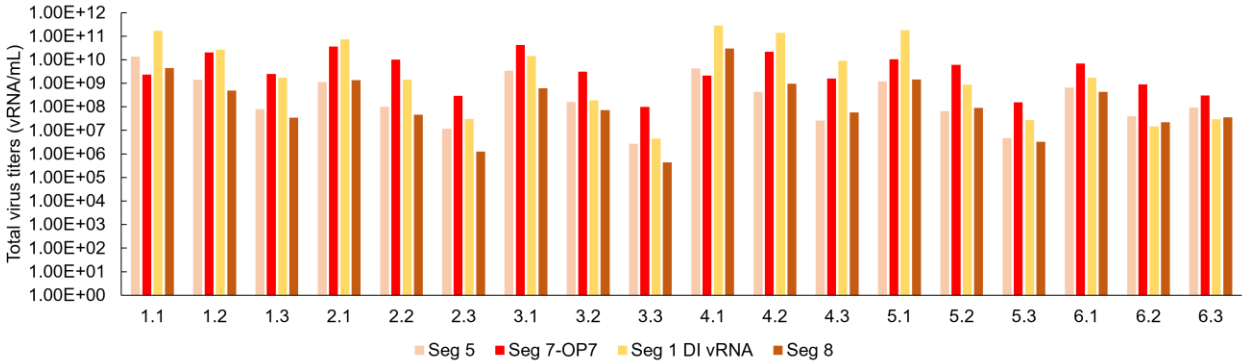

	Conditions labelled	virus type (genome constellation)	PR8 plasmids (1 µg)	DI plasmid	Seg7-OP7 plasmid	harvest time point	Passage number
HEK-PB2 + MDCK-PB2	1.1	Seg 1 Loser + OP7 (8+1)	Seg 2-8	Seg 1 Loser (50 ng)	50 ng	6 d.p.t.	1
	1.2	Seg 1 Loser + OP7 (8+1)	Seg 2-8	Seg 1 Loser (50 ng)	50 ng	6 d.p.t.	2
	1.3	Seg 1 Loser + OP7 (8+1)	Seg 2-8	Seg 1 Loser (50 ng)	50 ng	6 d.p.t.	3
	2.1	Seg 1 Loser + OP7 (8+1)	Seg 2-8	Seg 1 Loser (50 ng)	50 ng	8 d.p.t.	1
	2.2	Seg 1 Loser + OP7 (8+1)	Seg 2-8	Seg 1 Loser (50 ng)	50 ng	8 d.p.t.	2
	2.3	Seg 1 Loser + OP7 (8+1)	Seg 2-8	Seg 1 Loser (50 ng)	50 ng	8 d.p.t.	3
	3.1	Seg 1 Loser + OP7 (8+1)	Seg 2-8	Seg 1 Loser (50 ng)	50 ng	10 d.p.t.	1
	3.2	Seg 1 Loser + OP7 (8+1)	Seg 2-8	Seg 1 Loser (50 ng)	50 ng	10 d.p.t.	2
	3.3	Seg 1 Loser + OP7 (8+1)	Seg 2-8	Seg 1 Loser (50 ng)	50 ng	10 d.p.t.	3
	4.1	Seg 1 Winner + OP7 (8+1)	Seg 2-8	Seg 1 Winner (500 ng)	50 ng	6 d.p.t.	1
	4.2	Seg 1 Winner + OP7 (8+1)	Seg 2-8	Seg 1 Winner (500 ng)	50 ng	6 d.p.t.	2
	4.3	Seg 1 Winner + OP7 (8+1)	Seg 2-8	Seg 1 Winner (500 ng)	50 ng	6 d.p.t.	3
	5.1	Seg 1 Winner + OP7 (8+1)	Seg 2-8	Seg 1 Winner (500 ng)	50 ng	8 d.p.t.	1
	5.2	Seg 1 Winner + OP7 (8+1)	Seg 2-8	Seg 1 Winner (500 ng)	50 ng	8 d.p.t.	2
	5.3	Seg 1 Winner + OP7 (8+1)	Seg 2-8	Seg 1 Winner (500 ng)	50 ng	8 d.p.t.	3
	6.1	Seg 1 Winner + OP7 (8+1)	Seg 2-8	Seg 1 Winner (500 ng)	50 ng	10 d.p.t.	1
	6.2	Seg 1 Winner + OP7 (8+1)	Seg 2-8	Seg 1 Winner (500 ng)	50 ng	10 d.p.t.	2
	6.3	Seg 1 Winner + OP7 (8+1)	Seg 2-8	Seg 1 Winner (500 ng)	50 ng	10 d.p.t.	3

Figure 4.3.7. vRNA levels of reconstituted seg 1/loser or winner-OP7 chimera DIPs after serial passaging. RT-qPCR was used to quantify the total virus titers (segments 5 and 8 vRNA levels) and DI vRNA levels from seg 1 (loser or winner) and seg7-OP7. Details on the conditions used in the nine-plasmid reconstitution scheme and the specific harvest times assed (during rescue experiments) are given in the table.

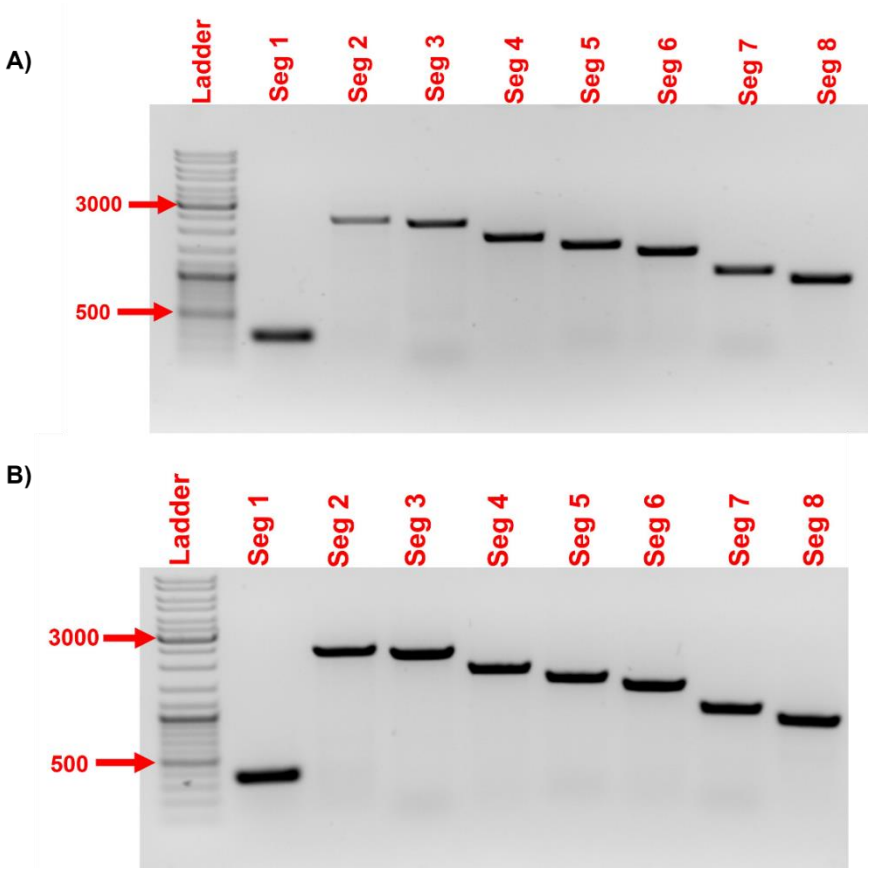

Figure 4.3.8. Purity of seg 1/loser and seg 1/winner-OP7 chimera DIPs. After reconstitution, the OP7 chimera DIPs were amplified in MDCK-PB2 cells. Resulting virus harvest were subjected to segment-specific RT-PCR analysis and agarose gel electrophoresis to detect any contamination by other DIPs or STV. A) Analysis was conducted on seg 1/loser-OP7 chimera DIPs and B) seg 1/winner-OP7 chimera DIPs, using samples from 6 d.p.t., the virus harvests were amplified blindly for one passage in MDCK-PB2 cells. To be precise, within the nine-plasmid system framework, 50 ng of seg 7-OP7 plasmid combined with either 50 ng of seg 1/loser or 500 ng of seg 1/winner were utilized. Ladder bands at 500 bp and 3000 bp (ladder) are highlighted.

4.3.6. Establishment of a new inference assay based on human lung cells

Interference studies using MDCK cell-based assays provide an effective means to evaluate the antiviral activity of newly developed DIPs against STV propagation. During co-infection in MDCK cells, DIPs can inhibit STV replication by competing for cellular resources without activating innate immune responses, as MDCK cells lack effective immune responses against human IAV strains [177]. In contrast, Calu-3 cell assays are more appropriate for detecting the antiviral activity of DIPs against STV, as they allow to assess both replication and innate immune response-based inhibition, closely mimicking the target tissue [178]. It is important to note that the PR8 virus exhibits slower growth in Calu-3 cells compared to MDCK cells due to the absence of exogenous trypsin. Hence, PR8 virus replication in Calu-3 cells depends on intrinsic trypsin-like proteases for viral cleavage and replication [179]. While MDCK cells supplemented with trypsin demonstrate higher viral growth rates, trypsin may degrade Type I IFNs and ISGs induced by STV or DIPs [56]. This section of the thesis investigates assays using human alveolar epithelial Calu-3 cells, incorporating findings from Ghada Hemissi's BSc thesis.

Calu-3 cells display an epithelial morphology but form cellular islands in vitro, complicating the culture conditions needed for a loosely packed monolayer. This monolayer is essential for uniform substrate and nutrient distribution. Additionally, maintaining cells in the logarithmic growth phase with high viability is crucial for reproducible results and high virus titers post-infection. Initial steps involved testing various well formats for seeding, and testing multiple seeding densities from 0.2×10^6 to 3×10^6 cells per well across 6, 12, 24, and 96 well plates (data not shown). Both enzymatic (trypsin-based) and mechanical (scrapers/pipettes) subculturing methods were evaluated for cell detachment (data not shown). Various volumes of 1X trypsin ranging from 0.5 mL to 2 mL were also tested to achieve rapid cell detachment while minimizing trypsin exposure to preserve cell viability (data not shown). Following seeding in culture plates and based on the time required to reach confluency, cells were incubated in a growth medium (details in the materials and methods section 3.7.2). This incubation lasted for a minimum of 24 h and up to 48 h post-seeding.

Optimal results were observed when Calu-3 cells were seeded in a 12-well format and incubated for 24 h, forming a monolayer that could be easily detached using 1 mL of 1X trypsin, achieving a single cell suspension within 15 min of incubation. The viability of cells under these culturing conditions was consistently above 90%, and the procedures were reproducible (data not shown).

Subsequently, the efficacy of above established culturing conditions in promoting the propagation of STV PR8 to relatively high titers was evaluated. STV growth dynamic experiments were performed in duplicate, as illustrated in Figure 4.3.9. In this study, STV infection in Calu-3 cells was monitored at an MOI of 0.05 for up to 60 h.p.i., with cell-free virus harvests collected at 24 and 48 h.p.i. For STV, relatively high average infectious virus titers of 2.0×10^7 PFU/mL at 24 h.p.i. (Figure 4.3.9) were achieved, which stabilized at about 60 h.p.i. with an average infectious virus titer of 4.2×10^7 PFU/mL. A similar pattern was observed for HA values. Specifically, low HA titers of 0.9 HAU/100 µL were recorded at 24 h.p.i., increasing to 1.5 HAU/100 µL at 48 h.p.i. and further to 1.7 HAU/100 µL at 60 h.p.i. Overall, it was demonstrated that STV can be propagated to relatively high titers in Calu-3 cells without trypsin supplementation. The established assay was therefore considered suitable for assessing the antiviral activity of DIPs, by measuring Type I IFN stimulation (such as IFN-β) and replication inhibition.

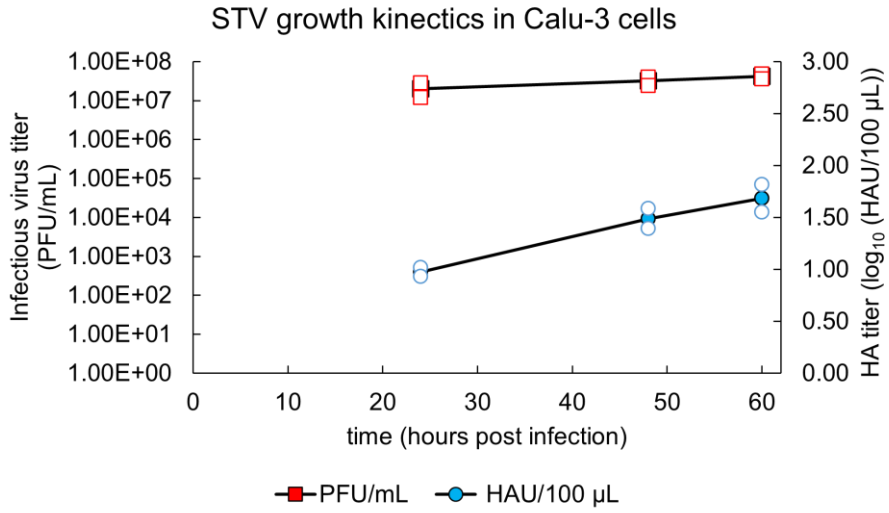

Figure 4.3.9. Growth dynamics of STV (PR8) in Calu-3 cells. Calu-3 cells were cultured in a 12-well plate. The cells were infected with STV at a MOI of 0.05. The harvested virus-containing supernatants were analysed using plaque (red label) and HA (blue label) assays to evaluate the infectious and overall virus yields, respectively. Experiments were conducted in duplicates (n=2), and the solid mean line shows the average of replicates.

4.3.7. OP7 chimera DIP material shows strong antiviral efficacy in human lung cells in vitro

An in vitro interference assay using Calu-3 cells was conducted to assess the antiviral efficacy of purified OP7 chimera DIPs. The comparison was made between OP7 chimera DIP material produced before and after process optimization (conducted by Lars Pelz [4]). Briefly, MDCK-PB2 cells were grown in shake flasks at 37°C, followed by a complete medium exchange (CME) before infection with seg 1/winner-OP7 chimera DIPs. In addition, an optimized production with a 1:2 medium dilution (MD) instead of a complete medium exchange, and a reduction of the temperature to 32°C for infection, was conducted. This increased virus titers by 11- fold to 3.2 $\log_{10}$ HAU/100 µL compared to the original process. The virus was then purified using a Steric exclusion chromatography (SXC)-based method [4].

To determine if antiviral activity was improved by process optimization, viral yields from co-infections were compared using the Calu-3 interference assay, with both the 37°C CME and 32°C medium dilution downstream production (MD DSP) condition. In this assay, Calu-3 cells were infected with STV at an MOI of 0.05 for 24 h, resulting in an average infectious virus titer of 2.3×10^7 PFU/mL (Figure 4.3.10A). Co-infection with seg 1/winner-OP7 chimera from the 37°C CME significantly reduced infectious virus titers to 2.2×10^5 PFU/mL. In contrast, co-infection with the OP7 chimera DIP produced at 32°C MD DSP appeared to interfere more, reducing infectious virus titers to 1.0×10^4 PFU/mL (Figure 4.3.10A). This reduction was not statistically significant (ns, $p>0.05$, one-way ANOVA with Tukey's multiple comparison test, Figure 4.3.10A). When comparing the IFN-β stimulation by STV alone to STV co-infections with different DIP preparations (32°C MD DSP or 37°C CME) over time, an early and strong increase in IFN-β was observed at 6 h.p.i. with 32°C MD DSP co-infections compared to STV or 37°C CME. (Figure 4.3.10B). This early IFN-β stimulation (at 6 h.p.i.) was significantly increased in the 32°C MD DSP preparations compared to 37°C CME (*, $p<0.05$;), as determined by one-way ANOVA followed by Dunnett's test (Figure 4.3.10C) [4]. This early IFN-β stimulation may explain part of the strong antiviral activity exerted by the OP7 chimera DIPs.

In summary, co-infection studies were performed utilizing a newly developed Calu-3 cell-based interference assay to evaluate the antiviral efficacy of OP7 chimera DIPs generated under different conditions. A substantial decrease in infectious virus titers and an early induction (6 h.p.i.) of IFN-β were revealed when chimera DIPs were produced under optimized conditions.

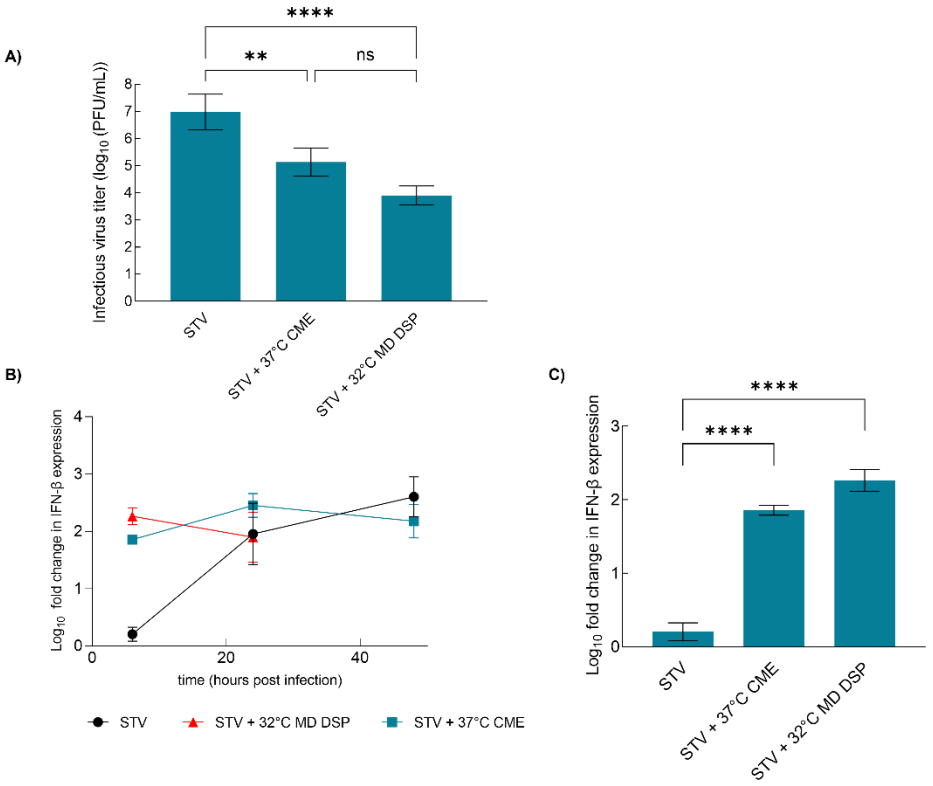

Figure 4.3.10. Interfering assay in Calu-3 cells with OP7 chimera DIP material. Calu-3 cells were infected with STV at an MOI of 0.05 or were co-infected with 125 µL of OP7 chimera DIP material. A) Comparison of infectious STV titers when infected alone or co-infected with OP7 chimera DIP material. The DIP material was produced in shake flasks at 37ºC with a complete medium change (37ºC CME) or DIP material produced at 32ºC with medium dilution (32ºC MD), followed by SXC purification (n=3) (OP7 DIP material produced by Pelz et al., [4]. The significance of the findings was determined using ANOVA analysis with Tukey's comparison test. B) Fold change in IFN-ß expression from RT-qPCR analysis. STV infections, six independent experiments and co-infections with OP7 chimera DIP material, three experiments. C) The fold change in IFN-ß expression at 6 h.p.i. ANOVA analysis with Dunnett's comparison test to evaluate significance. A p-value <0.05 was marked as significant (*) and a p-value >0.05 as not significant (ns). SD is indicated. Figure is adapted from Pelz et al., [4].

4.3.8. High in vivo tolerability and antiviral efficacy of OP7 chimera DIP material

The tolerability and antiviral effectiveness of OP7 chimera DIP material in mice were evaluated using DIPs that were produced at 37°C in shake flasks with MDCK-PB2 cells at a MOI of 1E-4 and purified by SXC (performed by Lars Pelz and Pavel Marichal-Gallardo). The final product contained 8.96×10^9 virions/mL (calculated based on Seg 5 vRNA concentrations), with a fraction of 60.1% OP7 chimera DIP fraction (calculated based on Seg 7-OP7 and Seg 7-WT vRNA concentrations), determined by RT-qPCR quantifications. In Figure 4.3.11A, mice received an intranasal dose of 20 µL of active OP7 chimera DIPs (8.96×10^7 virions) or PBS. Minimal lung tissue damage was observed in PBS-treated mice, a typical reaction observed upon an intranasal liquid application. No clinically relevant histopathological changes were noted in mice treated with OP7 chimera DIP material. Furthermore, OP7 chimera DIP material's intranasal administration at the high dose in mice did not lead to any clinical scores for disease, thereby indicating good tolerability of the DIPs (Figure 4.3.11B).

Subsequently, as shown in Figure 4.3.11C-E, mice were treated with a lethal dose of 1000 focus-forming units (FFU) of STV (PR8) in 20 µL PBS. In addition, a co-infection with a lethal dose of STV along with active or inactive OP7 chimera DIPs (in 20 µL volume) was tested in mice. The inactive OP7 chimera DIP preparation was inactivated by exposure for 24 min with UV light until no further interfering efficacy was detected (previously shown by Hein et al., [38]), was used as negative control. PBS co-treated mice experienced severe weight loss (Figure 4.3.11C), high clinical score (Figure 4.21D) and 100% mortality (Figure 4.3.11E) due to lethal STV infection, similar to those treated with inactive OP7 chimera DIPs. Conversely, mice co-treated with active OP7 chimera DIPs showed no weight loss and survived the lethal IAV challenge without showing clinical signs of influenza infection (Figures 4.3.11C, D, and E).

In summary, intranasal administration of OP7 chimera DIP material was highly tolerable in mice, and administration of active OP7 chimera DIPs provided complete protection against a lethal IAV challenge. This demonstrated their safety and potent antiviral efficacy in vivo.

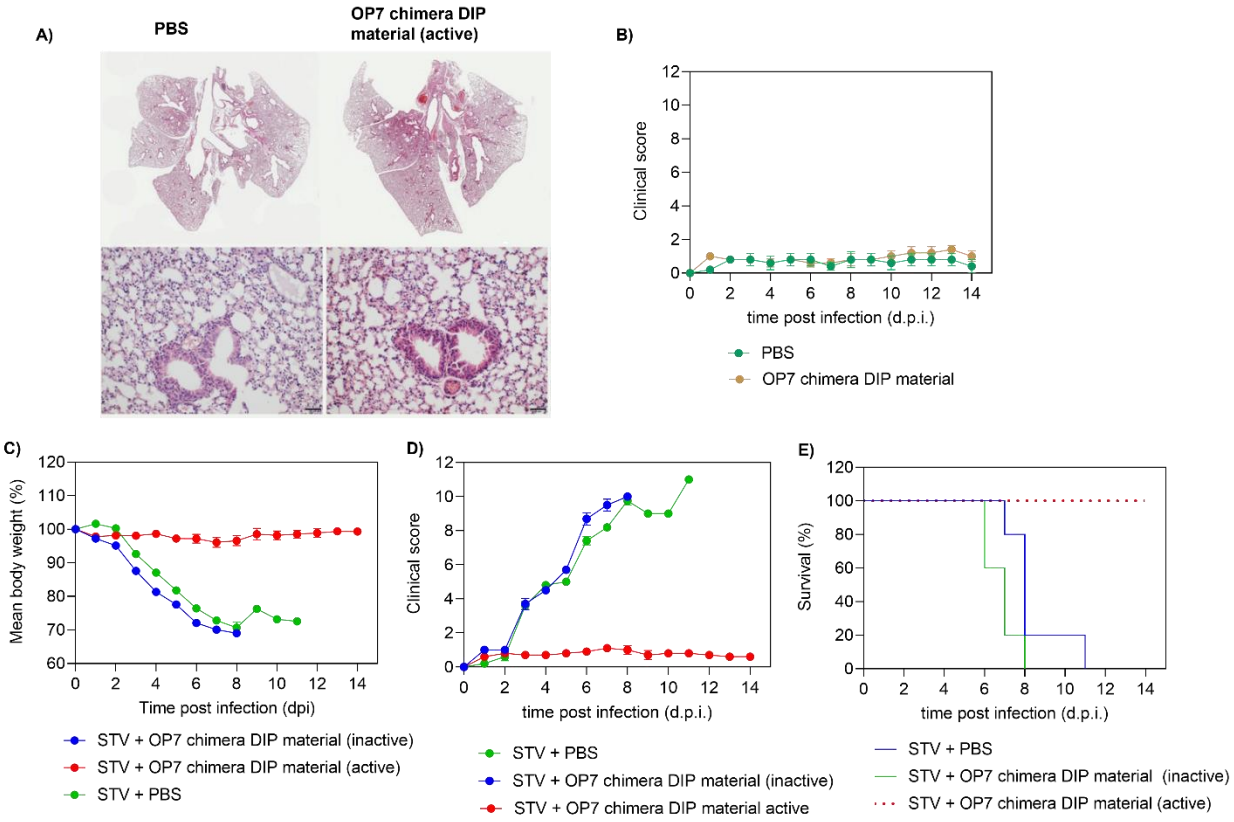

Figure 4.3.11. In vivo tolerability and antiviral activity of OP7 chimera DIP material in mice. A) Lung histology of D2(B6).A2G-Mx1r/r mice following OP7 chimera DIP or PBS administration. Mice (12–24 weeks old, n=5) received an intranasal dose of 20 µL OP7 chimera DIPs (8.96×10^7 virions/mouse) or PBS. Hematoxylin-eosin staining 14 days post-administration showed no significant histological differences between OP7 chimera DIP-treated and PBS control lungs. B) Disease severity scores in mice after intranasal delivery of 20 µL OP7 chimera DIPs or PBS. C-E) Response of mice to intranasal co-treatment with a lethal STV dose (1000 FFU strain PR8) and OP7 chimera DIP (active or inactive i.e., UV treated for 24 min) or PBS (n=5 for PBS, n=10 for each DIP group) in a 20 µL volume. C) Average body weight change, showing statistically significant protection by active OP7 chimera DIP material compared to PBS control (mixed effects models, Tukey's test, $p<0.0001$). D) clinical disease scores post-treatment. E) Survival rates, with Kaplan-Meier curves indicating significantly higher survival in mice co-treated with active OP7 chimera DIPs versus those receiving STV with PBS (log-rank test). Error bars represent the standard error of the mean (SEM). Figure adapted from Dogra et al., [3].

4.3.9. Discussion III

The recently identified OP7 DIP is characterized by a unique mutation profile [5]. Unlike conventional IAV DIPs, the seg 7-OP7 vRNA contains 37 point mutations. Specifically, 33 of these mutations are located in the coding regions, which include sequences encoding the M1 and M2 proteins, as well as additional point mutations

in packaging signal sequences and promoter regions. Despite the presence of mutations across various functional areas of the seg 7 vRNA, identifying the exact nucleotide alteration responsible for OP7's defect in virus replication remains challenging [5, 38]. As illustrated in Figure 4.3.1, generating a clonal OP7 DIP using a co-culture of MDCK-WT and HEK-WT cells was not feasible. This finding supports the hypothesis that OP7 virions are indeed defective in virus replication, as previously suspected [5, 38]. However, it is still essential to identify the source of the defect by analysing and characterizing the various mutations in the functional regions of seg 7-OP7 vRNA to enable clonal OP7 DIP production.

In prior investigations, Kupke et al., demonstrated a significant accumulation of M1-OP7 and vRNPs in the cell nucleus during co-infection experiments with STV [5]. It was hypothesized that defects in the M1-OP7 protein would also impact M1 protein's regulatory roles, including binding to vRNPs in the nucleus and their nuclear export [65, 180, 181]. Ruediger et al., developed mathematical models that support these experimental findings [84]. Model simulations suggested that defects in M1-OP7 proteins may lead to no or weak binding to the vRNPs in the nucleus, thereby tentatively halting the virus replication, as nuclear export of vRNPs is prevented.

The interaction of M1 proteins with vRNPs in the nucleus, inhibiting their transcription, was initially demonstrated by Perez et al., through a cell-free mini-replicon assay [182]. This assay evaluated transcriptional activity from the polymerase complex—comprising PB2, PB1, PA, and NP proteins—which associates with vRNA to initiate transcription. Early stages of IAV infection are characterized by heightened transcription to produce substantial protein quantities. The binding of M1 proteins to vRNP suppresses polymerase complex activity, thereby reducing transcription [183]. The inhibitory effect of M1 proteins on polymerase activity was assessed using a mini-replicon assay in HEK-WT cells. Here, cells were transfected with plasmids encoding polymerase complex proteins, NP protein, and a reporter gene for chloramphenicol acetyltransferase (CAT), flanked by seg 8 UTRs [182]. The introduction of M1 protein-encoding plasmids in varying concentrations revealed a dose-dependent decrease in reporter activity, indicating polymerase inhibition. This methodology can be extended in the future

experiments to assess the activity of the M1-OP7 protein in mini-replicon assays, aiming to investigate its interaction with vRNPs and subsequent inhibition of reporter protein transcription. In this experimental setup, control plasmids encoding the M1-WT protein can be utilized to compare the transcription inhibition activity between mutated and non-mutated M1 proteins.

Besides, it is conceivable that mutations in the M1-OP7 proteins may contribute to the limitations observed in the reconstitution of clonal OP7 DIPs (Figure 4.3.1). These mutations could result in a defective OP7 DIP phenotype, preventing independent replication. Therefore, it would be apparent to reconstitute OP7 clonal DIPs using complementing cell lines, similar to the approach used for seg 1 DIPs, which contain deletions in seg 1 vRNA and require PB2 protein supplementation from the cell lines for clonal DIP propagation. In this context, future studies could be conducted with M1 protein-expressing cells such as MDCK and HEK could be utilized in an eight-plasmid system. This system would include seven plasmids encoding seg 1-6 and seg 8 WT, along with an eighth plasmid encoding seg 7-OP7.

Furthermore, a co-infection of OP7 seed virus and STV, resulted in reductions in the vRNA levels from other segments such as seg 5 and 8 [5, 38]. It was hypothesized that this effect might be due to superpromoter (G3A/C8U) mutations on seg 7 vRNA, which suppress other vRNA segments while disproportionately increasing the replication of the affected segment [5, 184, 185]. Moreover, Ruediger et al., applied a mathematical model to this experimental dataset and suggested that the presence of superpromoter-carrying segments leads to increased replication of these segments, thereby reducing viral resources available for the replication of other vRNA segments [84]. This, in turn, can exert an antiviral effect. This finding aligns with previous studies where the presence of a superpromoter on the polymerase seg 2 and 3 showed increased replication of the superpromoter-carrying segments and a reduction in other vRNA segments [184]. When viruses with G3A/C8U mutations on seg 2 or 3 were rescued, they exhibited attenuated growth, confirming the interfering phenotype caused by these mutations [184]. The mechanism by which these mutations enhance the replication of their respective segments—whether through stronger polymerase binding due to

altered RNA structures or a lesser preference for other segments by unidentified mechanisms—remains to be elucidated.

In previous studies, increased gene expression (due to increased vRNA replication) from a reporter-encoding segment carrying the superpromoter mutations was demonstrated in a mini-replicon assay [184]. Similarly, the mini-replicon assay can be used to evaluate a plasmid encoding seg 7 vRNA with the G3A/C8U mutation when co-transfected into cells. This method would allow for the determination of whether the replication of this superpromoter containing vRNA leads to a reduction in luciferase activity (compared to co-transfection with a plasmid encoding seg 7 vRNA without the superpromoter mutation), thereby indicating an inhibitory effect of the G3A/C8U mutation on virus replication and demonstrating the antiviral effect of OP7.

The challenge of achieving purely clonal OP7 has been a significant milestone for our research group. Initial efforts to cultivate OP7 alongside STV have paved the way for assessing its antiviral potential and establishing its production in suspension cell culture [38]. This thesis focused on successfully rescuing the OP7 as a chimera DIP that is free of infectious STV, circumventing the need for UV inactivation.

To generate clonal OP7 DIPs devoid of infectious STV, a mammalian PB2-expression system was employed using a reverse genetics approach specific for seg 1 DIP generation. The reconstitution of seg 1 DIPs utilized eight plasmids, with seg 1 encoding the DI vRNA. The addition of a ninth plasmid encoding seg 7-OP7 resulted in a population of DIPs, including a seg 1 DIP (Figure 4.3.2 C) and an OP7 chimera DIP (Figure 4.3.2 E or Figure 4.3.5) [3]. Due to deletions in seg 1, these DIPs are restricted to grow in PB2-expressing cells and final viral harvests are free from infectious STV. The OP7 chimera DIPs were further enriched to 99.7% in the final virus harvest using optimised cell culture-based processes [4].

An initial examination of the blind amplification of OP7 chimera DIPs in MDCK-PB2 adherent cells revealed a decrease in infectious virus titers, alongside a slow decrease in HA titer (Figures 4.3.3 and 4.3.6). This indicated that the seg 1 DIP, acting as a surrogate STV, was likely being outcompeted by the OP7 chimera DIP, as evidenced by the rising OP7 vRNA titers across passages and the diminishing

seg 1 DI vRNA levels (Figures 4.3.4 and 4.3.7). Such findings underscored the necessity to optimize the growth conditions for these complex DIP populations in suspension cell cultures, to achieve high total and infectious virus titers and a high fraction of seg 7-OP7 [4]. Hence, condition 7.1 in Figure 4.3.6B was selected for cultivating the seg 1/winner-OP7 chimera in suspension MDCK-PB2 cells for MODIP screening in MDCK-PB2 suspension cells (refer to Supplement figure 7.6) [3].

MODIP screening, involved infecting MDCK-PB2 cells with varying MOI of OP7 chimera DIPs to identify conditions that yield high total DIP titers (Supplement figure 7.6) and demonstrate potent interference efficacy in vitro using MDCK cells-based assays (Supplement figure 7.8). For the OP7 chimera DIPs, optimal production was achieved with MODIP ranging from E-5 to E-2 in MDCK-PB2 suspension cells incubated in shake flasks at 37°C [3]. Specifically, MODIP of E-4 and E-3 were found to be most effective for producing OP7 chimera DIPs (high fractions of OP7 chimera DIPs based on vRNA quantifications), and with significant interfering activity (Supplement figure 7.7), highlighting the critical role of MODIP in optimizing DIP production.

Later on, the DIP material produced at 37°C in shake flasks was SXC purified to concentrate the virus to high doses for in vivo testing [3]. A mouse model D2(B6).A2G-Mx1$^{r/r}$, expressing the Mx1 gene, which is crucial for antiviral response, was used to mimic human infection closely [186]. The high-dose intranasal administration of OP7 chimera DIP material in these mice did not cause any disease symptoms or significant lung histopathological changes, indicating good tolerability and safety compared to PBS controls (Figure 4.3.11A–B). This outcome suggests that using high doses of DIP in vivo does not lead to adverse effects like cytokine storms or lung damage, while still eliciting a strong antiviral response. This was further supported by the 100% survival rate of mice after co-administration of a lethal dose of STV and OP7 chimera DIPs (Figure 4.3.11E), highlighting the potential of DIPs as effective antivirals [3, 37, 38]. Although the study was performed in mice, future studies in animals such as ferrets and in non-human primates should be performed to confirm these claims. The production of these chimera DIPs using cell culture is currently under evaluation for GMP-compliant manufacturing at Fraunhofer ITEM, Braunschweig. This step is crucial

for further assessing the DIP's toxicity and safety, paving the way for clinical trials and, ultimately, market authorization.

Calu-3 cells serve as optimal in vitro models for evaluating the antiviral efficacy of IAV DIPs against STV propagation. Until now, interference assays utilizing MDCK cells or preclinical studies in murine models have been employed to elucidate the fundamental mechanisms of DIPs. However, in vitro models using target tissues or cell types can closely mimic in vivo conditions, allowing for drug screening under more controlled conditions. As a result, these in vitro models are invaluable, offering significant savings in time and resources, and minimizing the necessity for animal use.

The previous experiments used MDCK cells to assess replication inhibition among various DIPs in co-infection scenarios with STV. However, MDCK cells, lack a fully functional innate immune system capable of combating human IAV infections [177]. Specifically, these cells produce canine Mx proteins (Mx1 and Mx2), which are not effective for defending against human IAV infections [177]. Moreover, any interferons produced by MDCK cells are susceptible to proteolytic breakdown by trypsin, which is added to the culture medium to facilitate multiple rounds of IAV replication [56]. This breakdown occurs because HA proteins from the STV PR8 strain, essential for virus entry into host cells through membrane fusion [187], need to be cleaved into HA1 and HA2 subunits for activation, a process facilitated by trypsin [188, 189]. Therefore, trypsin is externally added to the infection medium for MDCK cells, however this trypsin supplementation May degrade any interferons produced.

In contrast, human-derived cell lines like Calu-3 intrinsically express trypsin like proteases, eliminating the need for external trypsin and preventing interferon degradation [179, 189]. Additionally, human cell lines such as A549 and Calu-3, derived from lung tissues possess a fully functional interferon signalling pathway against human IAV infection [190, 191]. This pathway enables the expression of ISGs specific to human IAV upon infection [191, 192]. Thus, human-origin cell lines with an intact interferon signalling system are more suitable for conducting interference studies. The use of A549 cells as a potential platform for testing interfering capacities of IAV DIPs has limitations as they lack constitutive trypsin

expression, necessitating the exogenous addition of trypsin or the adaptation of the virus strain to one that does not require HA protein cleavage, such as IAV/A/WSN/33 (H1N1) [187, 192, 193]. Using WSN as a backbone, due to its capability for trypsin-independent replication, may prevent the need for long-term trypsin supplementation in the infection medium. However, there are concerns regarding the use of WSN as a backbone for virus-based antiviral therapies. Research by Bdeir et al., highlights an innovative approach using A549 cells in an interference assay, where the backbone of DIPs was switched to a combination of PR8 DI vRNA within the WSN backbone [138]. However, the neurovirulence and poor growth characteristics of WSN-based viruses, compared to the PR8 backbone, limit their practical application, particularly in the context of DIP production for treating IAV infections [156, 157]. The decision to focus on the PR8 backbone for DIP generation in our studies was driven by the need for a system compatible with later market approval processes.

The use of Calu-3 cells was a superior alternative for cultivating the virus without trypsin supplementation, allowing for more accurate quantification of IFN-β stimulation upon DIP or STV infection. This approach has shown promising results in evaluating the antiviral activity of PR8-backbone DIPs against PR8 STV in Calu-3 cells, as evidenced by Figure 4.3.10. Despite these advancements, there remains significant room for improvement of the methodology. For instance, optimizing the cell culture medium by supplementing 1% amino acids could potentially enhance Calu-3 cell propagation [178]. Apart from measuring reliably the IFN-β gene expression, the expression of human IAV-specific ISGs such as Mx1, RSAD2, RIG-I, ITIM3, etc. [7, 194, 195], would also provide more information on the stimulated of the innate immune system by DIPs. Moreover, incorporating IFN-β stimulated cells as a control and screening various IFN-β concentrations could provide deeper insights into the suppression of STV propagation. This would not only refine the assay but also contribute to the evaluation of DIPs as a potential prophylactic treatment, comparing their efficacy against traditional IFN treatments in terms of costs and therapeutic value. The establishment of a more robust in vitro model that could pave the way for more complex in vivo studies. The goal also accommodates assessing the viability of DIPs as a therapeutic alternative to IFN, potentially offering a more cost-effective solution to managing IAV infections.

In further research in our group [4], we optimized OP7 chimera DIP production using MDCK-PB2 suspension cells. Subsequent SXC purification removed contaminants, producing a highly purified product, termed 32°C MD+SXC. This product was tested in Calu-3 cell interference assays, showing superior interfering activity compared to DIPs produced in the original process at 37°C with complete medium exchange (Figure 4.3.10).

For a long time, since DI244 was identified by Dimmock, IAV DIPs have been advocated for use as antivirals. This recommendation stems from research involving DI244, in which mice received DI244 treatment one week before being infected with a lethal dose of STV. The findings revealed that this pre-treatment offered complete protection. In addition, DIPs also demonstrated efficacy as a treatment when administered one- or two-days post-exposure to a lethal STV infection [2]. Furthermore, IAV DIPs have demonstrated protective effects against a variety of non-homologous, IFN-sensitive viruses [17, 29-31]. This underscores the potential of DIPs as broad-spectrum antiviral agents. They could be administered as a nasal spray, when there is a pandemic or in high-risk environments such as nursery or quarantine areas, thereby reducing the spread of infections from other respiratory viruses including IAV.

Furthermore, current research by Dunja Bruder (HZI, Braunschweig) employs mouse models to assess OP7 chimera DIPs as a mucosal vaccine. These studies investigate the adaptive immune responses elicited by the intranasal administration of OP7 chimera DIPs. They observed that intranasal administration of OP7 chimera DIPs resulted in a robust systemic antibody response, along with strong mucosal antibody responses and cellular immune responses, as indicated by the presence of interferon-gamma (IFN-γ) producing cells (unpublished data). Consequently, DIPs emerge as a promising vaccine candidate for the treatment of IAV. Dimmock et al., also showed the use of DI244 (at a very high concentration of 12 µg) as an intranasal vaccine, showed complete protection against the challenge STV [2]. In some case, DIP administration also mounted an adaptive immune response to the STV challenge strains [2]. However, in these studies with DI244, the DIP preparations were produced with an infectious STV in the final DIP harvest, which was UV-inactivated. More specifically, these DIP preparations were produced using egg-based cultivations, which have their known shortcomings

compared to the cell-based cultivations. The DIP produced is therefore promising not just as an antiviral but as a vaccine.

Future research will focus on utilizing OP7 as a live DIP vaccine, in addition to its currently identified role as an antiviral, to further expand its potential applications. This will be complemented by the development of robust manufacturing processes and comprehensive toxicology studies, thereby enhancing the likelihood of market approval as a medical drug.

5. Conclusion and Outlook

Previous studies have demonstrated the potential of IAV DIPs for antiviral use in outbreaks [1, 17, 30, 34, 37, 38]. A modified IAV reverse genetics system has enabled the production of specific DIPs without the need for co-cultivation with STV [6, 137]. This allowed to overcome previous production challenges. In this thesis, this approach was employed to produce new seg 1-based DIP constructs [6], which do not contain infectious STV, for use as antivirals or live vaccines.

Newly identified seg 1 DIPs with enhanced antiviral activity

In a collaborative project, a semi-continuous production process was employed for evolution studies [1], and novel deletion junctions were identified via NGS analysis [77]. These deletion junctions, suspected to be highly competitive and interfering, accumulated to high titers during long-term infections [1]. To determine the antiviral activity of the new DIPs, reverse genetics was used to reconstitute seg 1 DIPs.

The DIP rescue experiments demonstrated that varying the amount of DI plasmid during transfection significantly influenced the rescue efficiency of the DIPs, likely due to a self-interfering activity during their own reconstitution. Specifically, using 50 ng of DI plasmid combined with 1 µg of seven full-length plasmids per well resulted in successful reconstitution of both seg 1 winner and loser constructs, while higher amounts of DI plasmids (1 µg) were only effective for the seg 1 winner construct. Subsequent amplification in adherent MDCK-PB2 cells yielded high infectious virus titers for both seg 1 winner and loser constructs. In contrast, the seg 1 De novo construct (reconstituted using 50 ng DI plasmid) required additional rounds of amplification in suspension MDCK-PB2 cells to achieve detectable titers.

Next, these seg 1 DIP constructs were subjected to an in vitro interference assay in MDCK cells to analyse their capacity to interfere with STV replication. Results supported the hypothesis that the newly identified deletion junctions exhibit strong antiviral activity, with highly competitive DIPs demonstrating a higher antiviral effect than DI244 and slower growing DIPs [1].

While specific determinants of rapidly proliferating DIPs could not be identified, observations indicated that highly competitive DIPs were primarily encoded within

seg 1, 2, and 3 of the IAV polymerase genes. These DIPs exhibited an optimal length that included essential incorporation signals for packaging of the vRNA into progeny virions. Although seg 1 DIPs were successfully reconstituted using a modified reverse genetics system, difficulties were encountered in rescuing and amplifying DIPs derived from seg 2 and 3. This highlighted the necessity for further investigation into the factors affecting DIP rescue and proliferation.

Future studies should explore different viral strain backbones, such as WSN, to determine if DIPs with specific deletion junctions could be rescued more effectively compared to the PR8 backbone. Additionally, it is possible that the reconstitution of specific deletion junctions in polymerase seg 2 and 3 require particular sizes and locations. Various deletion junctions on the PR8 or WSN backbones could be tested to provide further insights. Alternatively, a chimeric approach could be employed as described in a previous study to rescue seg 3 DIPs devoid of any infectious STV [138]. Here, seg 3 deletion was presented in the PR8 strain and rescued using the WSN backbone, which provided the remaining seven vRNA segments. These reconstituted DIPs could then be subjected to interference assays to evaluate their antiviral activity.

Overall, this study offered a thorough examination of viral evolution and replication processes, emphasizing the significance and potential of IAV DIPs. The application of reverse genetics provided a proof of concept by enabling the reconstitution of specific DIPs and their assessment of antiviral activity in vitro. The newly identified DIPs will serve as a foundational platform for developing innovative antivirals and vaccines, as addressed in other parts of this thesis.

A DIP-based live vaccine for mucosal administration

Following the success of identifying and reconstituting a new seg 1 DIP with superior antiviral activity than DI244, the next goal was to develop a LAIV based on this construct. This aimed to create a construct with strong antiviral activity and the ability to stimulate adaptive immune responses to seasonal IAV infections. Utilizing DIPs as a platform for production of LAIVs offers options to achieve a broader safety profile compared to currently available LAIVs [165], as conventional seg 1 DIPs can only multiply in cells that express PB2, significantly reducing safety concerns.

In the scope of this thesis, a vaccine construct was engineered by substituting the surface antigens (HA and NA) of seg 1 DIP with those from the pandemic strain Cal H1N1. While a Cal H1N1 virus-based CVV with a 5+3 genome constellation in the PR8 backbone was successfully reconstituted, efforts to reconstitute a seg 1-based DIP vaccine expressing Cal H1N1 were not successful. This outcome suggested potential incompatibilities between the seg 1 DIP and the pandemic strain, indicating the need for further molecular-level investigations to optimize the DIP-vaccine construct.

This includes assessing the compatibility of the UTRs and packaging signals of the seg1 DIP and Cal H1N1 vRNA segments. A mismatch between the UTRs or the absence of packaging signals due to large internal deletions may hinder RNA-RNA interactions, leading to unsuccessful packaging and the generation of functional virions. Future experiments are planned that involve substituting the UTRs of Cal H1N1 with those of PR8 to create a DIP platform with compatible UTR ends. This would facilitate the availability of packaging signals, thereby enabling the bundling and incorporation of all vRNA segments to generate functional virions. Additionally, it may be necessary to provide more packaging signals to ease the bundling and incorporation process, which would involve testing for deletion junctions shorter than the seg 1 winner DI vRNA that was previously tested.

Overall, with the increasing risk of pandemics, prioritizing methods for fast vaccine development, particularly using the PR8 backbone for its growth efficiency, is vital [158]. Efforts should focus on overcoming obstacles in DIP utilization for creating adaptable virus constructs and establishing a DIP platform that allows for easy manipulation, fast screening and high-yield virus production. This includes adopting a "plug and play" approach to incorporate WHO-recommended vaccine strain surface glycoproteins into the DIP backbone, and bypassing strain-specific internal gene requirements for effective virus growth. Advances in cell culture technology may allow for the production of these DIP-based live vaccines to high titers. Thereby, these DIP-based vaccine candidates would be easily accessible.

Reconstitution of OP7 chimera DIPs

OP7 is a new type of IAV DIP with 37-point mutations, demonstrating stronger antiviral activity than DI244 both in vitro and in vivo [5, 37, 38]. This PhD thesis

showed initial attempts to reconstitute OP7 DIPs using an eight-plasmid rescue scheme. Unsuccessful reconstitution of STV-free OP7 DIPs, underscored the need to identify specific mutations responsible for the DIP's replication defect and its inhibitory effect on STV propagation.

Understanding the unique characteristics of OP7 is essential for its potential use as an antiviral or live vaccine. This requires initial characterization of its defects to elucidate its interference mechanism. Future studies can employ techniques like mini replicon assays to investigate the interactions between the mutated M1-OP7 protein and the vRNP complexes [65, 180, 181]. A better characterization of the impact of superpromoter mutations on seg 7-OP7 vRNA and the level of other vRNAs could provide insights into its broader effects on viral replication and packaging [184, 185].

Due to the strong antiviral activity of OP7, developing a reconstitution system devoid of infectious STVs was essential. Rescue experiments indicated that OP7 was defective and relied on gene complementation from full-length seg 7 vRNA. A nine-plasmid system based on modified IAV reverse genetics was employed to create OP7 chimera DIPs, overcoming previous reconstitution challenges. This system allowed for the evaluation of the antiviral capabilities of OP7 chimera DIPs [3].

Subsequent studies allowed to establish a cell culture-based production and purification process for OP7 chimera DIPs in suspension MDCK-PB2 cells [4]. Post-production, the antiviral preparations were tested in mice by Dunja Bruder's lab. The administration of OP7 chimera DIPs was well tolerated, showing no adverse effects such as cytokine storms or infiltration of immune cells into the lungs [3]. Moreover, these studies revealed that the DIPs were highly effective antivirals, leading to a 100% survival rate in mice exposed to lethal STV infections without any disease symptoms [3].

Additionally, the produced OP7 chimera DIP material achieved a purity level of at least 99.7%, making the process suitable for large-scale industrial production [4]. Comparative studies using material from these optimized processes in a new human lung cell-based assay (using Calu-3 cells) showed a strong, early IFN-β response, indicating enhanced contribution to the antiviral activity [4].

Future studies should aim for exploring the broader potential of OP7 chimera DIPs, including their use as a mucosal LAIV vaccine, in addition to their potential use as antiviral. In summary, this PhD work demonstrated the potential for cell culture-based production of OP7 chimera DIPs, which is crucial for GMP-compliant manufacturing, toxicity and safety evaluations, clinical trials, and eventual market approval.

6. References

1. Pelz, L., et al., *Semi-continuous Propagation of Influenza A Virus and Its Defective Interfering Particles: Analyzing the Dynamic Competition To Select Candidates for Antiviral Therapy.* J Virol, 2021. **95**(24): p. e0117421.
2. Dimmock, N.J., et al., *Influenza virus protecting RNA: an effective prophylactic and therapeutic antiviral.* J Virol, 2008. **82**(17): p. 8570-8.
3. Dogra, T., et al., *Generation of "OP7 chimera" defective interfering influenza A particle preparations free of infectious virus that show antiviral efficacy in mice.* Sci Rep, 2023. **13**(1): p. 20936.
4. Pelz, L., et al., *Production of antiviral "OP7 chimera" defective interfering particles free of infectious virus.* Appl Microbiol Biotechnol, 2024. **108**(1): p. 97.
5. Kupke, S.Y., et al., *A Novel Type of Influenza A Virus-Derived Defective Interfering Particle with Nucleotide Substitutions in Its Genome.* J Virol, 2019. **93**(4).
6. Bdeir, N., et al., *A system for production of defective interfering particles in the absence of infectious influenza A virus.* PLoS One, 2019. **14**(3): p. e0212757.
7. Goraya, M., et al., *Web of interferon stimulated antiviral factors to control the influenza A viruses replication.* Microb Pathog, 2020. **139**: p. 103919.
8. Hoffmann, E., et al., *A DNA transfection system for generation of influenza A virus from eight plasmids.* Proc Natl Acad Sci U S A, 2000. **97**(11): p. 6108-13.
9. Krammer, F., et al., *Influenza.* Nat Rev Dis Primers, 2018. **4**(1): p. 3.
10. Singh, P., et al., *Influenza A virus and its antiviral drug treatment options.* Medicine in Microecology, 2023. **16**.
11. Zheng, W. and Y.J. Tao, *Structure and assembly of the influenza A virus ribonucleoprotein complex.* FEBS Lett, 2013. **587**(8): p. 1206-14.
12. G. B. D. Chronic Respiratory Diseases Collaborators, *Global burden of chronic respiratory diseases and risk factors, 1990-2019: an update from the Global Burden of Disease Study 2019.* EClinicalMedicine, 2023. **59**: p. 101936.
13. Iuliano, A.D., et al., *Estimates of global seasonal influenza-associated respiratory mortality: a modelling study.* Lancet, 2018. **391**(10127): p. 1285-1300.
14. Johnson, N.P. and J. Mueller, *Updating the accounts: global mortality of the 1918-1920 "Spanish" influenza pandemic.* Bull Hist Med, 2002. **76**(1): p. 105-15.
15. Krammer, F. and P. Palese, *Advances in the development of influenza virus vaccines.* Nat Rev Drug Discov, 2015. **14**(3): p. 167-82.
16. Trombetta, C.M., et al., *Influenza Viruses and Vaccines: The Role of Vaccine Effectiveness Studies for Evaluation of the Benefits of Influenza Vaccines.* Vaccines (Basel), 2022. **10**(5).
17. Dimmock, N.J. and A.J. Easton, *Cloned Defective Interfering Influenza RNA and a Possible Pan-Specific Treatment of Respiratory Virus Diseases.* Viruses, 2015. **7**(7): p. 3768-88.
18. Frensing, T., *Defective interfering viruses and their impact on vaccines and viral vectors.* Biotechnol J, 2015. **10**(5): p. 681-9.
19. Huo, C., et al., *Safety, Immunogenicity, and Effectiveness of Defective Viral Particles Arising in Mast Cells Against Influenza in Mice.* Front Immunol, 2020. **11**: p. 585254.
20. Huo, C., et al., *Defective Viral Particles Produced in Mast Cells Can Effectively Fight Against Lethal Influenza A Virus.* Front Microbiol, 2020. **11**: p. 553274.
21. Genoyer, E. and C.B. Lopez, *The Impact of Defective Viruses on Infection and Immunity.* Annu Rev Virol, 2019. **6**(1): p. 547-566.
22. Vasilijevic, J., et al., *Reduced accumulation of defective viral genomes contributes to severe outcome in influenza virus infected patients.* PLoS Pathog, 2017. **13**(10): p. e1006650.

23. Vignuzzi, M. and C.B. Lopez, *Defective viral genomes are key drivers of the virus-host interaction.* Nat Microbiol, 2019. **4**(7): p. 1075-1087.
24. Yang, Y., et al., *The Antiviral and Antitumor Effects of Defective Interfering Particles/Genomes and Their Mechanisms.* Front Microbiol, 2019. **10**: p. 1852.
25. Nayak, D.P., T.M. Chambers, and R.K. Akkina, *Defective-interfering (DI) RNAs of influenza viruses: origin, structure, expression, and interference.* Curr Top Microbiol Immunol, 1985. **114**: p. 103-51.
26. Marriott, A.C. and N.J. Dimmock, *Defective interfering viruses and their potential as antiviral agents.* Rev Med Virol, 2010. **20**(1): p. 51-62.
27. Manzoni, T.B. and C.B. Lopez, *Defective (interfering) viral genomes re-explored: impact on antiviral immunity and virus persistence.* Future Virol, 2018. **13**(7): p. 493-503.
28. Wu, M., et al., *Defective Interfering Particles of Influenza Virus and Their Characteristics, Impacts, and Use in Vaccines and Antiviral Strategies: A Systematic Review.* Viruses, 2022. **14**(12).
29. Rand, U., et al., *Antiviral Activity of Influenza A Virus Defective Interfering Particles against SARS-CoV-2 Replication In Vitro through Stimulation of Innate Immunity.* Cells, 2021. **10**(7).
30. Pelz, L., et al., *Broad-Spectrum Antiviral Activity of Influenza A Defective Interfering Particles against Respiratory Syncytial, Yellow Fever, and Zika Virus Replication In Vitro.* Viruses, 2023. **15**(9).
31. Scott, P.D., et al., *Defective interfering influenza A virus protects in vivo against disease caused by a heterologous influenza B virus.* J Gen Virol, 2011. **92**(Pt 9): p. 2122-2132.
32. Harding, A.T. and N.S. Heaton, *Efforts to Improve the Seasonal Influenza Vaccine.* Vaccines (Basel), 2018. **6**(2).
33. Ziegler, C.M. and J.W. Botten, *Defective Interfering Particles of Negative-Strand RNA Viruses.* Trends Microbiol, 2020. **28**(7): p. 554-565.
34. Dimmock, N.J. and A.J. Easton, *Defective interfering influenza virus RNAs: time to reevaluate their clinical potential as broad-spectrum antivirals?* J Virol, 2014. **88**(10): p. 5217-27.
35. Scott, P.D., et al., *Defective interfering virus protects elderly mice from influenza.* Virol J, 2011. **8**: p. 212.
36. Dimmock, N.J., et al., *Cloned defective interfering influenza virus protects ferrets from pandemic 2009 influenza A virus and allows protective immunity to be established.* PLoS One, 2012. **7**(12): p. e49394.
37. Hein, M.D., et al., *Cell culture-based production and in vivo characterization of purely clonal defective interfering influenza virus particles.* BMC Biol, 2021. **19**(1): p. 91.
38. Hein, M.D., et al., *OP7, a novel influenza A virus defective interfering particle: production, purification, and animal experiments demonstrating antiviral potential.* Appl Microbiol Biotechnol, 2021. **105**(1): p. 129-146.
39. Bouvier, N.M. and P. Palese, *The biology of influenza viruses.* Vaccine, 2008. **26 Suppl 4**(Suppl 4): p. D49-53.
40. Dou, D., et al., *Influenza A Virus Cell Entry, Replication, Virion Assembly and Movement.* Front Immunol, 2018. **9**: p. 1581.
41. Lee, N., et al., *Genome-wide analysis of influenza viral RNA and nucleoprotein association.* Nucleic Acids Res, 2017. **45**(15): p. 8968-8977.
42. Li, H.C., C.H. Yang, and S.Y. Lo, *Strategies of Influenza A Virus to Ensure the Translation of Viral mRNAs.* Pathogens, 2022. **11**(12).
43. Ferhadian, D., et al., *Structural and Functional Motifs in Influenza Virus RNAs.* Front Microbiol, 2018. **9**: p. 559.
44. Goto, H., et al., *The genome-packaging signal of the influenza A virus genome comprises a genome incorporation signal and a genome-bundling signal.* J Virol, 2013. **87**(21): p. 11316-22.

45. Carter, T. and M. Iqbal, *The Influenza A Virus Replication Cycle: A Comprehensive Review.* Viruses, 2024. **16**(2).
46. Noda, T. and Y. Kawaoka, *Structure of influenza virus ribonucleoprotein complexes and their packaging into virions.* Rev Med Virol, 2010. **20**(6): p. 380-91.
47. Noda, T., et al., *Three-dimensional analysis of ribonucleoprotein complexes in influenza A virus.* Nat Commun, 2012. **3**: p. 639.
48. Chlanda, P., et al., *Structural Analysis of the Roles of Influenza A Virus Membrane-Associated Proteins in Assembly and Morphology.* J Virol, 2015. **89**(17): p. 8957-66.
49. Skehel, J.J. and D.C. Wiley, *Receptor binding and membrane fusion in virus entry: the influenza hemagglutinin.* Annu Rev Biochem, 2000. **69**: p. 531-69.
50. Liu, L., et al., *Receptor Binding Properties of Neuraminidase for influenza A virus: An Overview of Recent Research Advances.* Virulence, 2023. **14**(1): p. 2235459.
51. Iwasaki, A. and P.S. Pillai, *Innate immunity to influenza virus infection.* Nat Rev Immunol, 2014. **14**(5): p. 315-28.
52. Noda, T., *Native morphology of influenza virions.* Front Microbiol, 2011. **2**: p. 269.
53. Nelli, R.K., et al., *Comparative distribution of human and avian type sialic acid influenza receptors in the pig.* BMC Vet Res, 2010. **6**: p. 4.
54. Isin, B., P. Doruker, and I. Bahar, *Functional motions of influenza virus hemagglutinin: a structure-based analytical approach.* Biophys J, 2002. **82**(2): p. 569-81.
55. Sun, X., et al., *Modifications to the hemagglutinin cleavage site control the virulence of a neurotropic H1N1 influenza virus.* J Virol, 2010. **84**(17): p. 8683-90.
56. Seitz, C., et al., *Trypsin promotes efficient influenza vaccine production in MDCK cells by interfering with the antiviral host response.* Appl Microbiol Biotechnol, 2012. **93**(2): p. 601-11.
57. Mtambo, S.E., et al., *Influenza Viruses: Harnessing the Crucial Role of the M2 Ion-Channel and Neuraminidase toward Inhibitor Design.* Molecules, 2021. **26**(4).
58. Pinto, L.H. and R.A. Lamb, *The M2 proton channels of influenza A and B viruses.* J Biol Chem, 2006. **281**(14): p. 8997-9000.
59. Schreiber, A., et al., *Dissecting the mechanism of signaling-triggered nuclear export of newly synthesized influenza virus ribonucleoprotein complexes.* Proc Natl Acad Sci U S A, 2020. **117**(28): p. 16557-16566.
60. Hutchinson, E.C. and E. Fodor, *Nuclear import of the influenza A virus transcriptional machinery.* Vaccine, 2012. **30**(51): p. 7353-8.
61. Fodor, E., *The RNA polymerase of influenza a virus: mechanisms of viral transcription and replication.* Acta Virol, 2013. **57**(2): p. 113-22.
62. Deng, T., F.T. Vreede, and G.G. Brownlee, *Different de novo initiation strategies are used by influenza virus RNA polymerase on its cRNA and viral RNA promoters during viral RNA replication.* J Virol, 2006. **80**(5): p. 2337-48.
63. Te Velthuis, A.J. and E. Fodor, *Influenza virus RNA polymerase: insights into the mechanisms of viral RNA synthesis.* Nat Rev Microbiol, 2016. **14**(8): p. 479-93.
64. Rossman, J.S. and R.A. Lamb, *Influenza virus assembly and budding.* Virology, 2011. **411**(2): p. 229-36.
65. Brunotte, L., et al., *The nuclear export protein of H5N1 influenza A viruses recruits Matrix 1 (M1) protein to the viral ribonucleoprotein to mediate nuclear export.* J Biol Chem, 2014. **289**(29): p. 20067-77.
66. Noda, T., *Selective Genome Packaging Mechanisms of Influenza A Viruses.* Cold Spring Harb Perspect Med, 2021. **11**(7).
67. Bancroft, C.T. and T.G. Parslow, *Evidence for segment-nonspecific packaging of the influenza a virus genome.* J Virol, 2002. **76**(14): p. 7133-9.
68. Odagiri, T. and M. Tashiro, *Segment-specific noncoding sequences of the influenza virus genome RNA are involved in the specific competition between*

defective interfering RNA and its progenitor RNA segment at the virion assembly step. J Virol, 1997. **71**(3): p. 2138-45.
69. Duhaut, S.D. and J.W. McCauley, *Defective RNAs inhibit the assembly of influenza virus genome segments in a segment-specific manner.* Virology, 1996. **216**(2): p. 326-37.
70. Von Magnus, P., *Propagation of the PR8 strain of influenza A virus in chick embryos. III. Properties of the incomplete virus produced in serial passages of undiluted virus.* Acta Pathol Microbiol Scand, 1951. **29**(2): p. 157-81.
71. Von Magnus, P., *Propagation of the PR8 strain of influenza A virus in chick embryos. II. The formation of incomplete virus following inoculation of large doses of seed virus.* Acta Pathol Microbiol Scand, 1951. **28**(3): p. 278-93.
72. Huang, A.S. and D. Baltimore, *Defective viral particles and viral disease processes.* Nature, 1970. **226**(5243): p. 325-7.
73. Welch, S.R., et al., *Inhibition of Nipah Virus by Defective Interfering Particles.* J Infect Dis, 2020. **221**(Suppl 4): p. S460-S470.
74. Lazzarini, R.A., J.D. Keene, and M. Schubert, *The origins of defective interfering particles of the negative-strand RNA viruses.* Cell, 1981. **26**(2 Pt 2): p. 145-54.
75. Perrault, J., *Origin and replication of defective interfering particles.* Curr Top Microbiol Immunol, 1981. **93**: p. 151-207.
76. Piasecka, J., A. Jarmolowicz, and E. Kierzek, *Organization of the Influenza A Virus Genomic RNA in the Viral Replication Cycle-Structure, Interactions, and Implications for the Emergence of New Strains.* Pathogens, 2020. **9**(11).
77. Alnaji, F.G., et al., *Sequencing Framework for the Sensitive Detection and Precise Mapping of Defective Interfering Particle-Associated Deletions across Influenza A and B Viruses.* J Virol, 2019. **93**(11).
78. Alnaji, F.G., et al., *Influenza A Virus Defective Viral Genomes Are Inefficiently Packaged into Virions Relative to Wild-Type Genomic RNAs.* mBio, 2021. **12**(6): p. e0295921.
79. Fodor, E., et al., *A single amino acid mutation in the PA subunit of the influenza virus RNA polymerase promotes the generation of defective interfering RNAs.* J Virol, 2003. **77**(8): p. 5017-20.
80. Alnaji, F.G. and C.B. Brooke, *Influenza virus DI particles: Defective interfering or delightfully interesting?* PLoS Pathog, 2020. **16**(5): p. e1008436.
81. Fan, H., et al., *Structures of influenza A virus RNA polymerase offer insight into viral genome replication.* Nature, 2019. **573**(7773): p. 287-290.
82. Laske, T., et al., *Reprint of "Modeling the intracellular replication of influenza A virus in the presence of defective interfering RNAs.* Virus Res, 2016. **218**: p. 86-95.
83. Hein, M.D., et al., *Cell culture-based production of defective interfering influenza A virus particles in perfusion mode using an alternating tangential flow filtration system.* Appl Microbiol Biotechnol, 2021. **105**(19): p. 7251-7264.
84. Ruediger, D., et al., *Mathematical model calibrated to in vitro data predicts mechanisms of antiviral action of the influenza defective interfering particle "OP7".* iScience, 2024. **27**(4): p. 109421.
85. Hutchinson, E.C., et al., *Mutational analysis of cis-acting RNA signals in segment 7 of influenza A virus.* J Virol, 2008. **82**(23): p. 11869-79.
86. Roux, L., A.E. Simon, and J.J. Holland, *Effects of defective interfering viruses on virus replication and pathogenesis in vitro and in vivo.* Adv Virus Res, 1991. **40**: p. 181-211.
87. Frensing, T., et al., *Impact of defective interfering particles on virus replication and antiviral host response in cell culture-based influenza vaccine production.* Appl Microbiol Biotechnol, 2014. **98**(21): p. 8999-9008.
88. Isken, B., Y. Genzel, and U. Reichl, *Productivity, apoptosis, and infection dynamics of influenza A/PR/8 strains and A/PR/8-based reassortants.* Vaccine, 2012. **30**(35): p. 5253-61.

89. Ruediger, D., et al., *Multiscale model of defective interfering particle replication for influenza A virus infection in animal cell culture.* PLoS Comput Biol, 2021. **17**(9): p. e1009357.
90. Frensing, T., et al., *Continuous influenza virus production in cell culture shows a periodic accumulation of defective interfering particles.* PLoS One, 2013. **8**(9): p. e72288.
91. Lamb, R.A. and P.W. Choppin, *The gene structure and replication of influenza virus.* Annu Rev Biochem, 1983. **52**: p. 467-506.
92. Luytjes, W., et al., *Amplification, expression, and packaging of foreign gene by influenza virus.* Cell, 1989. **59**(6): p. 1107-13.
93. McGeoch, D., P. Fellner, and C. Newton, *Influenza virus genome consists of eight distinct RNA species.* Proc Natl Acad Sci U S A, 1976. **73**(9): p. 3045-9.
94. Mendes, M. and A.B. Russell, *Library-based analysis reveals segment and length dependent characteristics of defective influenza genomes.* PLoS Pathog, 2021. **17**(12): p. e1010125.
95. Goraya, M.U., et al., *Web of interferon stimulated antiviral factors to control the influenza A viruses replication.* Microb Pathog, 2020. **139**: p. 103919.
96. Baum, A. and A. Garcia-Sastre, *Differential recognition of viral RNA by RIG-I.* Virulence, 2011. **2**(2): p. 166-9.
97. Doly, J., et al., *Type I interferons: expression and signalization.* Cell Mol Life Sci, 1998. **54**(10): p. 1109-21.
98. Haller, O. and G. Kochs, *Mx genes: host determinants controlling influenza virus infection and trans-species transmission.* Hum Genet, 2020. **139**(6-7): p. 695-705.
99. Vasou, A., et al., *Targeting Pattern Recognition Receptors (PRR) for Vaccine Adjuvantation: From Synthetic PRR Agonists to the Potential of Defective Interfering Particles of Viruses.* Viruses, 2017. **9**(7).
100. Mercado-Lopez, X., et al., *Highly immunostimulatory RNA derived from a Sendai virus defective viral genome.* Vaccine, 2013. **31**(48): p. 5713-21.
101. Xiao, Y., et al., *A defective viral genome strategy elicits broad protective immunity against respiratory viruses.* Cell, 2021. **184**(25): p. 6037-6051 e14.
102. Wang, S., et al., *Subgenomic RNA from Dengue Virus Type 2 Suppresses Replication of Dengue Virus Genomes and Interacts with Virus-Encoded NS3 and NS5 Proteins.* ACS Infect Dis, 2020. **6**(3): p. 436-446.
103. Johnson, D.M., et al., *Lassa Virus Vaccine Candidate ML29 Generates Truncated Viral RNAs Which Contribute to Interfering Activity and Attenuation.* Viruses, 2021. **13**(2).
104. Kuge, S., I. Saito, and A. Nomoto, *Primary structure of poliovirus defective-interfering particle genomes and possible generation mechanisms of the particles.* J Mol Biol, 1986. **192**(3): p. 473-87.
105. Wang, C., et al., *Influenza Defective Interfering Virus Promotes Multiciliated Cell Differentiation and Reduces the Inflammatory Response in Mice.* J Virol, 2023. **97**(6): p. e0049323.
106. Scott, P.D., et al., *Defective interfering influenza virus confers only short-lived protection against influenza virus disease: evidence for a role for adaptive immunity in DI virus-mediated protection in vivo.* Vaccine, 2011. **29**(38): p. 6584-91.
107. Boergeling, Y., et al., *Evidence for a Novel Mechanism of Influenza Virus-Induced Type I Interferon Expression by a Defective RNA-Encoded Protein.* PLoS Pathog, 2015. **11**(5): p. e1004924.
108. Ghanem, A., et al., *Peptide-mediated interference with influenza A virus polymerase.* J Virol, 2007. **81**(14): p. 7801-4.
109. Wunderlich, K., et al., *Identification of a PA-binding peptide with inhibitory activity against influenza A and B virus replication.* PLoS One, 2009. **4**(10): p. e7517.

110. Ranum, J.N., et al., *Cryptic proteins translated from deletion-containing viral genomes dramatically expand the influenza virus proteome.* Nucleic Acids Res, 2024. **52**(6): p. 3199-3212.
111. Hubsher, G., M. Haider, and M.S. Okun, *Amantadine: the journey from fighting flu to treating Parkinson disease.* Neurology, 2012. **78**(14): p. 1096-9.
112. Han, J., et al., *Influenza Virus: Small Molecule Therapeutics and Mechanisms of Antiviral Resistance.* Curr Med Chem, 2018. **25**(38): p. 5115-5127.
113. Wintermeyer, S.M. and M.C. Nahata, *Rimantadine: a clinical perspective.* Ann Pharmacother, 1995. **29**(3): p. 299-310.
114. O'Hanlon, R. and M.L. Shaw, *Baloxavir marboxil: the new influenza drug on the market.* Curr Opin Virol, 2019. **35**: p. 14-18.
115. Meijer, A., et al., *Oseltamivir-resistant influenza virus A (H1N1), Europe, 2007-08 season.* Emerg Infect Dis, 2009. **15**(4): p. 552-60.
116. Le, Q.M., et al., *Avian flu: isolation of drug-resistant H5N1 virus.* Nature, 2005. **437**(7062): p. 1108.
117. Kiso, M., et al., *Resistant influenza A viruses in children treated with oseltamivir: descriptive study.* Lancet, 2004. **364**(9436): p. 759-65.
118. Cochran, K.W., et al., *Studies on the antiviral activity of amantadine hydrochloride.* Ann N Y Acad Sci, 1965. **130**(1): p. 432-9.
119. Chen, W., et al., *Approaches for discovery of small-molecular antivirals targeting to influenza A virus PB2 subunit.* Drug Discov Today, 2022. **27**(6): p. 1545-1553.
120. Wood, J.M. and J.P. Weir, *Standardisation of inactivated influenza vaccines-Learning from history.* Influenza Other Respir Viruses, 2018. **12**(2): p. 195-201.
121. Lee, M.S. and A.Y. Hu, *A cell-based backup to speed up pandemic influenza vaccine production.* Trends Microbiol, 2012. **20**(3): p. 103-5.
122. Kilbourne, E.D., *Future influenza vaccines and the use of genetic recombinants.* Bull World Health Organ, 1969. **41**(3): p. 643-5.
123. Robertson, J.S., et al., *The development of vaccine viruses against pandemic A(H1N1) influenza.* Vaccine, 2011. **29**(9): p. 1836-43.
124. World Health Organization. *Availability of a candidate reassortant vaccine virus for the novel influenza A (H1N1) vaccine development*. 2009; Available from: https://cdn.who.int/media/docs/default-source/influenza/cvvs/archive-2009/20090527_x179aa.pdf?sfvrsn=3eaa581e_14.
125. Belshe, R., et al., *Safety, immunogenicity and efficacy of intranasal, live attenuated influenza vaccine.* Expert Rev Vaccines, 2004. **3**(6): p. 643-54.
126. Kendal, A.P., et al., *Development of Cold-Adapted Recombinant Live, Attenuated Influenza-a Vaccines in the USA and Ussr.* Antiviral Research, 1982. **1**(6): p. 339-365.
127. AstraZeneca. *European Commission approves Fluenz Tetra for the prevention of seasonal influenza in children*. 2013; Available from: https://www.astrazeneca.com/media-centre/press-releases/2013/fluenz-tetra-european-commission-approval-seasonal-influenza-prevention-children-06122013.html#.
128. Doroshenko, A. and S.A. Halperin, *Trivalent MDCK cell culture-derived influenza vaccine Optaflu (Novartis Vaccines).* Expert Rev Vaccines, 2009. **8**(6): p. 679-88.
129. Minskaia, E.L., G. *Reverse Genetics of the Negative-Sense Influenza A Virus: Aspects and Applications*. 2015; Available from: https://symbiosisonlinepublishing.com/virology-retrovirology/virology-retrovirology07.php.
130. Palese, P., et al., *Negative-strand RNA viruses: genetic engineering and applications.* Proc Natl Acad Sci U S A, 1996. **93**(21): p. 11354-8.
131. Honda, A., et al., *Identification of the RNA polymerase-binding site on genome RNA of influenza virus.* J Biochem, 1987. **102**(5): p. 1241-9.
132. Zobel, A., G. Neumann, and G. Hobom, *RNA polymerase I catalysed transcription of insert viral cDNA.* Nucleic Acids Res, 1993. **21**(16): p. 3607-14.

133. Pleschka, S., et al., *A plasmid-based reverse genetics system for influenza A virus.* J Virol, 1996. **70**(6): p. 4188-92.
134. Neumann, G., et al., *Generation of influenza A viruses entirely from cloned cDNAs.* Proc Natl Acad Sci U S A, 1999. **96**(16): p. 9345-50.
135. Chaturvedi, S., et al., *Identification of a therapeutic interfering particle-A single-dose SARS-CoV-2 antiviral intervention with a high barrier to resistance.* Cell, 2021. **184**(25): p. 6022-6036 e18.
136. Tapia, F., et al., *Production of Defective Interfering Particles of Influenza A Virus in Parallel Continuous Cultures at Two Residence Times-Insights From qPCR Measurements and Viral Dynamics Modeling.* Front Bioeng Biotechnol, 2019. **7**: p. 275.
137. Yamagata, Y., et al., *Generation of a purely clonal defective interfering influenza virus.* Microbiol Immunol, 2019. **63**(5): p. 164-171.
138. Bdeir, N., et al., *Evidence that two instead of one defective interfering RNA in influenza A virus-derived defective interfering particles (DIPs) does not enhance antiviral activity.* Sci Rep, 2021. **11**(1): p. 20477.
139. Hoffmann, E., et al., *Eight-plasmid system for rapid generation of influenza virus vaccines.* Vaccine, 2002. **20**(25-26): p. 3165-70.
140. Andreou, A.I. and N. Nakayama, *Mobius Assembly: A versatile Golden-Gate framework towards universal DNA assembly.* PLoS One, 2018. **13**(1): p. e0189892.
141. Andreou, A.I. and N. Nakayama, *Mobius Assembly.* Methods Mol Biol, 2020. **2205**: p. 201-218.
142. Seitz, C., *Der Einfluss der Wirtszell-Interferonantwort auf die Influenza-Impfstoffproduktion in MDCK-Zellen*. 2012.
143. Kalbfuss, B., et al., *Monitoring influenza virus content in vaccine production: precise assays for the quantitation of hemagglutination and neuraminidase activity.* Biologicals, 2008. **36**(3): p. 145-61.
144. Frensing, T., et al., *Influenza virus intracellular replication dynamics, release kinetics, and particle morphology during propagation in MDCK cells.* Appl Microbiol Biotechnol, 2016. **100**(16): p. 7181-92.
145. G., H., *An assay to assess the antiviral effect of influenza A virus defective interfering particles in vitro using human lung cells*. 2022.
146. Kawakami, E., et al., *Strand-specific real-time RT-PCR for distinguishing influenza vRNA, cRNA, and mRNA.* J Virol Methods, 2011. **173**(1): p. 1-6.
147. Ruediger, D., et al., *Multiscale modeling of influenza A virus replication in cell cultures predicts infection dynamics for highly different infection conditions.* PLoS Comput Biol, 2019. **15**(2): p. e1006819.
148. Davis, A.R. and D.P. Nayak, *Sequence relationships among defective interfering influenza viral RNAs.* Proceedings of the National Academy of Sciences of the United States of America, 1979. **76**(7): p. 3092-6.
149. Saira, K., et al., *Sequence analysis of in vivo defective interfering-like RNA of influenza A H1N1 pandemic virus.* J Virol, 2013. **87**(14): p. 8064-74.
150. Widjaja, I., et al., *Competition between influenza A virus genome segments.* PLoS One, 2012. **7**(10): p. e47529.
151. Fujii, Y., et al., *Selective incorporation of influenza virus RNA segments into virions.* Proceedings of the National Academy of Sciences of the United States of America, 2003. **100**(4): p. 2002-7.
152. Meyer, W.J., et al., *Influence of host cell-mediated variation on the international surveillance of influenza A (H3N2) viruses.* Virology, 1993. **196**(1): p. 130-7.
153. Katz, J.M. and R.G. Webster, *Efficacy of inactivated influenza A virus (H3N2) vaccines grown in mammalian cells or embryonated eggs.* J Infect Dis, 1989. **160**(2): p. 191-8.

154. Rezelj, V.V., et al., *Defective viral genomes as therapeutic interfering particles against flavivirus infection in mammalian and mosquito hosts.* Nature communications, 2021. **12**(1): p. 2290.
155. Levi, L.I., et al., *Defective viral genomes from chikungunya virus are broad-spectrum antivirals and prevent virus dissemination in mosquitoes.* PLoS Pathog, 2021. **17**(2): p. e1009110.
156. Nakajima, S. and A. Sugiura, *Neurovirulence of influenza virus in mice. II. Mechanism of virulence as studied in a neuroblastoma cell line.* Virology, 1980. **101**(2): p. 450-7.
157. Sugiura, A. and M. Ueda, *Neurovirulence of influenza virus in mice. I. Neurovirulence of recombinants between virulent and avirulent virus strains.* Virology, 1980. **101**(2): p. 440-9.
158. Nogales, A. and L. Martinez-Sobrido, *Reverse Genetics Approaches for the Development of Influenza Vaccines.* Int J Mol Sci, 2016. **18**(1).
159. Giria, M., et al., *Reverse genetics vaccine seeds for influenza: Proof of concept in the source of PB1 as a determinant factor in virus growth and antigen yield.* Virology, 2016. **496**: p. 21-27.
160. Mehle, A. and J.A. Doudna, *Adaptive strategies of the influenza virus polymerase for replication in humans.* Proc Natl Acad Sci U S A, 2009. **106**(50): p. 21312-6.
161. Almeida, F., et al., *Optimization of A(H1N1)pdm09 vaccine seed viruses: The source of PB1 and HA vRNA as a major determinant for antigen yield.* Virus Res, 2022. **315**: p. 198795.
162. Vincent, A.L., et al., *Live attenuated influenza vaccine provides superior protection from heterologous infection in pigs with maternal antibodies without inducing vaccine-associated enhanced respiratory disease.* J Virol, 2012. **86**(19): p. 10597-605.
163. Tang, P.C.H., et al., *Can live-attenuated SARS-CoV-2 vaccine contribute to stopping the pandemic?* PLoS Pathog, 2022. **18**(9): p. e1010821.
164. Rudenko, L., et al., *Development and approval of live attenuated influenza vaccines based on Russian master donor viruses: Process challenges and success stories.* Vaccine, 2016. **34**(45): p. 5436-5441.
165. Zhou, B., et al., *Reversion of Cold-Adapted Live Attenuated Influenza Vaccine into a Pathogenic Virus.* J Virol, 2016. **90**(19): p. 8454-63.
166. World Health Organization. *Candidate vaccine viruses and potency testing reagents*. 2024 [cited 2024; Available from: https://www.who.int/teams/global-influenza-programme/vaccines/who-recommendations/candidate-vaccine-viruses.
167. Wanitchang, A., J. Kramyu, and A. Jongkaewwattana, *Enhancement of reverse genetics-derived swine-origin H1N1 influenza virus seed vaccine growth by inclusion of indigenous polymerase PB1 protein.* Virus Res, 2010. **147**(1): p. 145-8.
168. Mostafa, A., et al., *The PB1 segment of an influenza A virus H1N1 2009pdm isolate enhances the replication efficiency of specific influenza vaccine strains in cell culture and embryonated eggs.* J Gen Virol, 2016. **97**(3): p. 620-631.
169. Cobbin, J.C., et al., *Influenza virus PB1 and neuraminidase gene segments can cosegregate during vaccine reassortment driven by interactions in the PB1 coding region.* J Virol, 2014. **88**(16): p. 8971-80.
170. Rigby, C.V., et al., *Evolution of transient RNA structure-RNA polymerase interactions in respiratory RNA virus genomes.* Virus Evol, 2023. **9**(2): p. vead056.
171. Dadonaite, B., et al., *The structure of the influenza A virus genome.* Nat Microbiol, 2019. **4**(11): p. 1781-1789.
172. Gao, J., et al., *Balancing the influenza neuraminidase and hemagglutinin responses by exchanging the vaccine virus backbone.* PLoS Pathog, 2021. **17**(4): p. e1009171.

173. Zheng, A., et al., *Enhancing Neuraminidase Immunogenicity of Influenza A Viruses by Rewiring RNA Packaging Signals.* J Virol, 2020. **94**(16).
174. Ozawa, M., et al., *Nucleotide sequence requirements at the 5' end of the influenza A virus M RNA segment for efficient virus replication.* J Virol, 2009. **83**(7): p. 3384-8.
175. Hutchinson, E.C., et al., *Genome packaging in influenza A virus.* J Gen Virol, 2010. **91**(Pt 2): p. 313-28.
176. Furuse, Y. and H. Oshitani, *Evolution of the influenza A virus untranslated regions.* Infect Genet Evol, 2011. **11**(5): p. 1150-4.
177. Seitz, C., et al., *High yields of influenza A virus in Madin-Darby canine kidney cells are promoted by an insufficient interferon-induced antiviral state.* J Gen Virol, 2010. **91**(Pt 7): p. 1754-63.
178. Sanchez-Guzman, D., et al., *Long-term evolution of the epithelial cell secretome in preclinical 3D models of the human bronchial epithelium.* Sci Rep, 2021. **11**(1): p. 6621.
179. Bottcher-Friebertshauser, E., et al., *Inhibition of influenza virus infection in human airway cell cultures by an antisense peptide-conjugated morpholino oligomer targeting the hemagglutinin-activating protease TMPRSS2.* Journal of virology, 2011. **85**(4): p. 1554-62.
180. Bui, M., G. Whittaker, and A. Helenius, *Effect of M1 protein and low pH on nuclear transport of influenza virus ribonucleoproteins.* J Virol, 1996. **70**(12): p. 8391-401.
181. Bui, M., et al., *Role of the influenza virus M1 protein in nuclear export of viral ribonucleoproteins.* J Virol, 2000. **74**(4): p. 1781-6.
182. Perez, D.R. and R.O. Donis, *The matrix 1 protein of influenza A virus inhibits the transcriptase activity of a model influenza reporter genome in vivo.* Virology, 1998. **249**(1): p. 52-61.
183. Hankins, R.W., et al., *Mechanism of influenza virus transcription inhibition by matrix (M1) protein.* Res Virol, 1990. **141**(3): p. 305-14.
184. Belicha-Villanueva, A., et al., *Recombinant influenza A viruses with enhanced levels of PB1 and PA viral protein expression.* J Virol, 2012. **86**(10): p. 5926-30.
185. Maamary, J., et al., *Attenuated influenza virus construct with enhanced hemagglutinin protein expression.* J Virol, 2012. **86**(10): p. 5782-90.
186. Shin, D.L., et al., *Protection from Severe Influenza Virus Infections in Mice Carrying the Mx1 Influenza Virus Resistance Gene Strongly Depends on Genetic Background.* J Virol, 2015. **89**(19): p. 9998-10009.
187. Lazarowitz, S.G. and P.W. Choppin, *Enhancement of the infectivity of influenza A and B viruses by proteolytic cleavage of the hemagglutinin polypeptide.* Virology, 1975. **68**(2): p. 440-54.
188. Klenk, H.D., et al., *Activation of influenza A viruses by trypsin treatment.* Virology, 1975. **68**(2): p. 426-39.
189. Bottcher-Friebertshauser, E., H.D. Klenk, and W. Garten, *Activation of influenza viruses by proteases from host cells and bacteria in the human airway epithelium.* Pathog Dis, 2013. **69**(2): p. 87-100.
190. Hsu, A.C.-Y., et al., *Human influenza is more effective than avian influenza at antiviral suppression in airway cells.* American journal of respiratory cell and molecular biology, 2011. **44**(6): p. 906-13.
191. To, K.K., et al., *Human H7N9 virus induces a more pronounced pro-inflammatory cytokine but an attenuated interferon response in human bronchial epithelial cells when compared with an epidemiologically-linked chicken H7N9 virus.* Virol J, 2016. **13**: p. 42.
192. Dittmann, M., et al., *A serpin shapes the extracellular environment to prevent influenza A virus maturation.* Cell, 2015. **160**(4): p. 631-643.

193. Lazarowitz, S.G., A.R. Goldberg, and P.W. Choppin, *Proteolytic cleavage by plasmin of the HA polypeptide of influenza virus: host cell activation of serum plasminogen.* Virology, 1973. **56**(1): p. 172-80.
194. Hinay, A.A., Jr., et al., *Pro-Inflammatory Cytokines and Interferon-Stimulated Gene Responses Induced by Seasonal Influenza A Virus with Varying Growth Capabilities in Human Lung Epithelial Cell Lines.* Vaccines (Basel), 2022. **10**(9).
195. Mesev, E.V., R.A. LeDesma, and A. Ploss, *Decoding type I and III interferon signalling during viral infection.* Nat Microbiol, 2019. **4**(6): p. 914-924.

7. Supplements

7.1.1. Production of seg 1 DIP candidates in MDCK-PB2 suspension cells

Seg 1 DIP candidates were rescued in HEK-PB2 and MDCK-PB2 co-cultures using the transfection conditions specified in Table 4.5B (lower panel). Rescue harvests from 13 d.p.t., underwent amplification followed by MODIP screening in MDCK-PB2 suspension cells, conducted by Lars Pelz. The MODIP screening revealed high total and infectious (data not shown) virus titers for all seg 1 DIP candidates, including the seg 1 de novo DIP, which was previously undetectable using adherent MDCK-PB2 cell-based amplifications (Figures 4.1.5 B, C). The virus harvest from the MODIP screening was further analysed using segment-specific DIP PCR and agarose gel electrophoresis (Supplement figure 7.2), to confirm the presence of the seg 1 de novo DIP band on the agarose gel.

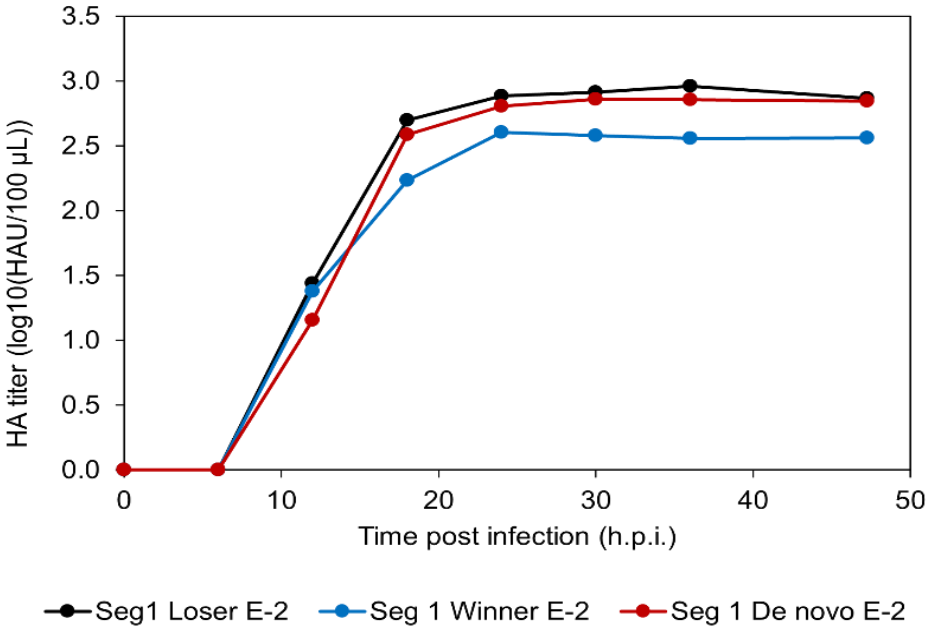

Supplement figure 7.1. Production of seg 1 DIP candidates. MDCK-PB2 suspension cells were grown in 125 mL shake flasks with a working volume of 50 mL. Cells at a density of 2 × 10^6 cells/mL were infected with MODIP of E-2 to grow top seg 1 loser, winner, and de novo candidate DIPs. The cell-free supernatants were subsequently assessed for total virus titers using the HA assay. Data generated by Lars Pelz (unpublished).

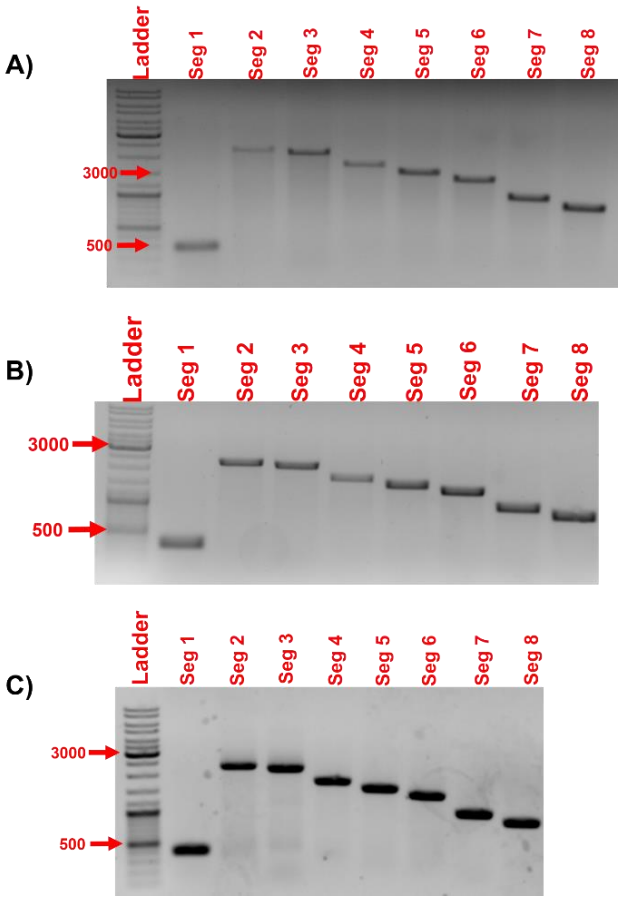

Supplement figure 7.2. Growth and purity of seg 1 DIP candidates in MDCK-PB2 suspension cells. Purity of seg 1 DIP candidates (produced at different MODIP) in MDCK-PB2 suspension cells with respect to other contaminating DIPs. MODIP used are A) E-4 for loser B) E-3 for winner and C) E-2 for de novo. Viral harvests were subjected to segment-specific RT-PCR followed by agarose gel electrophoresis. Arrows indicate ladder band size. Data generated by Lars Pelz [1]

7.1.2. Western blots for single and triple IAV polymerase expressing cells

To reconstitute seg 2 and 3 DIP candidates (Figure 4.1.8) that lack functional PB1 and PA proteins, respectively, genetically engineered HEK and MDCK cells expressing the IAV polymerase proteins were developed by collaborators at the DPZ, Göttingen. These engineered cell lines were essential for the reconstitution and amplification processes. Both single and triple IAV polymerase-expressing cell lines were created and subsequently analysed using western blotting to confirm

stable expression of the IAV proteins in the adherent cell lines (Supplement figure 7.3).

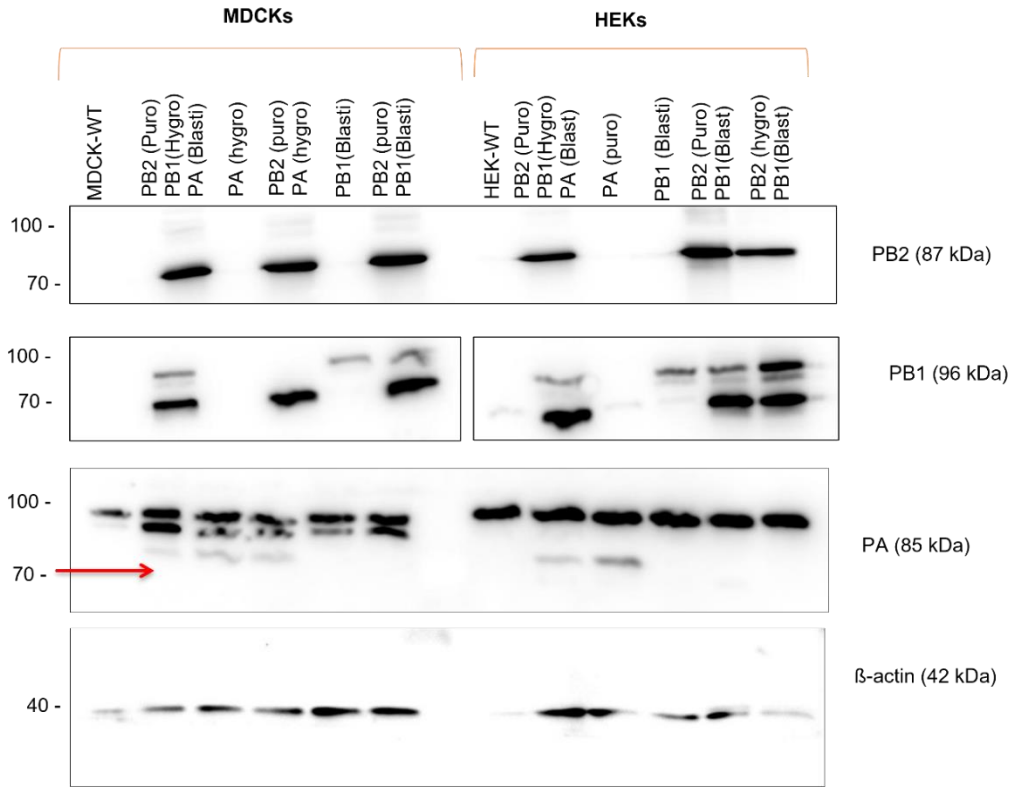

Supplement figure 7.3. Western blot analysis of the IAV polymerase protein expressing cell lines. 0.5 × 10^6 cells cells from various complementing cell lines were lysed in 200 µl of 1x SDS lysis buffer and heated at 94°C for 10 min before western blot analysis. Non-transduced parental MDCKs and 293Ts served as negative controls. Proteins were separated on gels of different percentages: PA on 8%, PB2 on 12%, and PB1 on 10%, with 7 µl of each sample loaded per lane in a 15-well chamber. Primary antibodies used were: PB2 (rabbit, 1:5000), PB1 (rabbit, 1:1000), PA-C-Term (rabbit, 1:1000), and ß-actin (mouse, 1:1000). All primary antibodies were diluted in 5% milk powder (MP) and incubated overnight at 4°C. The secondary antibody, anti-rabbit HRP, was used at 1:10000 dilution in 5% MP/PBS-T and incubated for 1 h at room temperature. Please note the antibiotics for maintenance of single and triple positive MDCK-PB2-PB1-PA cells were switched and mentioned in the Material and Methods section 3.1. Data was generated at the Stefan Pöhlmann lab, DPZ, Göttingen.

7.1.3. Reconstitution of OP7 DIPs

In addition to the rescue attempts to generate clonal OP7 DIPs with HEK-WT and MDCK-WT co-cultures, as detailed in section 4.3.1, similar efforts were previously made by collaboration partners at DPZ, Göttingen, as illustrated in Supplement figure 7.4.

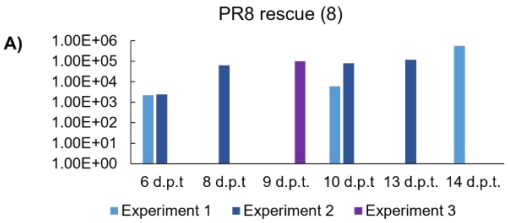

HEK-WT + MDCK-WT	Virus type	Seg 1-8	Seg 7-OP7
	STV (PR8)	1 µg	

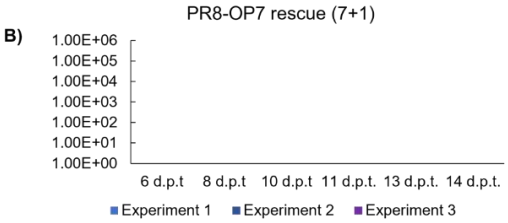

HEK-WT + MDCK-WT	Virus type	Seg 1-6, 8	Seg 7-OP7
	PR8-OP7	1 µg	1 µg

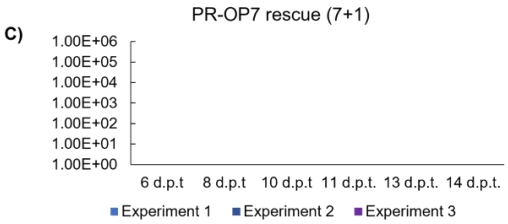

HEK-WT + MDCK-WT	Virus type	Seg 1-6, 8	Seg 7-OP7
	PR8-OP7	1 µg	50 ng

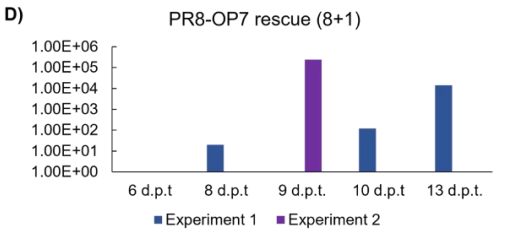

HEK-WT + MDCK-WT	Virus type	Seg 1-8	Seg 7-OP7
	PR8-OP7	1 µg	1 µg

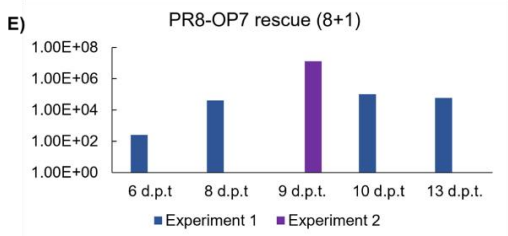

HEK-WT + MDCK-WT	Virus type	Seg 1-8	Seg 7-OP7
	PR8-OP7	1 µg	50 ng

Supplement figure 7.4. Efforts to reconstitute clonal OP7 DIPs using reverse genetics. Collaborative efforts with DPZ, Gottingen, involved two independent reverse genetics experiments to reconstitute clonal OP7 DIPs, with a third attempt (performed in our lab) detailed in Figure 4.3.1 and revisited here for context. HEK-WT and MDCK-WT cells were co-transfected with eight plasmids (1 µg per well) A) encoding WT segments to generate a PR8 control virus. B) For OP7 DIP reconstitution, the standard eight-plasmid approach was modified by substituting the seg 7 plasmid with one encoding seg 7-OP7 at 1 µg per well C) or 50 ng. D-E) Additionally, a 9-plasmid scheme was used, combining eight WT segment plasmids with a ninth for seg 7-OP7 at D) 1 µg (D) or E) 50 ng per well. Infectious virus titers post-rescue were quantified via plaque assay

7.1.4. Experimental conditions for recovering OP7 chimera DIPs

The use of two distinct DI vRNA types (seg 1 DI and seg 7-OP7 vRNA) introduced significant uncertainty in virus rescue. Various plasmid amounts were tested for reconstitution. Supplement figure 7.5 shows the adjusted plasmid quantities for DI244 and OP7. This involved increasing both DI vRNA-encoding plasmids (1 µg) or increasing DI244 (2 µg) with seven full-length plasmids (2 µg), keeping OP7 at 50 ng per well. Additional combinations are detailed in Supplement figure 7.5. These combinations aimed to facilitate seg 1 DIP rescue, counteracting OP7's antiviral effects. Using 2 µg of seven full-length and DI244 plasmids with 50 ng of OP7 yielded detectable virus titers after two propagation rounds in MDCK-PB2 cells (conditions 1, 2, 3 in Supplement figure 7.5). Conversely, using 1 µg of DI244 and seven full-length plasmids with 50 ng of OP7 failed to produce detectable titers after three passages. This aligns with unsuccessful rescue attempts using 1 µg of OP7 with other plasmids at 1 µg (conditions 4, 5, 6 in Supplement figure 7.5). However, it contrasts with successful rescue using 1 µg of OP7 and seven full-length plasmids (Figure 4.3.3). Thus, establishing a fixed plasmid concentration for DIP rescue is challenging with two distinct DI vRNA types.

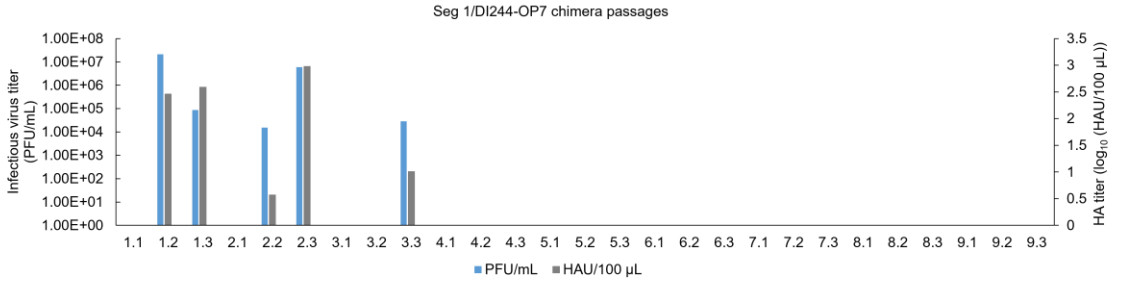

	Conditions labelled	Virus type (genome constellation)	PR8 plasmids	DI244 plasmid	Seg 7-OP7 plasmid	harvest time point	Passage
HEK-PB2 + MDCK-PB2	1.1	DI244+OP7	Seg 2-8 (2 µg)	2 µg	50 ng	6 d.p.t.	1
	1.2	DI244+OP7	Seg 2-8 (2 µg)	2 µg	50 ng	6 d.p.t.	2
	1.3	DI244+OP7	Seg 2-8 (2 µg)	2 µg	50 ng	6 d.p.t.	3
	2.1	DI244+OP7	Seg 2-8 (2 µg)	2 µg	50 ng	8 d.p.t.	1
	2.2	DI244+OP7	Seg 2-8 (2 µg)	2 µg	50 ng	8 d.p.t.	2
	2.3	DI244+OP7	Seg 2-8 (2 µg)	2 µg	50 ng	8 d.p.t.	3
	3.1	DI244+OP7	Seg 2-8 (2 µg)	2 µg	50 ng	10 d.p.t.	1
	3.2	DI244+OP7	Seg 2-8 (2 µg)	2 µg	50 ng	10 d.p.t.	2
	3.3	DI244+OP7	Seg 2-8 (2 µg)	2 µg	50 ng	10 d.p.t.	3
	4.1	DI244+OP7	Seg 2-8 (1 µg)	1 µg	1 µg	4 d.p.t.	1
	4.2	DI244+OP7	Seg 2-8 (1 µg)	1 µg	1 µg	4 d.p.t.	2
	4.3	DI244+OP7	Seg 2-8 (1 µg)	1 µg	1 µg	4 d.p.t.	3
	5.1	DI244+OP7	Seg 2-8 (1 µg)	1 µg	1 µg	6 d.p.t.	1
	5.2	DI244+OP7	Seg 2-8 (1 µg)	1 µg	1 µg	6 d.p.t.	2
	5.3	DI244+OP7	Seg 2-8 (1 µg)	1 µg	1 µg	6 d.p.t.	3
	6.1	DI244+OP7	Seg 2-8 (1 µg)	1 µg	1 µg	8 d.p.t.	1
	6.2	DI244+OP7	Seg 2-8 (1 µg)	1 µg	1 µg	8 d.p.t.	2
	6.3	DI244+OP7	Seg 2-8 (1 µg)	1 µg	1 µg	8 d.p.t.	3
	7.1	DI244+OP7	Seg 2-8 (1 µg)	1 µg	50 ng	4 d.p.t.	1
	7.2	DI244+OP7	Seg 2-8 (1 µg)	1 µg	50 ng	4 d.p.t.	2
	7.3	DI244+OP7	Seg 2-8 (1 µg)	1 µg	50 ng	4 d.p.t.	3
	8.1	DI244+OP7	Seg 2-8 (1 µg)	1 µg	50 ng	6 d.p.t.	1
	8.2	DI244+OP7	Seg 2-8 (1 µg)	1 µg	50 ng	6 d.p.t.	2
	8.3	DI244+OP7	Seg 2-8 (1 µg)	1 µg	50 ng	6 d.p.t.	3
	9.1	DI244+OP7	Seg 2-8 (1 µg)	1 µg	50 ng	8 d.p.t.	1
	9.2	DI244+OP7	Seg 2-8 (1 µg)	1 µg	50 ng	8 d.p.t.	2
	9.3	DI244+OP7	Seg 2-8 (1 µg)	1 µg	50 ng	8 d.p.t.	3

Supplement figure 7.5. Varied plasmid amounts tested for OP7 chimera DIP rescue. The figure's accompanying table illustrates the experimentation with plasmids encoding full-length WT segments, ranging from 1 µg to 2 µg per plasmid per well. For DI244 plasmids, amounts varied from 1 µg to 2 µg per well, and for OP7, from 50 ng to 1 µg. The absence of significant infectious (quantified in plaque assay) or total virus titers (measured in HA assay) after three consecutive blind amplifications in MDCK-PB2 cells is shown in the graph for various conditions.

7.1.5. MODIP screening for OP7 chimera DIPs

Based on the findings in sections 4.3.2–4.3.5, reconstitution of the OP7 chimera DIPs is achievable. However, the decreasing infectious and total titers over successive passages pose significant challenges for production of the DIP material as antivirals. The growth of seg 1 DIPs is crucial in this population of DIPs (Figure 4.3.2C) as they act as surrogate STV for propagating OP7 chimera DIPs, which otherwise inhibit seg 1 DIP propagation. Using a lower MOI may reduce the likelihood of co-infections between OP7 chimera DIPs and seg 1 DIPs, facilitating the growth of both surrogate STVs and OP7 chimera DIPs. Careful evaluation of these infections in MDCK-PB2 suspension cells is necessary to optimize the growth of OP7 chimera DIP material. This study, conducted by Lars Pelz [4], involved MODIP screening using of adherent culture-amplified OP7 chimera DIP material in MDCK-PB2 suspension cells at MOIs ranging from 1E-2 to 1E-5

(Supplement figure 7.6). As previously noted, (section 4.3.4) both seg 1 candidate DIP backbones were initially utilized to reconstitute OP7 chimera DIPs (Figure 4.3.5–4.3.8). Subsequently, the seg 1/winner-OP7 chimera was selected for suspension cell-based process optimization due to strong interfering activity.

From Supplement figure 7.6, it is evident that at lower MOIs, there are high total virus titers, as indicated by HA titers (Supplement figure 7.6A), and a high proportion of OP7 chimera DIPs, as determined by extracellular vRNA quantifications of seg 7-OP7 and WT seg 7 via RT-qPCR (Supplement figure 7.6B) [3]. This observation can be attributed to the inhibitory effect of accumulating OP7 chimera DIPs at higher MOIs. For instance, OP7 chimera DIPs constituted 94.4% at an MOI of 1E-2 and 24.2% at an MOI of 1E-5, based on RT-qPCR data. As previously shown (sections 4.3.2–4.3.5), infectious virus titers decreased over time, underscoring the importance of selecting optimal harvest times. DIP harvesting was therefore carried out when HA titers near-plateau and before onset of significant cell death to minimize cell debris and host DNA contamination [3]. Final viral harvests were devoid of contaminating DIPs, as RT-PCR results showed no significant accumulation of other DI vRNAs in seg 2–8 (Supplement figure 7.7) [3].

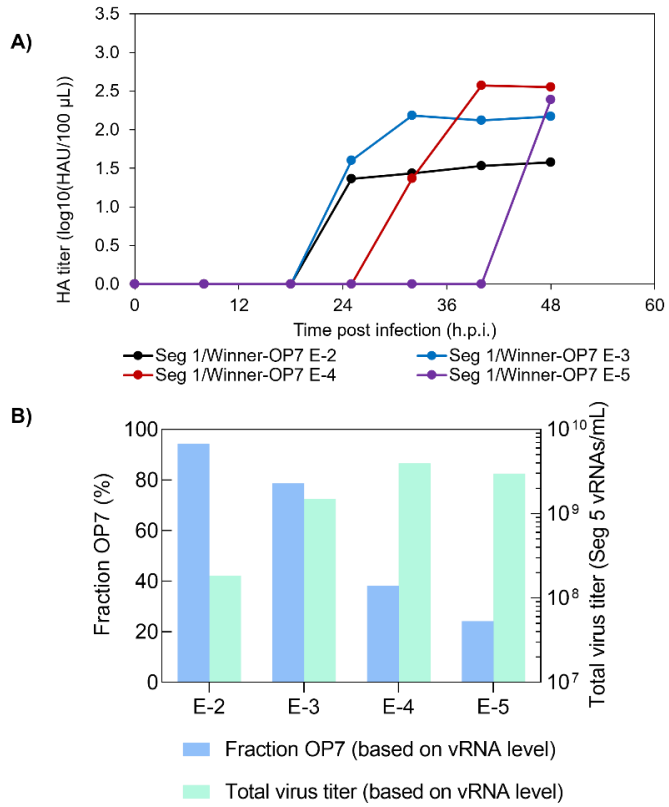

Supplement figure 7.6. Production of OP7 chimera DIP enriched material via MODIP screening. MDCK-PB2 cells were grown in 125 mL shake flasks (50 mL working volume) and infected at MODIP of E-2, E-3, E-4, and E-5 with OP7 chimera constructs (based on seg 1 winner) for 48 h. A) Complete medium exchange was performed prior to infection. Virus titers in cell-free supernatants were determined using the HA assay. B) Quantification of OP7 chimera DIPs by RT-qPCR. The fraction of extracellular seg 7-OP7 to seg 7-WT vRNA. Data generated by Lars Pelz [3].

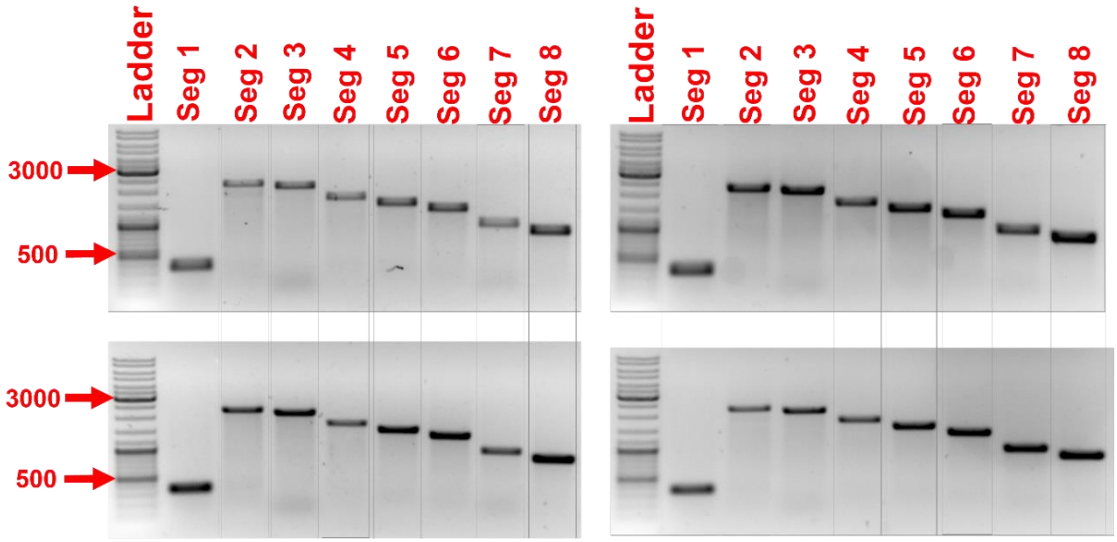

Supplement figure 7.7. Produced OP7 chimera DIP material is devoid of contaminating DIPs. OP7 chimera-enriched DIPs were produced in MDCK-PB2 suspension cells at different MODIP. Supernatants at 48 h.p.i. were subjected to segment-specific RT-PCR and agarose gel electrophoresis. (A) MOI 1E-2, (B) MOI 1E-3, (C) MOI 1E-4, and (D) MOI 1E-5. Arrows indicate the ladder band size. Cropped gels are shown. Data generated by Lars Pelz. [3]

7.1.6. Interfering capacity of OP7 chimera DIPs produced at various MODIP

The interfering assay was used to find the optimal MODIP to produce OP7 chimera DIP material with highest interfering activity (Supplement figure 7.8). MDCK-WT cells were infected either with STV at an MOI of 10 (negative control, NC) or co-infected with 125 µL of DIP material produced at various MOIs [3]. The results showed that DIPs produced at MOIs of 1E-3 and 1E-4 had the strongest interference, reducing infectious virus release by over two orders of magnitude, significantly more than the two-fold reduction at an MOI of 1E-2 ($p < 0.0001$) and the one-log reduction at an MOI of 1E-5 ($p < 0.001$, ANOVA analysis followed by Tukey's multiple comparison test). This trend was less pronounced for total virus release measured by HA titer (Supplement figure 7.8A) and extracellular seg 5 vRNA concentration (Supplement figure 7.8B). Additionally, co-infections with DIPs produced at MOIs of 1E-3 and 1E-4 showed a pronounced OP7 phenotype (Supplement figure 7.8B), indicating preferential replication of Seg 7-OP7 vRNA. Overall, the MOI significantly affects OP7 chimera DIP production, with

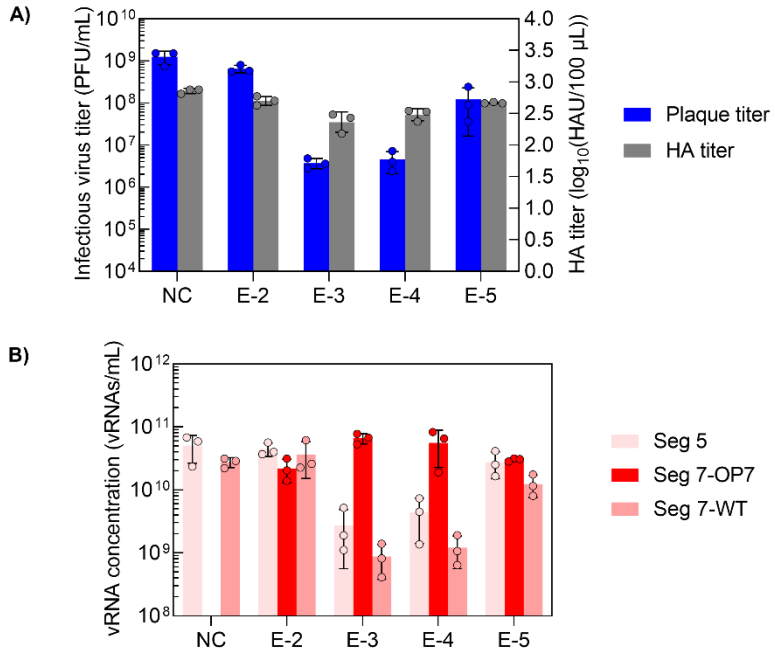

Supplement figure 7.8. OP7 chimera DIP enriched material demonstrates strong interfering activity. Cell-culture-based produced OP7 chimera DIPs (based on seg 1 winner backbone) in MDCK-PB2 suspension cells over a range of MODIP between E-2 to E-5. A-B) Evaluation of OP7 chimera DIPs' interfering activity in MDCK cells: A) Virus titers post-infection with STV (PR8 strain) or co-infection with DIP material (125 µL) measured via plaque and HA assays at 16 h.p.i.. B) RT-qPCR analysis of extracellular vRNA levels for segments 5, 7-OP7, and 7-WT. Data generated by Lars Pelz [3].

intermediate MOIs of 1E-3 and 1E-4 providing a balance between high DIP fractions and virus titers [3].

8. Standard operating procedures

Procedure	SOP number
Phosphate buffer saline preparation	SOP M/01
Cell culture media preparation	SOP M/02 and SOP M/03
1 X trypsin preparation	SOP M/07
HA assay	SOP V/05
Cell line freezing and thawing	SOP Z/02
Cell culturing	SOP Z/04
Working cell bank preparation	SOP Z/06

8.1.1. Plaque assay

Preparation of the cell culture flasks (Friday)

- Prepare T175 cell culture flasks on Friday
- At 13:00 prepare bottles with a cell density of 7 * 1E6 cells/bottle
- Prepare also enough cells for the following plaque assay
- With a T175 bottle, approx. 4 6-well plates can be prepared on Monday

Attaching the 6-well plates (Monday)

- On Monday at 14:00 6-well plates are prepared
- Trypsinate cells from the prepared T175 flasks
- Plaque (1 sample = 1 plate):
    - Measure cell concentration and adjust to 0.266 * 106 cells/mL with Z-medium
    - Using a Multi-Step pipette, add 3 mL to each well of the 6-well plate (0.8*106 cells/well)
    - Incubate cells for up to 76 h (Mon 14:00 -> Thur 17:00)

Infecting the cells (Thursday)

- First prepare V-Medium with 1v% trypsin (500U)
    - For dilution: 30 mL per 96-well plate
    - For agar: 10 mL per 6-well plate (do not add trypsin yet)
- Thaw the samples of the interfering assay and place them in a 96-well plate dilution series
    - Add 270 µL of V-Medium (+1 v% trypsin (500U)) to all wells
    - Add 30 µL sample to the first well, then transfer always 30 µL to the next row
    - Use multi-channel pipette, change tips after each pipetting step
- Wash the 6-well plates prepared on Monday 2 times with 1 mL PBS/well
- Apply the dilution series of one sample per plate (250 µL per well)
- Dilution depending on sample (usually 1E-2 – 1E-7; for RKI control: 1E-3 – 1E-8)
- Incubate plates for 1 h at 37°C (swivel every 15 min to avoid drying of the cells)
- Meanwhile, preheat medium to 45°C and melt 3% agar
- Mix medium and agar to achieve 1% agar and warm at 45 °C
- After the incubation remove the supernatant of the cells

- Take the 1% agar from the heat bath and add 1 v% trypsin (500U)
- overlay cells with 2 mL 1% agar per well
- Incubate 6-well plates at 37°C until Monday morning

Staining of the plaques (Monday)

- Add 1 mL cold methanol to each well
- Remove agar with a spatula (carefully, do not damage the cell layer)
- Collect the agar and place under a fume hood to evaporate the methanol
- Overlay the cell layer of each well with crystal violet and swivel to loosen cell debris
- Remove the Christallviolet and return it to the storage bottle
- Dry plates via ventilation
- count plaques

9. List of reagents

Reagent	Manufacturer	Article number
Agarose	AppliChem	A2114, 1000
Ampicillin	Roth	69-52-3
Blasticidin	Sigma-Aldrich	15205-25MG
Bovine serum albumin	Sigma-Aldrich	A1391
Crystal violet	Roth	C.I. 42555
Disodium hydrogen phosphate	Roth	2370.1
DMEM	Gibco	41966-029
dNTPs	Thermo Fisher Scientific	R0193
EDTA	Sigma-Aldrich	EDS-100g
Ethanol	Roth	9065.4
FastDigest Green Buffer	Thermo Fisher Scientific	B72
FBS	Pan Biotech	10270-106
Formaldehyde solution 37%	Roth	7398.1
G418	Roth	0239.4
GeneRuler DNA Ladder Mix	Thermo Fisher Scientific	SM0333
GeneRuler DNA Ladder Mix	Thermo Scientific	SM0333
Gentamycin	Invitrogen	15710064
GMEM powder	Gibco	22100-093
Hepes	Roth	HN78.3
Hygromycin B	Thermo Fisher Scientific	10687010
Isopropanol	Merck	1096342511
Maxima H Minus Reverse Transcriptase	Thermo Fisher Scientific	EP0751
Maxima H Minus Reverse Transcriptase first strand cDNA synthesis kit 5X RT buffer	Thermo Fisher Scientific	K1652
MEM	Thermo Fisher Scientific	41090093
Methanol	Roth	CP43.1
NucleoSpin RNA Virus kit	Macherey-Nagel	740956.250
oligo(dT) primer	Thermo Fisher Scientific	SO132
Peptone	Lab M	LAB204

Phusion High-Fidelity DNA Polymerase 5x Phusion HF buffer MgCl2	Thermo Fisher Scientific	F530L
Phusion Hot Start II DNA Polymerase	Thermo Scientific	F549L
Primers	Thermo Fisher Scientific	-
Puromycin	Thermo Fisher Scientific	#A1113803
QIAquick Gel Extraction Kit	Qiagen	28706
RevertAid First Strand cDNA Synthesis Kit	Thermo Fisher Scientific	K1631
RevertAid H minus Reverse transcriptase	Thermo Fisher Scientific	EP0451
RevertAid H Minus Reverse Transcriptase	Thermo Scientific	EP0451
RiboLock RNase Inhibitor	Thermo Fisher Scientific	EO0384
Roti-GelStain	Roth	3865.2
Rotor-Gene SYBR Green PCR Kit	Qiagen	204074
Sodium chloride	Sigma-Aldrich	S9625
TranscriptAid T7 High Yield Transcription Kit	Thermo Scientific	K0441
Tris	Roth	77-86-1
Trypan blue	Merck	1117320025
Trypsin	Gibco Sigma-Aldrich	1188797 T7409, T1426
β-Mercaptoethanol	Merck	44420

10. List of equipment and consumables

Equipment/consumable	**Manufacturer**	**Model name/article number**
12-well plates	Greiner BioOne	0358
6-well plates	Greiner BioOne	M8562
96-well-microtiter plates 96-	Greiner BioOne	656101
Agarose gel electrophoresis equipment	Biomed Analytics VWR Gibco	Agagel Maxi Biometra Power Source 300V BRL UV Transilluminator

	Biometra	BioDocAnalyzer
Autoclave	HP Medizintechnik	Varioklav 65T
Balance	Satorius	TE1502S Cubis precisuion
Biological safety cabinet	Thermo Fisher Scientific	Heraeus HERAsafe SAFE 2020
Cell counter	Beckman Coulter	ViCell XR cell counter
Centrifuge	Thermo Fisher Scientific Beckman Coulter	Heraeus BiofugePrimoR, Fresco 17 Avanti J 20, Optima LE 80K
Heat block	Grant Instruments	-
Incubator	Heraeus	HERAcell 240, 240i HERAcell T6060
Microplate reader	Tecan	Infinite 200 Pro NanoQuant
Microscope	Zeiss	Axioskop 2, observer.A1 Axiovert 25, 40C, S100
Multichannel and multistep pipet	Eppendorf	Xplorer plus 50-1200µL
PCR cabinet	Peqlab	PCR workstation Pro
pH meter	WTW	inoLab pH meter
Pipetting robot	Qiagen	QIAgility
Pump	Watson-Marlow	120 U/DV
Real-time PCR cycler	Qiagen	Rotor-Gene Q
Roller bottles	Greiner BioOne	0439
T-175 flasks	Greiner BioOne	C7356
T-75 flasks	Greiner BioOne	C7231
Thermocycler	Biometra	T3000 T professional Thermocycler
Ultrapure water purification system	Millipore	Milli-Q-Advantage A10
Vortexer	VWR	Genie G560 Votex-Genie 2 vortex-mischer 120V
Water bath	VWR Fluke	Ultrasonic cleaner Isotemp 202

11. List of figures

12. List of tables

13. List of publications (for Ph.D. thesis)

1. **Dogra, T**., Pelz, L., Boehme, J. D., Kuechler, J., Kershaw, O., Marichal-Gallardo, P., Baelkner, M., Hein, M. D., Gruber, A. D., Benndorf, D., Genzel, Y., Bruder, D., Kupke, S.Y., & Reichl, U. (2023). Generation of "OP7 chimera" defective interfering influenza A particle preparations free of infectious virus that show antiviral efficacy in mice. Scientific Reports, 13(1). https://doi.org/10.1038/s41598-023-47547-1
2. Pelz, L.*, Rüdiger, D. *, **Dogra, T. ***, Alnaji, F. G., Genzel, Y., Brooke, C. B., Kupke, S. Y., & Reichl, U. (2021). Semi-continuous propagation of influenza A virus and its defective interfering particles: Analyzing the dynamic competition to select candidates for antiviral therapy. Journal of Virology, 95(24). https://doi.org/10.1128/jvi.01174-21 **(*equal contribution)**
3. Hein, M. D., Kazenmaier, D., van Heuvel, Y., **Dogra, T**., Cattaneo, M., Kupke, S. Y., Stitz, J., Genzel, Y., & Reichl, U. (2023). Production of retroviral vectors in continuous high cell density culture. Applied Microbiology and Biotechnology, 107(19), 5947–5961. https://doi.org/10.1007/s00253-023-12689-9
4. van Heuvel, Y., Schatz, S., Hein, M., **Dogra, T**., Kazenmaier, D., Tschorn, N., Genzel, Y., & Stitz, J. (2023). Novel suspension retroviral packaging cells generated by transposition using transposase encoding mRNA advance vector yields and enable production in bioreactors. Frontiers in Bioengineering and Biotechnology, 11. https://doi.org/10.3389/fbioe.2023.1076524
5. Pelz, L., **Dogra, T**., Marichal-Gallardo, P., Hein, M. D., Hemissi, G., Kupke, S. Y., Genzel, Y., & Reichl, U. (2024b). Production of antiviral "OP7 chimera" defective interfering particles free of infectious virus. Applied Microbiology and Biotechnology, 108(1). https://doi.org/10.1007/s00253-023-12959-6